UNIVERSITÀ
DEGLI STUDI
DI PADOVA

Sede Amministrativa: Università degli Studi di Padova

Dipartimento di Scienze Chimiche

CORSO DI DOTTORATO DI RICERCA IN: SCIENZE MOLECOLARI

CURRICOLO: CHIMICA

CICLO: XXIX

On-Surface Supramolecular Networks: Structure and Dynamics of Formation in Ultra-High Vacuum and at the Solid/Liquid Interface

Direttore della Scuola : Ch.mo Prof. Antonino Polimeno

Supervisore: Ch.mo Prof. Mauro Sambi

Dottorando : Luciano Colazzo

ABSTRACT

On-surface supramolecular chemistry inspired the fabrication of a large variety of atomically controlled systems and on-surface synthesis allowed the production of low-dimensional materials with atomic precision. Since numerous surface-supported nanostructures are constantly developed, their possible applications stimulate diverse areas of research such as catalysis, organic electronics, surface sensing, surface functionalization and nanopatterning.

Several protocols and interfacial approaches have been developed for the production of surface-supported supramolecular networks by self-assembly and by far, the increasing interest for nanomaterials with innovative functionalities has boosted the search in on-surface activation of chemical reaction for the covalent stabilization of more complex molecular architectures.

Photochemistry was furthered as a promising approach for this purpose and pioneering examples allowed a deeper understanding of light-induced on-surface chemical reactions. However, the search in this field is still at its birth and further research is required. The Scanning Tunneling Microscope provides the necessary resolution for this studies in various conditions, including solid/liquid or solid/air interfaces or Ultra High Vacuum (UHV).

CONTENTS

INTRODUCTION 1
THE PH.D. ACTIVITY 5
1ST YEAR 6
2ND YEAR 6
3RD YEAR 7
METHODS 8
AMBIENT- AND UHV-SCANNING TUNNELING MICROSCOPY 8
SCANNING TUNNELING SPECTROSCOPY 9
X-RAY PHOTOELECTRON SPECTROSCOPY (XPS) 10
NEAR EDGE X-RAY ABSORPTION FINE STRUCTURE (NEXAFS) 10
LASER SOURCE 11
FUNDAMENTALS 12
ON-SURFACE SUPRAMOLECULAR NETWORKS 13
STRUCTURE AND DYNAMICS OF 2D AGGREGATES 16
DYNAMIC COVALENT CONTROL: THE CASE OF A STEREOSELECTIVE PHOTOPOLYMERIZATION 19
DYNAMERS 22
TWO DIMENSIONAL CRYSTALS 25
SELF-ASSEMBLED MONOLAYERS 25
HYDROGEN BOND INTERACTIONS 26
SELF-ASSEMBLED MONOLAYERS STABILIZED BY METAL-ORGANIC INTERACTIONS 31
COPPER TETRAMERIC UNITS EMBEDDED IN AN ON-SURFACE METAL-ORGANIC STRUCTURE 32
ON-SURFACE REACTIVITY 38
ON-SURFACE ACTIVATION OF CHEMICAL REACTIONS 38
ON-SURFACE ULLMANN COUPLING 39
WIDTH-DEPENDENT ENERGY GAP IN ARMCHAIR GRAPHENE NANORIBBONS: THE CASE OF PPP 39
ON-SURFACE GLASER COUPLING 42
PHOTOCHEMICAL ACTIVATION OF CHEMICAL REACTIONS 46
ON-SURFACE PHOTOCHEMISTRY OF PRE-ORDERED 1-METHYL-2-PHENYL-ACETYLENES: PHOTOSELECTIVE C-H BOND ACTIVATION AND INTERMOLECULAR COUPLING ON HOPG 48
METAL-FREE ON-SURFACE PHOTOCHEMICAL HOMOCOUPLING OF TERMINAL ALKYNES[54] 57
CONCLUSION AND OUTLOOK 70
REFERENCES 73
COMMUNICATIONS AT CONFERENCES 83
PUBLICATIONS 84
TEACHING EXPERIENCES 85
SELECTED PUBLICATIONS 86

INTRODUCTION

Gerhard Ertl remarked in his Noble Prize Lecture: “Surface chemistry can even explain the destruction of the ozone layer, as vital steps in the reaction actually take place on the surfaces of small crystals of ice in the stratosphere”.[1] Indeed, the surface of some forms of highly pure and ordered materials offers an ideal environment to investigate the physical and chemical properties of interfacial systems and atomistic phenomena.[2,3]

Supramolecular chemistry is the field of chemistry that deals with non-covalent interactions among molecules and the way in which the molecular assembly, folding and recognition occurs.[4] Early works dealing with supramolecular chemistry were solution-based and allowed to develop the fundamental concepts in this field. A variety of spectroscopic techniques were employed in the characterization of structures and dynamics of supramolecular assemblies and super-molecules. However, further details at the atomic level of such architectures were not available until microscopic visualization techniques in real space could be routinely performed in research laboratories.[5] With the invention of scanning tunneling microscopy (STM), information about the topography and a plethora of other surface properties could be finally obtained. The combination with the supramolecular chemistry research turned out to be useful to probe not only the organization of molecules at small scales, but also of molecular dynamics processes involved in assembly processes of molecules absorbed on surfaces.

The management of the assembly of nanostructured materials with architectures and properties that are directly influenced by the alteration of their smallest constituents (atoms and molecules), relies on the broad nanotechnological category of “bottom-up” fabrications. The combination of knowledge concerned with the design and testing of

molecular properties, behavior and supramolecular chemistry is encompassed by the term "crystal engineering".[6]

On-surface supramolecular chemistry has produced a large variety of atomically controlled systems, often obtained via molecular self-assembly.[7] The latter is a spontaneous phenomenon characterized by recognition and association of molecules, under equilibrium conditions, into structurally ordered and stable aggregates. In these molecular ensembles, molecules are held together by the highest possible number of non covalent, intermolecular interactions, e. g. hydrogen bonds, donor-acceptor, dipole-dipole and Van der Waals interactions.[8–10]

Within the building blocks of a generic surface-supported system exists also a delicate interplay between lateral and vertical interactions, i.e. molecule-molecule and molecule-substrate interactions, respectively. As a consequence, even slight modifications at the interface can produce dramatic changes either in the supramolecular network or at the single molecule level. Small and simple molecular architectures can in turn initiate a hierarchical path of self-aggregation between each other, leading eventually to nanostructured macroscopic materials. However, by properly choosing molecular building blocks, tailored supramolecular patterns can be obtained.[11,12]

Since molecular self-assembly is based on non-covalent interactions, the resulting two-dimensional (2D) crystals, are often rather labile and do not survive to the changing temperature or environment (vacuum Vs. solution or atmosphere). A way to overcome this limitation relies therefore, on the covalent stabilization of the self assembled nanoarchitectures. Commonly, this is obtained by using suitable reactants and by activating the covalent networking between the molecular precursors in a second stage, via chemical, thermal or photochemical reactions.[13–17]

So far, the on-surface covalent stabilization have been applied for the synthesis of 0D[18] objects, 1D[19] and 2D[20] polymers and well established chemical reactions could be applied on-surface, for the bottom-up

production of covalent organic frameworks. The ideal stabilization process implies the polymerization of preorganized precursors; however, if the functional groups which are involved in the stabilization networks are also used as reactive groups, possible side-reactions will irreversibly burden the propagation of an on-surface reaction.[21] This is explained by taking into account that precursors are unlikely to collectively diffuse on-surface in a coordinated manner. The more the degrees of freedom, the lower will be the probability that activated or highly reactive species will quench in an ordered fashion, e.g. with high reaction selectivity. On the other hand, defects formation is not a big issue if the reaction is carried out in reversible conditions because the dynamic equilibrium will possibly heal irregularities.[15,22]

Thermally activated reactions for the production of surface supported frameworks were the first tentative approaches in the field of on-surface synthesis.[23,24] As an example, organic halides have been used as precursors in thermally-activated coupling reactions as the carbon-halogen bond is relatively weak, (bond energy: 3.2 eV) compared with the stronger bond between two carbon atoms (bond energy: 4.8 eV).

The thermal activation often poses serious limitations to actual applications of these systems because in general, the resultant structures are intrinsically disordered and irregular. The formation of a covalent bond is an irreversible process that leads to interlinked building blocks which are not able to self-correct morphological defects that may occur during the reaction. Unwanted binding geometries are results of "kinetic trapping" effects, whose minimization is in general a difficult task because many parameters have to be optimized simultaneously. The most fundamental ones are: surface diffusion barriers, adsorption energies, substrate atomic symmetry and chemical nature and reactivity of the precursors.

Photochemical covalent stabilization is part of the expanding field of surface photochemistry.[25–28] The search for nanomaterials with novel structures and functionalities has recently boosted and on-surface

photochemistry resulted as a promising bottom-up approach towards complex molecular architectures.[29–31] New and more ordered types of supported architectures have been created by taking advantage of the fact that photochemical activation can eliminate some of the kinetic bottlenecks observed in thermal activation, e.g. photoinduced reactions can be triggered at lower temperatures than their thermo-induced counterparts.

Despite this field is still at its birth, few examples allowed to lay the groundwork of light-induced on-surface reactions and different synthetic approaches[32,33] led to the covalent stabilization of specific molecular networks[14,34,35] for technological applications in surface nanopatterning[36] and organic electronics.[37]

Among various on-surface covalent coupling reactions, the C-H bond activation towards the C-C bond formation has been tackled experimentally for the production of peculiar covalent assemblies.[38,39] Examples include site-specific coupling of methyl-rich molecules,[40] alkanes coupling,[41] and terminal alkyne homocoupling.[42] Such reactions are highly appealing because of the possibility of tailoring the topology of the resulting product by a proper design of the molecular precursors and - as far as alkynes are concerned, their application in the design of sp- and sp^2-hybridized nanomaterials is envisaged.[19,43–46]

On-surface C-H activation reactions are usually performed on metal substrates and triggered by thermal treatments in Ultra High Vacuum (UHV) conditions. The reaction mechanism on metal substrates, however, remains still an object of debate.[47,48] Alkynes at the metal interface indeed develop a complex on-surface chemistry when thermal energy is provided[47,48] and cyclotrimerizations,[49,50] generation of metal-organic species[51] and oligomers crosslinking[52] usually side a specific reaction.[53]

Few reports outline solutions for this chemical bottleneck and promising approaches for improving the reaction selectivity rely on alternative coupling schemes, as demonstrated by using topochemical

control protocols[54] or by using templating substrates,[41] soft activation methods, i.e. photochemical coupling,[55] or hindering groups close to the reactive centers.[42]

The actual role played by the metallic substrate, essential for the occurrence and propagation of on-surface reactions, or able to stray the C-H bond activation and the intermolecular C-C coupling into a multistep reaction pathway,[48] has never been tackled from an experimental point of view. Herein, the focus is on on-surface syntheses performed directly on metal surfaces and also as a comparison, in metal- and cofactor-free environments such as the solid/liquid interface. The surface of Highly Oriented Pyrolytic Graphite (HOPG) offers an extended board for molecular absorption and self-assembly of properly designed precursors. In this environment, the relatively low absorption energies and the lowering of the desorption barrier provided by the overflowing solvent,[56] allows to directly link the chemical reactivity to the most relevant molecular properties.

In this Thesis it will be shown that the molecular self-organization drives topochemically specific on-surface reactions. In addition, this study shows that once the precursors are thermally or photochemically activated on-surface, the complex recombination chemistry of the starting material and the detection and characterization of the reaction products is strongly affected by the environment in which the reaction takes place. Comparisons with the molecular behavior on metal and non-metal interfaces will be proposed. The necessary molecular resolution for this study has been provided by STM operating both at the solid/air, solid/liquid and UHV interfaces.

THE PH.D. ACTIVITY

During my Ph.D. I have mainly dealt with on-surface syntheses, providing innovative reaction protocols biased by the recent debate on the on-surface reactivity of terminal alkynes. The production of the

acetylene derivatives has been obtained via thermal and photochemical activation of simple molecular precursors under topochemical control and experiments are still running to better understand the behavior of the alkyne groups towards the rational synthesis of extended nano-materials.

Hereby a short summary is reported, including the overall activity and academic outcomes achieved by me during this three-year doctoral course, in the research group of Prof. Mauro Sambi.

1ST YEAR

During the first year of my Ph.D. I have mainly dealt with the commissioning of the newly acquired ambient-STM instrumentation: the Agilent 5500 SPM, i.e. a multipurpose STM and Atomic Force Microscope (AFM / AC-AFM) operating both at the solid/liquid and at the solid/air interface. The preliminary gathering of information and expertise allowed the production of different classes of nanostructured molecules layers, in different environments and from different media.

Additional data analysis of former synchrotron shifts were performed (@ ELETTRA, Trieste, Italy) for the characterization of the on-surface stereo-selective photopolymerization of tetraphenyl-porphyrin derivatives.[35]

As a side-project I participated in the STM characterization of singly and multiply doped graphene oxide quantum dots (GQD)s, which have been proven to be useful metal-free electrocatalysts in oxygen reduction reactions (ORR)s.[57]

2ND YEAR

During the second year of my Ph.D. I have mainly dealt with on-surface structure-reactivity relationships of alkyne compounds and I performed various experimental observations via both the environmental- and the UHV-STM. In particular, the focus has been put on the on-surface

photochemical activation of homo-molecular coupling among phenyl-acetylene derivatives self assembled on non-metallic surfaces.

Additional investigations and side projects have also been performed involving the surface characterization via AFM of various inorganic hereostructures.[58,59] A further insight regarding the possibility to use GQDs as highly efficient water remediation devices has also been investigated.[60]

Different synchrotron shifts (@ ELETTRA, Trieste, Italy) have been performed regarding the characterization of structural and electronic properties of donor-acceptor organic systems[61] and another, regarding a novel quinonic metal-organic frameworks with the XPS/XAS combination (paper in preparation).

3RD YEAR

During the third and last year of my Ph.D. I have finalized the on-surface syntheses and characterization performed via photochemical (and topochemical) activation starting from various alkyne compounds, thus providing an innovative reaction protocol regarding the on-surface reactivity of terminal alkynes.[54]

Further effort has been devoted to the synthesis and characterization via STM and STS of graphene nanoribbons with width-dependent energy gap (@ CIC nanoGUNE, San Sebastian, Spain)

Also, data analysis of former synchrotron shifts has been performed for the conclusive characterization of the structure and electronic features of the novel quinonic metal-organic framework (@ ELETTRA, Trieste, Italy).

METHODS

This section illustrates technical specification and functioning of the instrumentation used in this work. It is fascinating how trustful results can be obtained with such accuracy, by performing analysis on less than a single layer of molecules adsorbed on a surface. The basic laws of physics on which these tools are based are not discussed. For an in-depth description of the different techniques, the extended (and historical) literature can be used to further references.

AMBIENT- AND UHV-SCANNING TUNNELING MICROSCOPY

STM observations were performed at RT in constant current mode with a VT-Omicron (UHV STM) and an Agilent 5500 SPM (solid/liquid solid/air interfaces), equipped with a custom-built liquid cell. Within the latter, vibration insulation occurred by a bungee system enclosed in a sound-dumping chamber. STM tips were mechanically cut from a Pt-Ir (80:20) wire 0.25 mm in diameter. STM data were analyzed with the WSxM software[62] and the topography measurements were background-corrected.

Surface preparation in the case of metals in UHV was performed by repeated cycles of sputtering (1 keV Ar^+) and annealing (approximately 750 K) until a clean surface with sufficiently large terraces was confirmed by STM imaging. In the case of HOPG, the surface was prepared by adhesive tape cleaving.[63] Surfaces cleanness was accurately checked prior to each deposition of the molecule of interest. The deposition for the experiments in UHV were performed by means of a homebuilt effusion cell, while for the experiments at the HOPG surface a modified drop-coating method[64] and the conventional drop-

casting method have been used. For the preparations requiring $CHCl_3$ as the solvent, e.g. measurements at the solid/air interface, the drop-casting of the solution was used and measurements were carried out after the solvent evaporation.

For STM at the solid/liquid interface, the measurements were performed by scanning the solid-liquid interface after putting the non-insulated STM tip directly in 5-20 µL solution housed in the home-built liquid cell. The organic solvents commonly used in the solid/liquid interface experiments are 1,3,5, trichlorobenzene (TCB), 1-heptanoic acid (7COOH), phenyl-octane (Ph8). Their stagnation on the surface has been demonstrated to protect against air contamination and oxygen mediated reactions.[65] Since these are low polarity solvents, many molecules showed low solubility in them. The standard procedure for the preparation of the analysis solutions required the preliminary preparation of a saturated solution of the selected molecule. Then, short cycles of ultrasound bath are applied and the remaining precipitate is separated from the liquid phase via centrifugation. The resulting liquid is then put at rest for a few hours in order to exclude further precipitation of the solute and measurements are eventually carried out directly on these solutions.

SCANNING TUNNELING SPECTROSCOPY

Tunneling spectroscopy measurements (@ CIC nanoGUNE, San Sebastian, Spain) were performed on a custom-made low temperature scanning tunneling microscope, operating at 4.8 K. Lock-in techniques allowed to measure the differential conductance of the junction and to localize the energy alignment of molecular-derived resonances. Spatial maps of the differential conductance at the resonance voltage were drawn with an open feedback loop.

X-RAY PHOTOELECTRON SPECTROSCOPY (XPS)

In-house XPS measurements were performed by using an UHV chamber at a base pressure of $1x10^{-10}$ mbar, equipped with a Scienta M-780 Al Kα (1486.6 eV) monochromatic X-ray source and a Scienta SES-100 photoelectron analyzer fitted to the STM preparation chamber. Complementary experiments and XPS measurements were performed also at the ALOISA beamline[66] (@ ELETTRA, Trieste, Italy) by using a linearly polarized radiation. The spectra were obtained in normal emission geometry and overall XPS resolution of ≈ 0.3eV, by using grazing incident radiation and a home-built hemispherical electron analyzer equipped with a multichannel plate (MCP) detector.

NEAR EDGE X-RAY ABSORPTION FINE STRUCTURE (NEXAFS)

NEXAFS spectra were measured at the ALOISA beamline (@ ELETTRA, Trieste, Italy) in partial electron yield with a channeltron and a negatively biased (−230 V) grid in front of it to reject low-energy secondary electrons. The orientation of the surface with respect to the linearly polarized photon beam was changed by rotating the surface around the beam axis at a constant grazing incidence angle of ≈ 6° The polarization is defined by the orientation of the scattering plane with respect to either the electric or the magnetic field. Transverse electric (TE) polarization corresponds to s-polarization, whereas transverse magnetic (TM) closely corresponds to p-polarization (apart from the grazing angle). The spectra have been energy-calibrated a posteriori by the characteristic absorption signal of the carbon or oxygen K-edge in the I_0 signal (drain current on the last mirror).

LASER SOURCE

The monochromatic light source used in the surface photochemistry experiments was a tunable Nd:YAG laser system NT342A-SH (EKSPLA) equipped with an optical parametric oscillator (OPO). In order to perform irradiation tests at various wavelengths, the unfocused output beam (≈ 6 mm diameter, pulse frequency 30 Hz and pulse width 3.9 ns, output energy at 260nm, the wavelength mostly used in this work, was 1.71 mJ), additionally attenuated with an absorptive neutral density (OD1) filter, has been directed perpendicularly to the sample surface and the overlying solution by means of an Al-coated UV mirror. No temperature increase was detected on the samples during the irradiation. The selected attenuation provided a good balance between non-destructive beam intensity and short time of exposure to prevent atmospheric contamination of the sample and beam-induced heating.

FUNDAMENTALS

This section outlines some basic principles of surface science that are relevant to the understanding of this thesis work. The spatial arrangement of the atoms at the uppermost layer of a solid object, i.e. the surface atoms, determines specific chemical, electronic and mechanical properties of the materials in ways which are unpredictable on the basis of the properties of the bulk.

When a bulk specimen is broken in two pieces, the atoms on the two exposed surfaces suffer dramatic changes in their interactions. The surface separates the bulk from any outer environment and represents a discontinuity in the Bravais lattice of a crystal. It interrupts the translational symmetry in the direction normal to the surface plane, preserving it in the remaining in-plane dimensions. The energy that has been furnished to break interatomic bonds is partially released by means of lattice modifications, typically relaxations and reconstructions, involving from one to several atomic layers from the surface into the bulk.[67] The relaxation is a vertical variation of interplanar distances, e. g. a contraction or an extension with respect to a bulk value in the direction normal to the surface. The reconstruction is the variation of the in-plane periodicity of the surface with respect to the bulk. Additional factors to be considered are intrinsic and extrinsic defectiveness. The former are bulk defects, vacancies and self-adatoms, which are atoms of the substrate diffusing above its surface. The latter may also be purposely created by thermal or mechanical stress during the fabrication, e.g. if a surface is cut along a crystal plane with even a slight misalignment, a regular array of steps is introduced

From an experimental point of view, either the characterization of a surface structure and of a generic interfacial-system requires the use of various and complementary surface analysis techniques and both

theoretical and computational investigations are unquestionably useful to complement the experimental information.

On-Surface Supramolecular Networks

Upon on-surface adsorption, chemical species are allowed to diffuse. The most fundamental of the diffusive processes that may occur is the thermal migration of adsorbed molecules on the substrate terraces i.e. on the flat and uppermost layer of the substrate material. The model for the on-surface diffusion considers thermally activated jumps between adjacent sites in some particular direction.[68] Two adsorption minima are separated by a transition state, which implies that an activation barrier has to be overcome. The barrier is described as a combination of static and dynamic contributions, where the former is the difference in energy between the transition state and the adsorption minimum, while the latter is concerned with the variation in internal energy during the jump.[68]

Particles that lands on a surface (unit for measurements are atoms per unit surface and time), randomly diffuse, encounter each other and possibly aggregate to give dimers or oligomers. As the increasing number of stable synthons becomes comparable with the concentration of the monomers, the probability for a monomer of being captured by an existing cluster approaches the probability of creating new aggregates. When the on-surface density of stable aggregates increases, the mean separation between them is also reduced and becomes comparable to the mean free path of diffusing monomers. This scenario is called “island saturation” and growth occurs after saturation has been reached. Finally, after island coalescence occurs, molecular layers emerge.[68–70] As a general rule, the attachment of existing monomers to already existing aggregates is tailored by temperature and/or deposition rate modulations.[68–70]

The jump frequency ν, related to the diffusion coefficient D and to the number of visited absorption sites per unit time is described by the equation:

$$\nu = \frac{1}{z}\nu_0 exp\left(\frac{-E_{diff}}{kT}\right) \quad (1)$$

where z is the number of possible neighbouring adsorption sites, ν_0 the attempt frequency, a term of the order of 10^{12} s^{-1}, E_{diff} the activation barrier for surface diffusion, k the Boltzmann constant and T the temperature.

A minimalistic model relates the temperature, which affects the diffusion coefficient D, and the deposition flux F to the cluster density at saturation (n_x). This can be either identified with the mean island distance or, equivalently, with the mean free path of diffusing particles:

$$n_x = \eta(\Theta, i)\left(\frac{D}{F}\right)^{-\chi} exp\left[\frac{E_i}{(i+2)kT}\right] \quad \text{where} \quad \chi = \frac{i}{i+2} \quad (2)$$

in (2), $\eta(\Theta,i)$ is a pre-exponential numerical factors, which vary between 10^{-2} and 10 depending on the nature of aggregating species,[71] i denotes the critical cluster size and E_i the cluster binding energy. This model gives indications on the mean island density and size attained at saturation. In turn, the dependence of the saturation cluster density over a temperature interval gives information on the activation barrier E_{diff}.

On-surface self-assembly is unmistakably complicated by the presence of the substrate and by the role of the medium from which molecules are adsorbed onto. Both play a crucial role in the process, but the underlying substrates can direct the self-assembly by forcing molecules to retain particular packing configuration. As a result, long-range pattern organization is guided into epitaxial layers even if weak interactions between the adsorbed molecules and the substrate are

present.[72] The tendency of 2D molecular layer to comply with the local registry of a surface have revealed, experimentally and theoretically, significant changes in intermolecular parameters when compared to their three-dimensional counterparts.

A wise exploitation of the directing factors imposed by the registry requirements between molecules and substrate can actually advantage the fine-tuning of 2D self-assemblies since different substrates can be used to obtain different templating effects.[73]

When, on the other hand, the interactions that favour the epitaxial growth are overcome by intermolecular interactions, it is possible to obtain molecular self-assembly with less or no registry relationship with the underlying substrate. This phenomenon allows one to obtain an effective electronic decoupling between the supramolecular adlayer and the substrate,[74] and more favourable intermolecular interactions are obtained either by passivating or by introducing insulating layers on surface.[75,76] Ultimately, when intermolecular interactions prevail over molecule-substrate interactions, the medium may also affect the resulting molecular organization,[77,78] indeed it determines the deposition conditions and related thermodynamic or kinetic parameters of the self-assembly process. The case of the solid/liquid interface is thoroughly investigated, but insights are still lacking and are limited to direct experimental observations.

A wide range of atomically-flat metal surfaces are available under UHV, but obvious limitations do not allow to keep them stable under ambient conditions or in liquid environments. More inert material however exists, such as HOPG, Au(111), MoS_2 and $MoSe_2$, which demonstrated to perform well for numerous STM studies of on-surface physisorbed monolayers,[79,80] possibly allowing a comparison between UHV and environmental conditions.

STRUCTURE AND DYNAMICS OF 2D AGGREGATES

Surfaces serve as preferred binding sites for physically or chemically interacting particles. If such interfacial systems undergo chemical reactions, their dynamical behavior affects in turn the reaction outcomes. The study of on-surface dynamics is important in order to better understand the chemical reactions that occur at the solid/vacuum or solid/liquid interfaces.

The concept of lateral or rotational mobility of molecules adsorbed on-surface and of bare-surface dynamics are mostly described as a function of temperature and adsorbates that are commonly investigated span from small molecules with simple adsorption configurations to large organic molecules with additional internal degrees of freedom which need to be considered. Dynamics phenomena confined on-surface occur at characteristic timescales.

Bare surfaces are generally characterized by fast motions of surface atoms, which are thermally activated, and their imaging via STM emerge as time-averaged features in different temperature ranges.[81–83] Self-adatom and adsorbate diffusion are other phenomena that occur at intermediate timescales[84] and may in some cases be a sufficiently slow process to afford its study by collecting consecutive STM frames, lines or points over the same region.[85–87]

The common aspect that influences the on-surface molecular motion is the adsorption strength with the substrate. Molecules are subject to attractive interactions in the vicinity of a surface. In case of physisorption, molecules are bound to the surface by weak interactions, while adsorption energy is increased upon chemisorption, where chemical bonds between the molecule and the surface atoms are formed.

Irrespective of the environment, self-assembled monolayers (SAM) are differentiated in physisorbed and chemisorbed systems.[88] The former include weak interaction with the substrate, typically in the range 20-

25 kJ/mol, which is reversible and tunable e.g. by changing the temperature. The latter involve covalent bonds and commonly the directionality of the chemical bonds between molecules and the substrate atoms dictate the periodicity of a 2D crystalline domains.[89] Within a physisorbed system, most of the stabilization energy of a SAM is provided either by weak and cumulative intermolecular interactions.

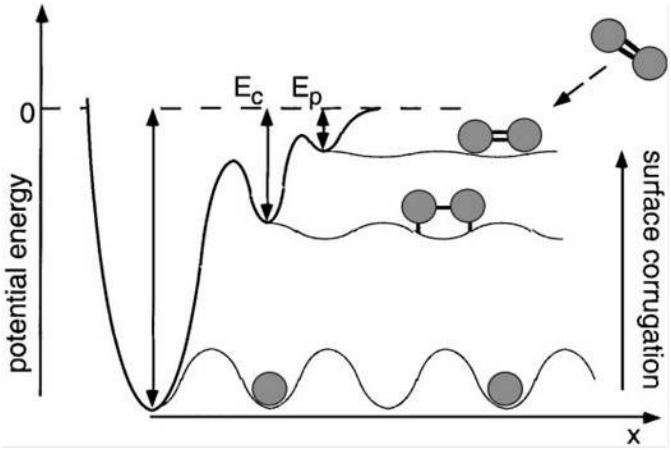

Figure 1. One-dimensional energy diagram for a diatomic molecular precursor with physisorbed, chemisorbed molecular and chemisorbed atomic state. potential energy barriers referred to the surface corrugation are expected to vary for the respective states as indicated. picture from ref. 84

Further stabilizations are possible in exothermic dissociative chemisorption, where intermolecular bonds break and dissociation products bond to the surface atoms. However, chemical bond formation or dissociative adsorption at a surface can be suppressed by a reduction of the substrate temperature. In the simple case of a diatomic chemisorbed precursor that comes to equilibrium with the substrate at low temperature, a sudden temperature increase may allow an exothermic bond scission and the released chemisorption energy may be transferred as kinetic energy to the evolving atoms. [84] In a one-dimensional energy diagram, this behavior contemplates energy barriers between molecular physisorption and dissociative

chemisorption, as illustrated in Figure 1. Such energy barriers indicate that molecules may experience transient stages of physisorbed state prior to chemisorption and molecular chemisorption prior to dissociation. These transiently physisorbed or chemisorbed molecules are commonly called precursors.[84]

The adsorbing molecules are said to have "hyperthermal"[90] energies prior to their stabilization in an energy minimum and an efficient lateral transport of hyperthermal species on-surface can be envisaged whenever the energy dissipation in physisorption or chemisorption is mediated by the molecular coupling to the substrate phonon bath or by formation of electron-hole pair couples.[91–93] The time evolution of molecular adsorption implies the dissipation of the released binding energy with the substrate; however, a one-dimensional problem may be inaccurate in case of absorption of organic molecules, due to the molecular degrees of freedom and the non-unique physisorbed or chemisorbed states that emerge from different configurations, e.g. an organic adsorbate considering the many possible combinations of binding sites and molecular orientations.[94]

Interesting consequences arise for on-surface chemical reactions from transient molecular mobility, i.e. the lateral motion of molecules (or atoms) in metastable states or in the process of thermalization at a surface. Transient mobility, indeed, may allow adsorbed species to attain reaction sites or reaction partners on a surface, and "hot" precursors may overcome energy barriers for reaction pathways that otherwise cannot be attained under equilibrium conditions.[95,96]

Theoretical studies for on-surface mobility phenomena employ molecular dynamics simulations[97,98] and the overall agreement is that the typical timescale for the thermalization is in the picosecond range.

After adsorption the atoms may diffuse along the surface for tens of nanometres before the equilibration of their tangential momentum and eventually, on-surface aggregation occurs when the intermolecular and molecule-to-substrate interactions are properly balanced. Molecules

that are not statically immobilized on the substrate and are free to diffuse achieve a 2D ordering driven by intermolecular interactions.
By far, on-surface dynamics are roughly referred to the colloidal chemistry theories and molecular properties are directly obtained if weak absorption strengths preserve the molecular electronic states.[99,100]

DYNAMIC COVALENT CONTROL: THE CASE OF A STEREOSELECTIVE PHOTOPOLYMERIZATION

Hereafter the study regarding the on-surface polymerization of a tetra-phenyl porphyrin derivative, namely 5,15-bis(4-aminophenyl)-10,20-diphenylporphyrin ($TPP(NH_2)_2$) on the Ag(110) surface is reported. More precisely, it is proven that a light stimulus can be used to trigger an intermolecular reaction and the results reveal that the reaction proceeds via the formation of azo-bridges (-TPP-N=N-TPP-) between the molecular building blocks. The initiation of the light-induced reaction was carefully controlled by modulating surface mobility with temperature. This study represents a step forward in the application of organic photochemistry to on-surface synthesis, and also represented a personal and solid base to start with further on-surface photochemical investigations. This work was published at the beginning of my Ph.D. program. My contribution has been given both as an undergraduate and an early Ph.D. student. It represents a proof on how the relationship between molecular surface mobility, chemical reactivity and temperature can be modulated for activating a polymerization reaction.

The lateral mobility of isolated molecules is routinely observed in UHV whenever experiments at low temperatures (< 100K) are performed. $TPP(NH_2)_2$ molecules are functionalized with aniline functional groups in para-positions at two meso phenyl rings. As shown in Figure 2a, they

are almost motionless and randomly disperse when their molecular vapors condense on the Ag surface held at low temperature (@ 100 K). By increasing the substrate temperature (195–230 K Figure 2b, c), they start aggregating in disordered small clusters, owing to a higher mobility, that eventually lead to a close-packed monomeric self-assembled configuration by proceeding with a temperature ramp towards room temperature (RT, Figure 2d). This particular aggregation phase is extensively described elsewhere.[61,101]

Interestingly, within the highly dispersed system at low T, by irradiating the sample at 405 nm during a linear heating ramp up to RT (approximately 12 h), the formation of a new superstructure could be observed. This phenomenon could be observed only in the submonolayer regime, since for a higher starting coverage the reaction did not occur and the oblique close-packed porphyrin self-assembly structure of Figure 2d developed. As a proof for the light-induced coupling, if molecules at 100 K are heated to RT in the dark, they organize into the oblique structure.

Within the extended photo-polymerized phase, the 2D overlayer lattice emerges with a lower density (0.37 nm^{-2}) than in the self-assembled phase (0.44 nm^{-2}). As observed for analogous self-organized structures of the TPP derivatives, the driving-force generating the close packed structures obtained by self-assembly, is the T interaction between meso-phenyl rings.[102,103] The peculiar arrangement of the photoinduced superstructure does not show such a close packed intermolecular configurations, hence, stronger interactions between the precursors have been proposed: covalent bonds.

Several photochemical studies show that photodissociation processes are directly activated on aniline in the gas phase[104] and absorption of light by metallic substrates produces a hot electron distribution[105,106] able to populate molecular empty states and possibly activate covalent bonds homolysis. The hypothesized reaction scheme, therefore, involves the N-H photodissociation of the *trans*-TPP(NH_2)$_2$ and a

recombination into an azo-bonds among close aniline functional groups (Ph-N=N-Ph). DFT simulations and XPS measurements[35] eventually confirmed that an N=N bond between porphyrin units occurs, affording a photodissociation of the N-H bond on the *trans*-TPP(NH_2)$_2$.

In conclusion, evidences demonstrate that light is able to induce reactions that would otherwise not occur. The growth of the new phase was obtained under dynamic control approach and by exploiting on-surface radical photodissociation towards covalent stabilization, an ordered and stable polymeric aggregate was obtained. A protocol for stereoselective photopolymerization under dynamic covalent control was eventually established.[107]

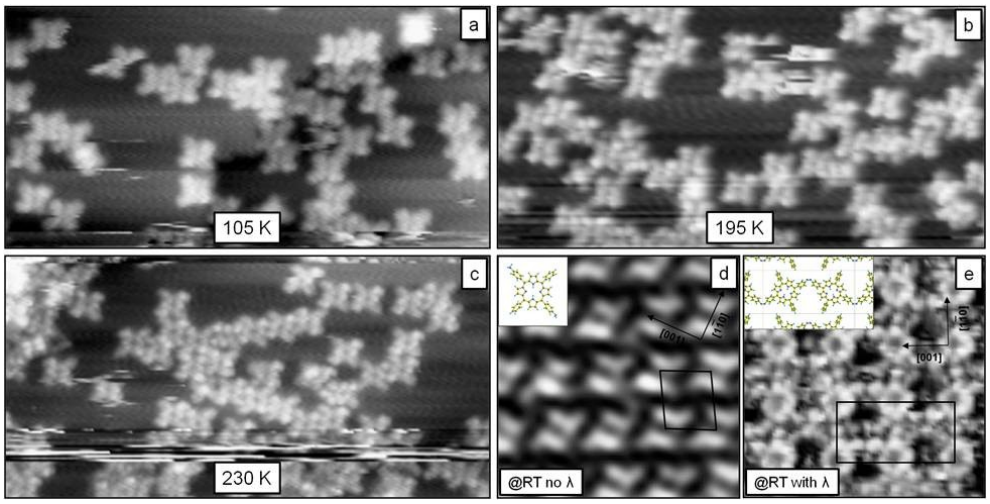

Figure 2. (a) 5,15-bis(4-aminophenyl)-10,20–diphenylporphyrin (TPP) deposited on the Ag(110) substrate held at 105 K. (b) TPP on the Ag (110) surface during the heating ramp. The surface is at 195 K. (c) TPP on the Ag (110) surface during the heating ramp. The surface is at 230 K. Lateral order of TPP is occasionally found. (d) close-packed TPP domains at RT on Ag(110). Ball and stick model, unit cell determination and main direction of the substrate are also reported. (e) covalently linked TPP domains at RT on Ag(110) after UV irradiation protracted during the heating ramp. Ball and stick model, unit cell determination and main direction of the substrate are also reported.

DYNAMERS

Alongside with lateral mobility, rotary motion of molecules is also frequently observed. Molecular rotors and motors have been thoroughly studied recently for their potential application in molecular electronic devices and exist as stand-alone units or as networks in which the rotor is confined into a static cavity.[108–113]

Remarkable is the case of 4,4′-(propane-2,2-diyl)diphenol (BPA), studied by Lloyd et al., which generates a monocomponent phase in which a periodic array of trimeric-rotors are included in a grid of hexagonally arranged trimeric-stator units on the weakly corrugated phase of Ag(111).[108] The switching of the aggregates between metastable positions by an azimuthal rotation movement is attributed to an instability caused by the strain induced by the surrounding molecular matrix, that forces the rotors into non-ideal adsorption sites.

In addition to excess SAM precursors trapped into monocomponent phases, other guest molecules can be also captured into a "dominant" porous SAM and undergo thermally activated azimuthal rotation. Briefly, nanoporous networks are a special class of 2D networks that expose surface sites through their nanometric voids while decorating a surface.[114] These systems are generally interconnected by weak and reversible supramolecular interactions and easily demonstrate their dynamic behavior through self-repair. They also result very useful in host-guest trapping experiments.[115] Guests molecules, which maintain a degree of motion when trapped in the voids of the network, are recognized as dynamers and exist both in UHV,[116] where their motion can be easily modulated by temperature, and at the solid/liquid interface.

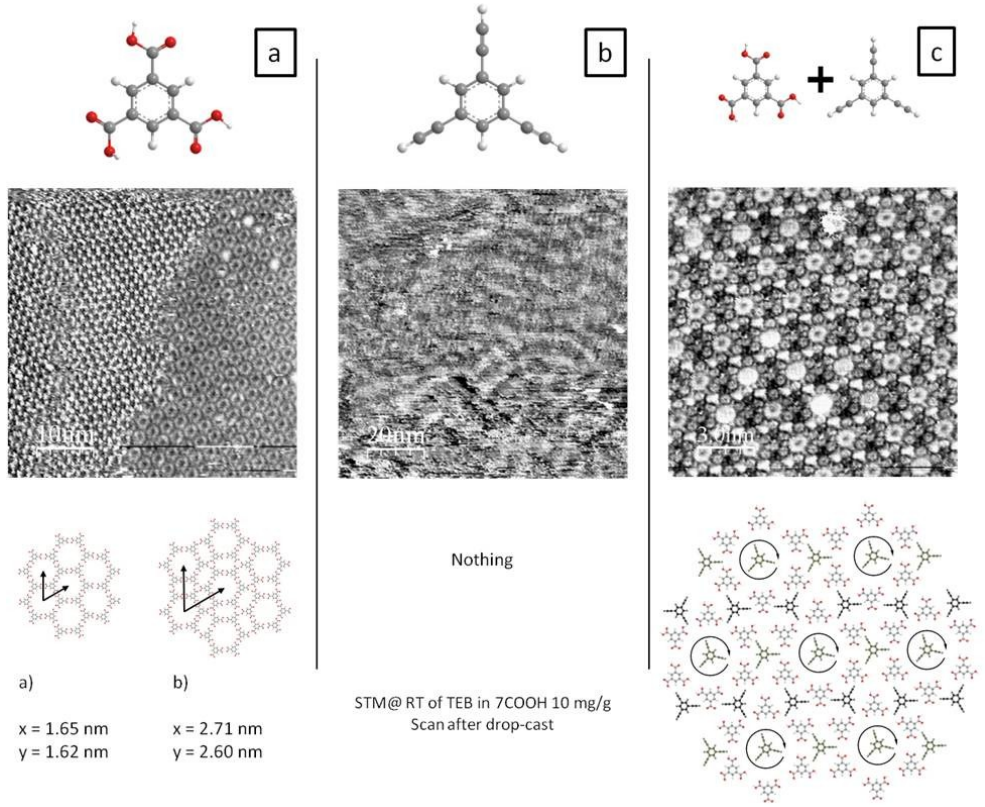

Figure 3. From top to bottom (a) ball and stick model of TMA, STM images of the well-known ordered TMA porous superstructures[78,100,118,119] and unit cell parameters for both the aggregation phases. (b) ball and stick model of TEB, on-surface aggregation is missing from STM images of the solid/liquid interface after the drop cast of a solution of TEB in 7COOH. (c) combination of TMA and TEB solution produced a novel co-crystal superstructure (middle) in which TEB molecules are trapped within the dominant TMA "flower" superstructure. A tentative model is reported in the bottom.

In Figure 3, a panel is shown for an in-house experimental observation, in which benzene-1 3 5-tricarboxylic acid (TMA, Figure 3a) acts as the host for 1,3,5-triethynylbenzene guest molecules (TEB, Figure 3b). TEB molecules are recognized as a versatile ingredient for the rational design of carbon scaffolds distinct from graphene.[117] The experiment has been performed at the solid/liquid interface (HOPG/7COOH) and at this interface TEB molecules alone are characterized by high on-surface diffusivity. Their imaging is impossible and only the TMA and TEB co-deposition resulted in an ordered co-crystal (Figure 3c) where TEB

molecules are the guests. In particular, within the TMA superstructure, TEB molecules are identified either as static units and as dynamers. The former are identified in Figure 3 as the bright features, intercalated within the "flower" structure of TMA; the latter appear as ring-like features, or bulges which owing to their azimuthal rotation, correspond to the convolution of the most stable configurations of the guest inside the pores, i.e. at RT their motion is faster than the scanning time regimes. A molecular ball-and-stick model is proposed for the host-guest structure of TMA and TEB (Figure 3c) as superposition of the molecular models with the STM images.

The co-crystal may in the future represent an opportunity for studies regarding acetylene derivatives and acetylenic coupling at interfaces, as sequential protocol with monolayer self-assembly and further crosslinking step provided encouraging results.[120]

Different dynamic phenomena are generally observed to originate at domain boundaries – not surprisingly, as these are typically regions with lower stability and enhanced dynamics.[121] Dynamic phenomena at the solid/liquid interface observed in-situ involve many variables that operate simultaneously.[122] Conformational dynamics of individual molecules within self-assembled monolayer occurs spontaneously, either in combination or as a result of heat, light treatment or by perturbations induced by the STM tip. The evolution towards the equilibrium state involves also island growth, phase transitions and coarsening, i.e. an increase in the characteristic dimensions of dominant structures, generally referred as self-healing.[123] These phenomena are routinely observed at RT, as the supernatant liquid environment easily influences the adlayer dynamics. Solvent properties and solute concentration as well as phase equilibria that occur in solution i.e. adsorption-desorption and dispersion-aggregation also strongly influence the molecular behavior at the interface.[124,125] The ability to perform tailored molecular processes is obtained with a careful control over these parameters.

TWO DIMENSIONAL CRYSTALS

Hereafter a survey on the structure and the driving forces for the formation of various 2D crystals is proposed. The focus is put on SAMs stabilized by hydrogen-bonds and metal-organic coordination. In addition to remarkable literature examples, selected examples of the results obtained during my Ph.D. program are proposed. They concern the preliminary results of the structure and reactivity of a phenyl-acetylene derivatives and a metal-organic framework. For the latter, an example regarding the formation of copper tetrameric units embedded in an on-surface metal-organic structure will be proposed. This experiment has been performed in collaboration with the University "La Sapienza" of Rome and with the King's College, Physics Department, London. In order to obtain a deep understanding of this system, multiple techniques have been employed (STM, LEED, XPS, NEXAFS, DFT) and a thorough joint effort from different researchers was required. My personal effort was put in the set-up of the experiment at the ALOISA beamline (@ ELETTRA, Trieste, Italy) in order to obtain information on the electronic structure of this promising tetrameric metal-organic structure by using synchrotron radiation techniques (NEXAFS/XPS).

SELF-ASSEMBLED MONOLAYERS

Among the possible intermolecular interactions exploited for the production of the majority of self-assembled monolayers, hydrogen-bonding and metal-ligand coordination are the interactions of choice as they are relatively strong and highly directional.[7] Organic building blocks generating ordered and dense molecular layers cover the range from small molecules adopting simple configurations to large organic

molecules, possibly flexible and with several internal degrees of freedom. Even simple molecules, which display phenyl rings cores, introduce degrees of freedom for the assembly phenomena such as the tilt of the backbone with respect to the surface normal, as well as the twist angle between adjacent building blocks need to be considered. [126]

HYDROGEN BOND INTERACTIONS

Benzoic acid (BA), phthalic acid (PA), isophthalic acid (ISA), terephthalic acid (TA) and trimesic acid (TMA) are classic example and simple cases of small organic molecules containing a progressively increasing number of carboxylic acid groups which act at the same time as donors and acceptors of highly directional hydrogen-bonds (HB). They are capable of generating a great variety of stable superstructures, with HB synthons of various symmetry and shape that aggregate in 1D and 2D motifs.[127–129] It is worth to point out that HBs also arise among other classes of functional groups,[130] e.g. alkynes.[49]

HB interactions provide extraordinary connectivity in various supramolecular aggregates and BA doubtless represent the archetypal unit. BA and BA-derived molecules posses only one carboxylic functionality and hardly self assemble because of such a reduced degree of functionalization. Indeed, a limited number of works are devoted to the interfacial behavior of BA. This molecule was mainly studied in electrochemical environments and various examples report its bias-dependent absorption geometry.[131–135] PA possesses two carboxylic functionalities, but its sterically hindered planarity prevents the stabilization of 2D networks. Yet, ISA and TA provide examples[136] of densely packed monolayers in which the molecular organization is dominated by various 1D HB chains, viz. “catemers”.[137] Finally, TMA is the textbook example of a 3-fold symmetry molecules with carboxylic acid functionality, that allows the formation of close packed and

honeycomb networks of fused cyclic hexamer arrays,[138] among other polymorphs.[139]

Within 2D crystals, HBs among mono-carboxylic species can be exploited to dictate the absorption geometry of molecular units[140,141] and, if any, the reciprocal positioning of other functional groups of the same precursor.[142–144] Recently, the interfacial behavior of BA on Au(100) was reported, providing information about structural transitions in an electrochemical environment.[129] In this case, it was observed that various 2D crystallographic phases, including similar to those formed by BA in the bulk,[145] could be stabilized. The key factors for the formation of ordered and flat-lying adlayers have been related to intermolecular interactions based on HB and weaker van der Waals interactions between phenyl rings. Interestingly, substrate-molecule interactions were predominant only following a bias-induced deprotonation. In the case of BA on the more reactive surface of Cu(110),[146] temperature dependent structural features and a phase variation were observed. In this case, the building blocks undergo deprotonation induced by the metal support even at low temperatures (120-170 K) and in turn change their bonding motifs.

An in-house investigation on the behavior of a BA-derivative, namely 4-ethynil benzoic acid (PEBA, Figure 4 a), on Ag(111) provides further proofs on the directing role of the carboxylic HB.

PEBA molecules are small π-systems, hetero-functionalized with an ethynyl end-group and a carboxylic group pointing apart on a benzene ring. The stabilization of molecular phases of mono-carboxylic species is generally hampered by high on-surface diffusivity, nonetheless, PEBA arranged in ordered clusters at RT on Ag(111), maintaining intact molecular features. Core level XPS measurements in the C 1s region (Figure 4b) confirm this assumption by providing predominantly the signal of an intact PEBA molecule.

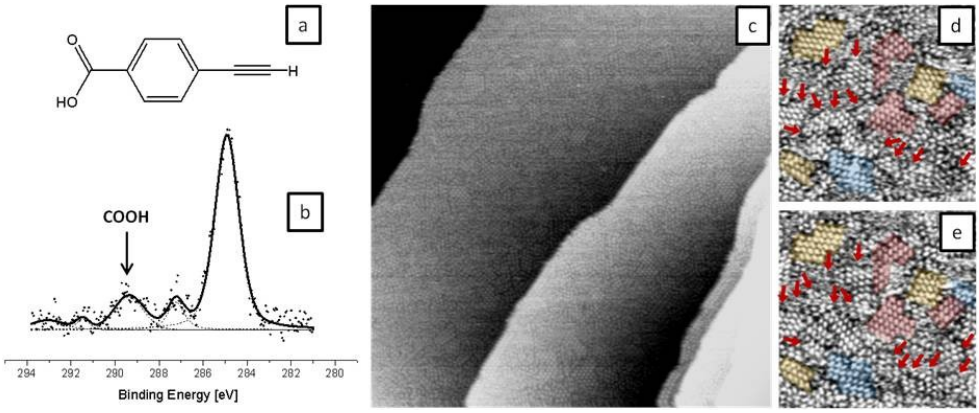

Figure 4. (a) Molecular structure of PEBA. (b) Al Kα excited c 1s XPS spectrum for PEBA on Ag(111) at RT. Intensity is reported in arbitrary units. (c) large scale STM image (100 nm × 100 nm) obtained at RT after the deposition of PEBA on Ag(111). Surface coverage is < 30%. (d) close-up STM image of figure c, (50 nm × 50 nm). Different orientations of PEBA domains have been highlighted with three different colors. Red arrows are pinpoints for the comparison of molecular features over successive frames. (e) close-up STM image, successive to the frame in figure d over the same area, (50 nm × 50 nm). Red arrows are in different positions with respect to the former frame and highlight dynamic changes that occurred on-surface.

A clear signature of phenyl-acetylene[147] and the protonated carboxylic group[148] are observed at 284.9 eV, i.e. the main peak with unresolved components, and 289.4 eV respectively. Corresponding shake-up satellite structures, due to π*←π excitations at the benzene ring emerge at 291.4 and 293.2. The peak at 287.2 could not be attributed to any functional group. The latter is common in analogous systems and is attributed to a partial oxidation of the monolayer[149,150] but may also be referred to CO absorption occurring during the deposition.[151] Figure 4c show a large area STM image obtained after dosing PEBA on Ag(111). Terrace decoration suggests that molecules diffuse freely at RT and preferentially saturate the step edges before nucleating on terraces. Relatively stable clusters also appear, within images dominated by streaks along the horizontal-scan direction. Streaks are attributed to single molecules or dimers, which diffuse under the field of the tip. Figures 4d and e are two successive close-up scans over the same area. Immobile clusters (rendered with different colors, accounting for the

orientation of the precursors) are actually observed from the comparison of the images. In addition, the highly fuzzy background and the variation of numerous features (highlighted with red arrows) suggest a high diffusion rate of single molecules or dimers at RT. Within the clusters, each bright feature measures 9.5 Å along its long axis, and is attributed to a single molecule.

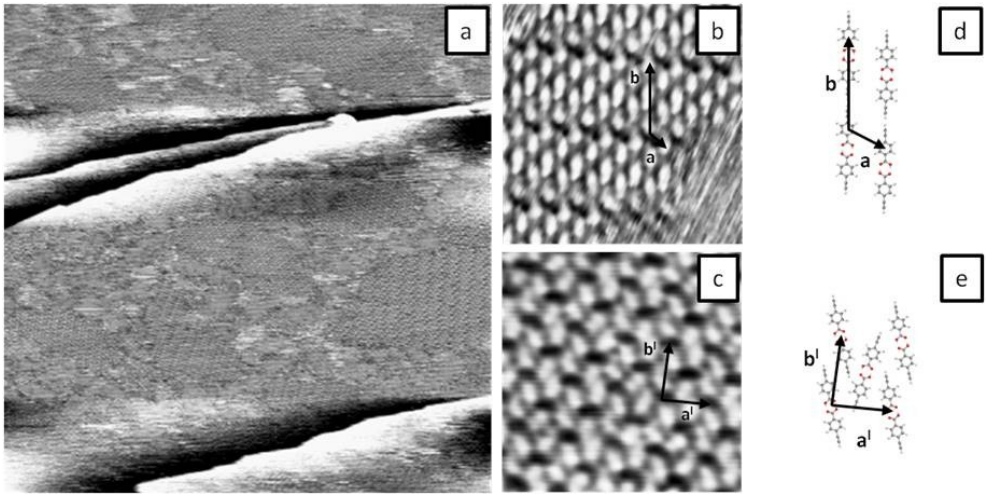

Figure 5. (a) Large scale STM image (100 nm × 100 nm) obtained at RT after the deposition of PEBA on Ag(111). Surface coverage is >50%. (b) close-up STM image of one aggregation phase of PEBA on Ag(111), (10 nm × 10 nm). Unit vectors a, b are superimposed as black arrows. (c) close-up STM image of another aggregation phase of PEBA on Ag(111), (10 nm × 10 nm). Unit vectors a, b are superimposed as black arrows. (d) tentative model of the unit cell of PEBA on Ag(111) for the aggregation phase reported in figure (b). (e) tentative model of the unit cell of PEBA on Ag(111) for the aggregation phase reported in figure (c).

At higher coverage surface diffusion was suppressed and distinct 2D crystalline domains were detected. The hetero-functionalization necessarily provided additional complicating factors and presumably the formation of different network was favored by a large number of local minima in the potential energy landscape that arise at the Ag(111)/PEBA interface. Noteworthy the interaction of alkynes with metal substrates is not negligible,[47] therefore the participation of the

substrates in the stabilization of the observed phases could not be excluded. In Figure 5a it is possible to observe two of the main assembly motifs observed on-surface, in a large scale STM image and reported as close-up images in Figure 5b and c. The phase reported in Figure 5b is described by unit vectors a = 2.12 ± 0.05 nm, b = 0.90 ± 0.05 and an angle α= 124 ± 2° between them. A tentative molecular model for this phase is reported in Figure 5d.

In analogy with similar sp^2 hybridized organic moieties, these systems have been recently described by means of a particular kind of intermolecular interaction, namely proton acceptor ring interaction (PARI).[152]

Major contributions to the stabilization energy originate from the whole electronic cloud of the ring and also part of the binding strength is related to the remote half of the benzene moiety, not directly involved in the carboxylic HB interaction. Alkyne groups provide additional stabilizing interactions, which are referred to as intermolecular hydrogen bonds as well. Parallel ethynyl groups are involved in a two-fold cyclic HB (C≡C–H•••C≡C) wherein the acidic hydrogen acts as a donor and the aromatic triple bond as an acceptor for hydrogen bonds. Additional interactions may occur among nearest neighbor aromatic systems.[49,130] Noteworthy, within this phase the molecular configuration is similar to what observed for the same molecule on HOPG,[54] even if the unit cell parameters are substantially different. This is reasonably due to a different accommodation on the underlying metal substrate, obtained as a consequence of a higher degree of interaction between PEBA and the metallic surface.[47]

The phase reported in Figure 5c is structurally similar to that of PEBA in the bulk[153] and is reproduced by unit vectors a = 1.96 ± 0.05 nm, b = 2.16 ± 0.05 and an angle α= 85 ± 1° between them. A tentative molecular model for this phase is reported in Figure 5e. It is characterized by an alternating dimers structure, in which the units are held by HBs among the carboxylate groups and a further “T-shaped”

weak C-H···π interaction among each end of the carboxylate dimer with the phenyl rings of nearest neighbor molecules.

Self-Assembled Monolayers Stabilized by Metal-Organic Interactions

Metals, especially d-block transition metals, afford the production of a large variety of 2D aggregates when they are coordinated to organic ligands. Their stoichiometry, strength and reversibility of binding are in principle modulated by means of a rational design of the building blocks, so that it is even possible to predict the bonding motif of 2D metal organic coordination networks (MOCN)s. MOCNs directly assemble on-surface at the solid/liquid interface and different examples of metal complexation at single ligand sites,[154] coordination polymers[155,156] and grid-like structures[157] are proposed in the literature. However, most of these studies are devoted to MOCNs in UHV conditions, as the medium-free environment grants the chemical stability of metal-ligand complexes.

A MOCN is generally obtained by performing thermal treatments on molecules containing carboxylic functionalities. In this case deprotonation occurs[158,159] and, in turn, carboxylates have the ability to establish coordination with metal centres. The latter can either be evaporated on-surface[160] or they can be directly included in a preformed molecular layer after they are extracted from the underlying substrates.[20]

As an example, within the experiment of Tseng et al.[161] the co-deposition of 7,7,8,8-tetracyanoquinodimethane (TCNQ) and Mn on the Cu(100) self-assembled in a 2D MOCNs. A long-range ordered square superstructure consisting of fourfold coordinated Mn centers with a Mn:TCNQ ratio of 1:2 was obtained. TCNQ coordinates to the substrate Cu atoms and with Mn adatoms by exploiting its two antipodal functional groups. By comparison of the XPS spectra of the powder

against the on-surface TCNQ aggregate, the authors demonstrated that the TCNQ acquired a significant negative charge following its absorption on Cu. Then, after dosing and embedding Mn atoms, the XPS signature of TCNQs MOCN remains unchanged. This is consistent with CN groups maintaining their full electron acceptor potential upon their coordination to Mn, despite a quenching of its electron acceptor capabilities would be bestowed. Finally it was proposed that Mn atoms are in a quasi-Mn^{2+} state and their role as independent magnetic centers was envisaged.

Copper Tetrameric Units Embedded in an On-Surface Metal-Organic Structure

Tetrahydroxyquinone (THQ) molecules (Figure 6a) offers a clear example of a multiple and long-range metal atom embedding of self-assembled on-surface metal-organic structure on the Cu(111) surfaces.

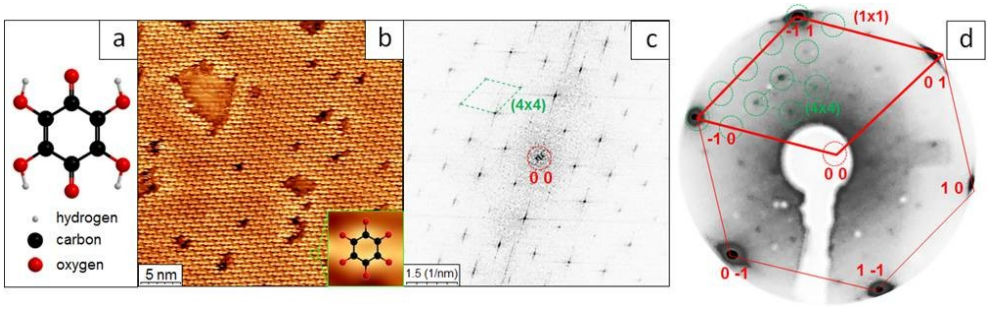

Figure 6. (a) Ball and stick model of the THQ molecule. (b) large scale STM image showing the self-assembly of TOQ molecules on Cu(111) after annealing to 383 K and TOQ anion shown in the bottom right corner. (c) corresponding Fast Fourier Transform (FFT) image and (d) low energy electron diffraction pattern acquired at an energy of 45 eV on the same sample. These data have been collected at the university of Padova in a collaboration project. Credits go to Matteo lo Cicero, Maria Gazia Betti, Carlo Mariani, Dipartimento di Chimica and Dipartimento di Fisica, Università di Roma "La Sapienza", Roma (Italy).

Within the following in-house experiment it was observed that THQ molecules, generate long range ordered islands (Figure 6b, c), upon annealing (@ 383 K), characterized by a 4x4 periodicity, as revealed by the combinations of STM and Low Energy Electron Diffraction (LEED) techniques (Figure 6d). In this phase, individual molecular units appear in the STM images as bright protrusions, with dimensions compatible with a single molecule. The homogeneity in their electronic features points toward a flat adsorption geometry of the molecule.

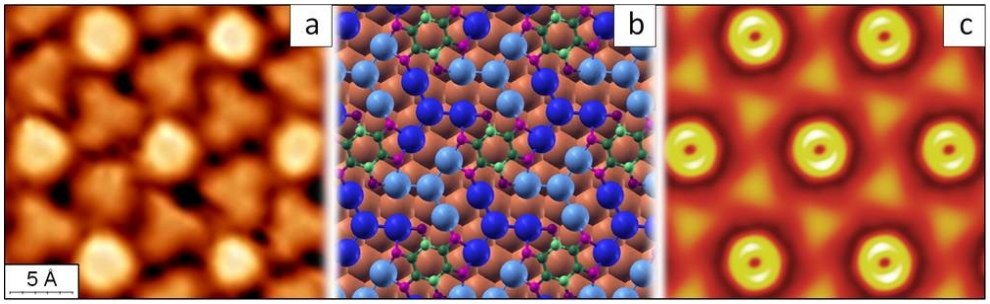

Figure 7. (a) STM image, (b) corresponding DFT calculated structure and (c) simulated STM image at 0.55 V obtained by using the Tersoff-Hammann approach[162] of the metal-organic network formed by TOQ on Cu(111) after an annealing to 383 K. Cu adatoms are represented as light and dark blue spheres in (b) for a better visualization of the copper tetramers, while TOQ anions are colored accordingly to XPS fitting (see below). The computed cell with parameters 10.22 Å is compatible with the experimental one observed by LEED and STM. These data have been collected at the university of Padova in a collaboration project. Credits for the stm image go to Matteo lo Cicero, Maria Gazia Betti, Carlo Mariani, Dipartimento di Chimica and Dipartimento di Fisica, Università di Roma "La Sapienza", Roma (Italy). Credits for the DFT simulations go to Massimo Riello and Alessandro de Vita, Physics Department, King's College, Strand, London (UK).

From high-resolution STM images, additional triangular features are observed between the THQ units (Figure 7a). These features are related to thermally released copper adatoms incorporated in a metal-organic network of 2,3,5,6-tetraoxyquinone tetra-anion (TOQ) units, after quadruple dehydrogenation of THQ, promoted by the annealing. In addition, the azimuthal orientation of the MOCN determines the

formation of two different chiral assemblies, with mirror-like mutual orientation.

DFT was used to model the system and the best THQ:$Cu_{(adatom)}$ ratio was 1:8, i.e. one radical and two Cu tetramers per unit cell, (see Figure 7b). Simulations corroborate that Cu adatoms generate a triangular-shaped tetrameric clusters with a central Cu adatom not interacting with the organic medium. Within each cluster, the triangular objects represent the tetrameric Cu clusters, while the bright doughnut-like protrusion correspond to the TOQ radical moieties (see Figure 7c).

The dehydrogenation of THQ molecules upon annealing is confirmed by high-resolution core-level spectroscopy measurements, performed before (Figure 8a, b) and after annealing (Figure 8c, d). At RT, the O_{1s} spectra display three peaks, at 530.29 eV, 530.68 eV and 532.49 eV. The component at 532.49 eV is associated to O-H oxygen, while the other two to C=O groups pointing towards and far from the surface, respectively.[163–165] Accordingly, the C 1s core level of as-deposited THQ molecules shows three contributions at 285.27 eV, 284.76 and 284.35 eV, corresponding to C-O-H (former peak) and C=O (latter peaks) carbon, respectively,[165] plus the shake-up peaks.

Upon annealing to 383 K, both O_{1s} and C_{1s} core level peaks change drastically (Figure 8). In particular, the peak associated with O-H, O_{1s} signal, disappears almost completely, as THQ undergoes dehydrogenation. Two main components appear in the spectrum at energies 530.36 eV and 531.16 eV (Figure 9c). The peak at 530.36 eV corresponds to oxygen atoms bound to two copper adatoms, while the peak corresponding to oxygen bound to one copper adatom appears at higher binding energy. The C_{1s} peak is characterized by an intense component at 284.87 eV, is associated to the C[-] atoms, and a second one at 284.16 eV, corresponds to the two equatorial C[+] atoms.

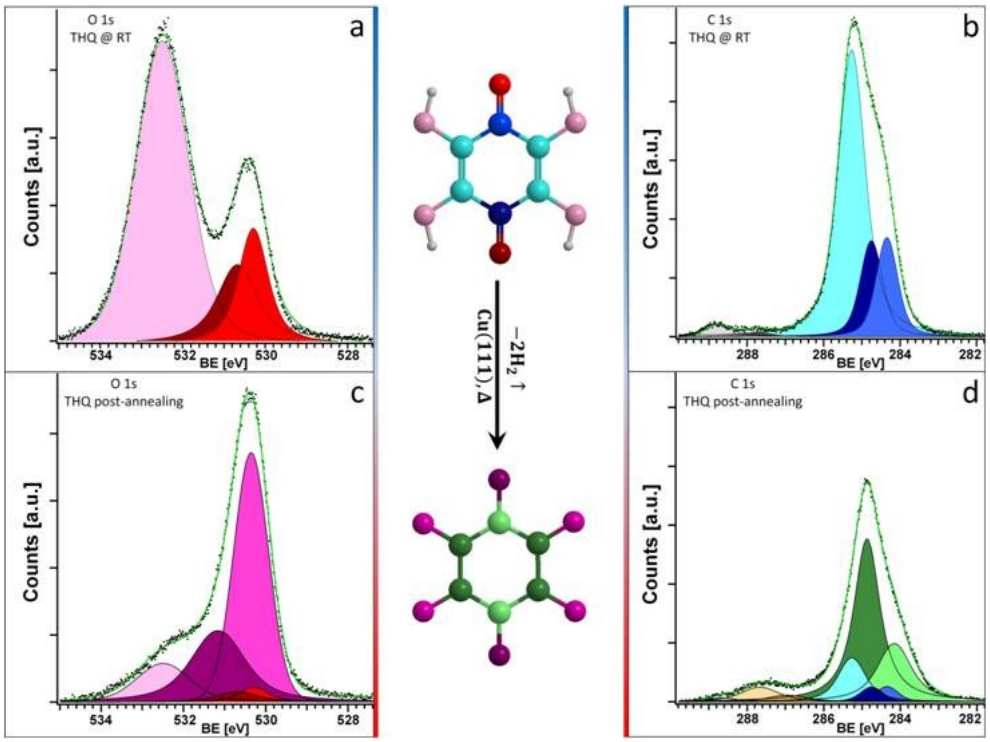

Figure 8. C 1s and O 1s core level X-ray photoelectron spectroscopic measurements performed on (a, b) THQ molecules deposited on a Cu(111) surface at room temperature and (c, d) after an annealing up to 383 K, respectively. The same color legend has been used in the fit components and in the sketches of the THQ molecule reported as insets: C-O-H and C=O of the intact THQ molecule are shown in pink, dark and light red in panel (a, c) and in three tonalities of blue in (b, d). C=O components for the post-annealing dehydrogenated TOQ anion are shown in light green and dark purple, while C=O groups binding to two copper adatoms are colored in light purple and dark green in (c, d). The pink, dark and light red components in (c, d) are associated to the C=O and C-O-H carbon atoms of intact THQ molecules. The grey and brown peaks in (b, d) are associated to the shake-up peaks for the O-H and C=O components of THQ and TOQ, respectively. These data have been collected at the ALOISA beamline (@ ELETTRA, Trieste, Italy) in a collaboration project. Credits for the XPS deconvolution go to Ada della Pia, Matteo lo Cicero, Maria Grazia Betti, Carlo Mariani, Dipartimento di Chimica, and Dipartimento di Fisica, Università di Roma "La Sapienza", Roma (Italy).

As a direct probe of the THQ unoccupied electronic structure and molecular positioning, the near-edge X-ray absorption fine structure (NEXAFS) spectra of the THQ phases at RT was compared with the same sample after an annealing at 375 K, at different orientations of the surface with respect to the electric field direction (Figure 9).

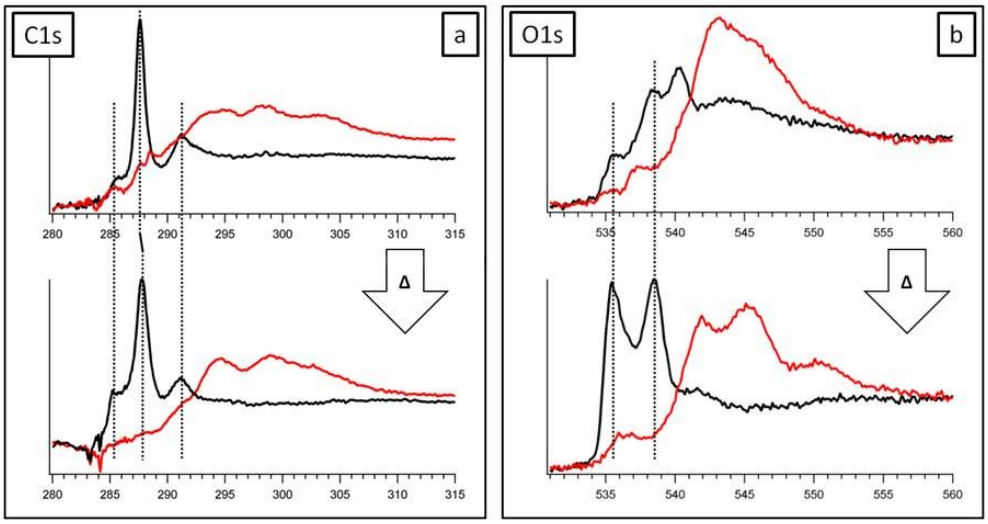

Figure 9. NEXAFS spectra measured by partial electron yield at the C K-edge and the O K-edge (a and b, respectively) for the THQ phase as-deposited at RT (top) and after an annealing at 375K protracted for 3 hours. Two spectra for each sample are reported, corresponding to transverse magnetic (black line) and transverse electric (red line) polarization. Dotted lines are guide for the eye.

C1s NEXAFS transverse-magnetic (TM) spectra of the THQ phase obtained ad RT (Figure 9a, black line) are dominated by the feature at approximately 287.5 eV, generated by C-OH-based π*←1s electronic transitions.[166] The evident shoulder on its lower excitation energy side at approximately 285.5 eV and the additional resonance at 291.2 eV have been associated with π*←1s excitations involving C=C and C=O, respectively.[166,167] Variations of the NEXAFS intensity resonances observed upon changing the orientation from TM to transverse-electric (TE, red line) suggest a tilted absorption of THQ at RT. In particular, the relatively large residual intensity measured in TE polarization at 285.5 and 287.5 eV reproduce the features obtained in the TM spectra, whereas the resonance at 291.2 eV vanishes in the TE polarization continuum.

O1s NEXAFS spectra of the THQ phase obtained at RT (Figure 9b, top) is mainly dominated by C-OH σ*←1s contributions in the TE polarization (red line). The resonances at 537.5 and 540.0 eV (TM polarization,

black line) have been attributed to a mix of higher order π*-symmetry molecular orbitals (MO)s and σ*-symmetry associated with C-OH bonds. C=O based π*←1s transitions appear with relatively low intensity at approximately 535.5 eV (Figure 9b, black line).[166]

After the thermal treatment at both TM and TE C and O K-edge NEXAFS spectra are affected in terms of line-shape features (Figure 9, bottom). In particular, the TM C-OH-based π*←1s electronic transition (Figure 9a, black line, bottom) is shifted towards higher binding energies at approximately 288.0 eV while the transitions at 285.5 eV and 291.2 eV, which have been attributed to the benzoquinonic (BQ, C=C and C=O) groups remain unchanged. Regarding the TE polarization curve (Figure 9a, red line, bottom), spectral features at lower binding energies result smoothened with respect to residual intensity measured at RT in accordance with the hypothesized thermally induced flattening of the THQ into TOQ, also found experimentally for similar systems.[168,169] Within the O K-edge NEXAFS spectra at high temperature, (Figure 9b, bottom) the π*←1s transitions at 535.5 and 538.0 eV (Figure 9b, black line, bottom) emerge with enhanced intensity while the component at 540.0 eV is suppressed. Such variations further corroborate the aforementioned hypothesis of the chemical transformation of THQ into TOQ species that occurs simultaneously with a conformational variation of the precursor upon annealing.

The combination of techniques used within this work led to a fully consistent characterization of the stable linkage structure of the tetrameric units within the 2D metal-organic layer. Eventually, the TOQ synthesis was possible only thanks to surface stabilization, as the ex-situ reactivity of such organic radicals would have limited their manipulation. These arrays of tetrameric Cu units are promising for applications in redox catalysis, particularly for CO_2 reduction to CO, CH_3OH and CH_4.[170]

ON-SURFACE REACTIVITY

Hereby a discussion is proposed regarding the main techniques for the on-surface activation of chemical reactions employed during my Ph.D. program. The discussion focuses mainly on thermally and photochemically activated on-surface reactions among halide- and alkyne-containing organic precursors. The synthesis and the characterization of the electronic structure of polymeric para-phenylene (PPP) on the surface of gold will be reported as part of a collaboration with Prof. Dimas de Oteyza, CFM, San Sebastian, Spain. Experiments and STM/STS characterization have been performed @ CIC nanoGUNE, San Sebastian, Spain. In addition, comparisons with the molecular behavior of the already discussed PEBA molecule on metal and non-metal surfaces will be proposed. Finally, two additional personal contributions regarding the on-surface photochemical reactivity under topochemical control will be proposed for two different alkyne containing organic precursors.

ON-SURFACE ACTIVATION OF CHEMICAL REACTIONS

Surfaces provide a peculiar energy landscape for various surface-overlayer interactions. They provide energetically favored adsorption sites, so that the energy minimization of 2D-crystals often deviate from the expected coordination structures of the bulk counterpart. In particular, known bulk coordination motifs are deeply influenced[171,172] and correlated molecular properties drastically change.[173] The driving forces defining the ultimate supramolecular 2D interaction network arise from a combination of substrate-mediated assembly geometries and interactions between the precursors in those positions. Substrates,

therefore, have an important influence on the assembly geometries and tailor the evolution and the reactivity of a specific molecular ensemble.

ON-SURFACE ULLMANN COUPLING

This reaction involves the thermal activation of halogenated precursors and leads to the formation of C-C bonds among reactants. The initial step is the thermal dissociation of the halogen from the organic scaffold. This occurs at lower energy than the carbon-carbon activation, for which reason the molecular core is generally preserved. Radical intermediates are reversibly stabilized, within specific temperature ranges, into metal-carbon protopolymers[174,175] and at higher temperature metal atom are released leading to the C-C bond formation.[176] The mostly studied halogen is bromine,[177] although successful reactions employing iodine[178] and chlorine[179] have also been reported. Noteworthy, Ullmann-like coupling reactions occur also on insulators,[180] granting a step forward for potential applications of the Ullmann coupling mechanism towards electronic devices.

WIDTH-DEPENDENT ENERGY GAP IN ARMCHAIR GRAPHENE NANORIBBONS: THE CASE OF PPP

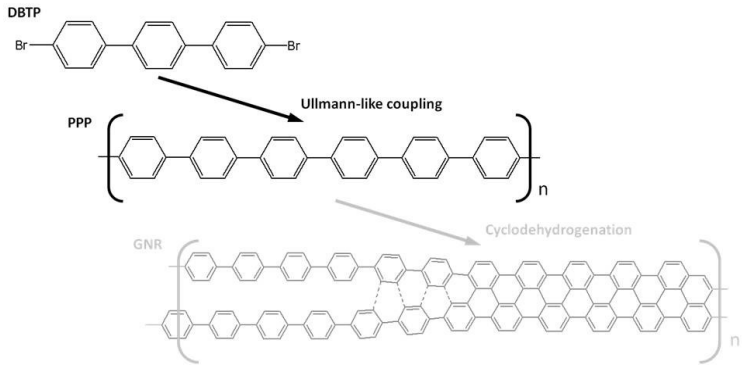

Figure 10. From top to bottom: schematic representation of the multi-step polymerization of DBTP

Poly-Para-Phenylene (PPP, Figure 10) is an ideally infinite chain of phenyl rings and represents one of the many precursors for the production of Graphene Nanoribbons (GNR)s. Its bottom-up synthesis is obtained with a surface-assisted Ullmann-like thermal polymerization of 4,4″-Dibromo-p-Terphenyl (DBTP, reaction scheme in Figure 10). Specifically, in a first step, DBTP precursors are thermally coupled into PPP wires (520 K), while GNRs are obtained in a second step of cylodehydrogenation activated at higher temperature (650 K).[19,181] This approach allows a fine-tuning of polymerization by temperature control. Indeed, PPP wires can be easily obtained on-surface in pure form.

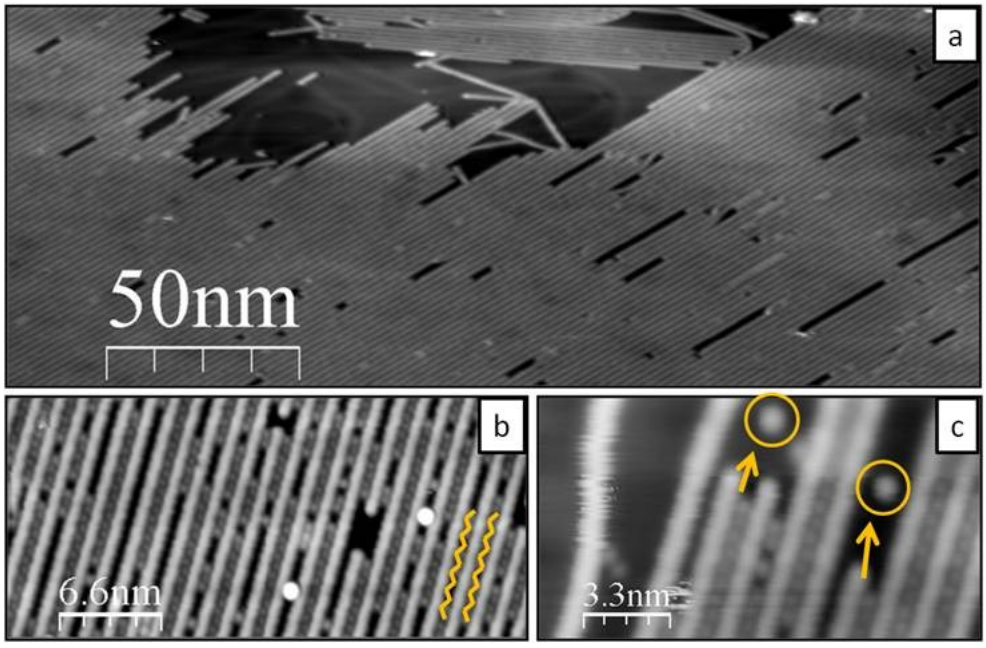

Figure 11. (a) Large scale STM image of close-packed PPP wires on Au(111) @4K; (b) small scale STM image of PPP wires with intercalated Br atoms. Yellow zig-zag lines are a guide for the eye and depict the peculiar aggregation pattern of Br atoms within the PPP wires; (c) detail of an STM image in which an isolated PPP (left side) is affected by a tip-induced perturbation and escaping Br atoms are highlighted with yellow circles.

After the annealing of DBTP on Au(111) at 520 K, close packed and isolated PPP wires emerge (Figure 11a). Samples show intercalated Br atoms among the PPP wires (Figure 11b). Their aggregation within the wires results in a "zig-zag" periodic pattern (see yellow lines in Figure 11b). However, random Br vacancies are detected. Residual surface diffusivity at 4K allows to detect the PPP termini as well as shorter oligomers and Br atoms moving on-surface during the scan. Isolated (escaping) Br atoms (Figure 11c yellow circles) are also observed on the substrate. Isolated PPPs are generally unstable and their imaging is not straightforward (see Figure 11c).

dI/dV single point measurements have been performed by STS on a PPP wire (Figure 12a) in order to obtain information on the electronic structure and on the band gap of this proto-GNR. The PPP wire shows two band onsets around -1.2 and +2.3 V (Figure 12b, experimental bias range of −1.6 to +2.5 V). The peak-to-peak band gap results E_{gap} = 3.48 ± 0.01 eV, which is in good agreement with the literature of other PPP wires characterized by an electronic structure poorly perturbed by the substrate.[182,183] PPP wires, as has been shown elsewhere,[181] physisorb with phenyl rings tilted by 20° to each other. In accordance with a recent study,[181] the lack of planarity along the polymer hinders the ideal delocalization of charge and results in a quasi-localization of molecular orbitals, i.e. HOMO and LUMO, clearly visible in correspondence of the phenyl rings (Figure 12c, d).

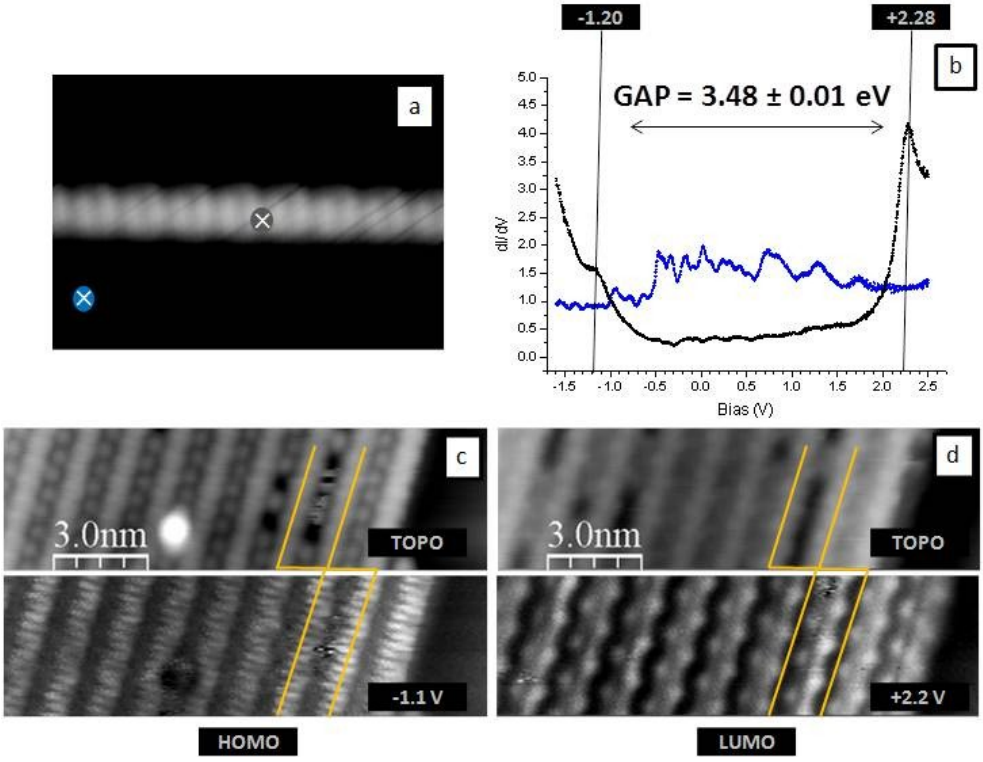

Figure 12. (a) STM image of an isolated PPP wire with two selected points for the dI/dV spectra. (b) comparison of dI/dV spectra with color code referred to (a), the band onset and the peak-to-peak gap in correspondence of the PPP wire is highlighted. (c) topographic and dI/dV 2D map collected at -1.1 v (HOMO onset) for closely packed PPP wires. (d) topographic and dI/dV 2D map collected at +2.2 v (LUMO onset) for the same PPP wires.

Noteworthy, following the cyclodehydrogenation step, the planarity of the ribbon increases, as consequently does the degree of conjugation. In turn, the bandgap decreases abruptly (down to E_g = 1.05 ± 0.01 eV for a ribbon made of five PPP wires fused together in-plane, these data are currently under elaboration).

On-Surface Glaser Coupling

The cuprous salts–catalyzed homocoupling of aryl-alkynes that occurs in ammonia and affords the buildup of bisacetylene derivatives through the air oxidation of Cu(I)phenyl acetylide is referred to as Glaser

coupling.[184] Variations of the metal catalyst or of the reaction environment are named Glaser-like or generally alkyne homocoupling reactions. On-surface Glaser coupling was developed on metal substrates in order to directly exploit surface atoms as catalysts,[185] and gained a growing interest for its possible application in the bottom-up fabrication of sp- and sp^2-hybridized nanomaterials.[43,44,186]

As far as the on-surface synthesis is concerned, it is well known that this reaction occurs on low Miller index Cu,[187] Ag[53] and Au[50] surfaces by providing heat to alkyne moieties. However, the strong adsorbate-substrate interaction often induces unwanted side-reactions (cyclotrimerizations,[49,50] generation of metal-organic species[51] and oligomers crosslinking[52]), which by far inhibit the production of extended and regular nanostructures.[53]

To date, a major effort has been put towards on-surface polymerization of symmetrical diethynyl-substituted π-system self-assembled superstructures and mostly statistical STM investigations outline trends within libraries of reaction products.[188,189] Yet by performing thermal annealing on properly functionalized precursors, the reaction between closely interacting alkynes can be promoted. Covalently bound nanostructures were certainly formed and several products were identified. The effort put in DFT investigations[48] validated the active role of the metal atoms in the stabilization of reaction intermediates, but did not provide conclusive information regarding the catalytic role of the surface for the coupling reaction. Apparently, the metal-alkyne interaction offers an energy landscape with many thermally accessible side reactions. Indeed, Glaser-like coupling, α- and β-hydroalkynylation of the terminal alkyne, dieyne, enediyne and cyclotrimerization products are obtained in the same batch.[188,189]

It was determined experimentally elsewhere, that the Au(111) and Ag(111) surfaces reveal some specificity regarding the relative frequency of occurrence of the competing reactions. Alkyne homocoupling resulted more efficient on Ag(111) than on Au(111). In

particular, the substrate-dependent selectivity was maintained for different kinds of alkyne precursors.[185] It has been established that ortho-substituents next to the alkyne functionality suppresses side reactions for steric reasons. However, ortho-substituents also limit an ordered propagation of the reaction by constraining the orientational degree of freedom of neighbor precursors during the coupling reaction.

The on-surface Glaser coupling is therefore not fully understood and the substrate-induced selectivity is far from being a general rule, as it does not hold for other alkyne-containing molecules.

The aforementioned PEBA, for example, although displaying a terminal alkyne, undergoes a different fate on Ag(111). By performing annealing at progressively higher temperature, an onset of on-surface intermolecular reactions was found at 400 K.

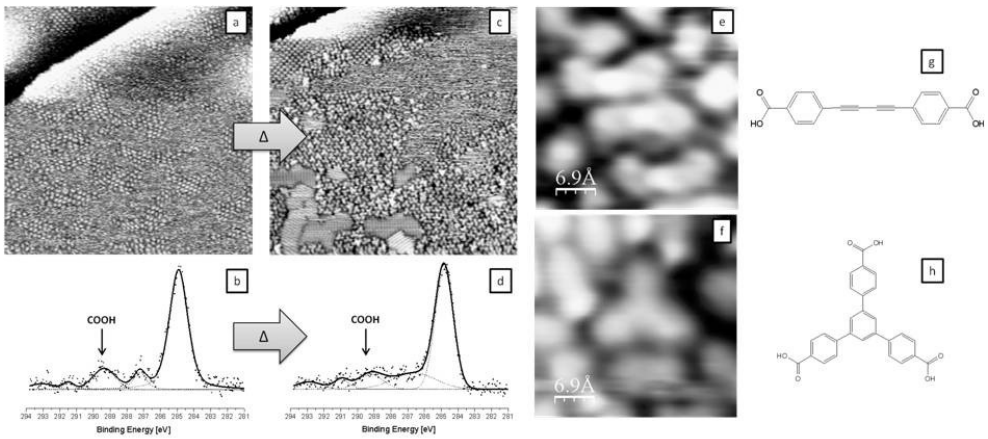

Figure 13. (a) STM image (50 nm × 50 nm) of PEBA molecules on Ag(111) obtained as deposited at RT (b) corresponding al Kα excited C 1s XPS spectra for PEBA on Ag(111) at RT. Intensity is reported in arbitrary units. (c) STM image (50 nm × 50 nm) of PEBA molecules on Ag(111) obtained after annealing at 400 K. (d) corresponding al Kα excited C 1s XPS spectra for PEBA on Ag(111) at 400 K. Intensity is reported in arbitrary units. (e, f) close up images of the predominant molecular structures found after the annealing. (g, h) tentative molecular models for the reaction products (e, f)

Within the previously discussed self assembled phase of PEBA on Ag(111) (Figure 13a, b) a covalent coupling occured at high temperature and a library of byproducts was identified (Figure 13c). In comparison with the diethynyl π-system,[53] the presence of two different antipodal functional groups inhibits the propagation of the reaction toward the on-surface polymerization, nonetheless the identification of the reaction product resulted straightforward as single molecules could be easily identified by STM imaging. The intermolecular reaction is believed to occur among alkyne groups, while the carboxylate groups ensure a HB interaction network among the reaction products. Decarboxylation does not occur in this temperature range (below 400 K) and it is known to occur at higher temperature for similar systems,[190] indeed, the signal of the carboxylic carbon is still present in the XPS spectrum (Figure 13d), despite the occurrence of a substantial thermally induced desorption.

Reaction products have been identified for alkyne homocoupling and cyclotrimerization reactions, reported in Figure 13e and f, and occurring among two and three molecular units, respectively. Tentative molecular models are proposed in Figure 13g and h. The relative ratio of these products reveals an unprecedented behavior: it was found that the alkyne homocoupling occurred less efficiently (approximately 18%) if compared with the cyclotrimerization reaction (approximately 79%). In the case of diethynyl π-system[53] the selectivity of these reactions was reversed. A minor quantity of tetramers and unreacted starting materials have also been observed. Tetrameric structure have been tentatively assigned to the enediyne moiety.

Overall, the multitude of reaction products that has been detected indicates that the catalytic activity of the Ag(111) surface is non-selective. With these scenarios and the lack of an extended literature on this subject, the real challenge still remains to take control of the many possible reaction pathways. Besides the use of templating substrates[191] or the adoption of steric hindering groups,[53] promising approaches to

overcome this limit rely also on non-thermal activation processes of supported alkynes.[54,55]

PHOTOCHEMICAL ACTIVATION OF CHEMICAL REACTIONS

The increasing interest for nanomaterials with innovative functionalities has recently boosted the search in on-surface photochemistry as a promising bottom-up approach towards complex molecular architectures.[29–31] The search in the field of on-surface synthesis is still at its birth, however, few examples allowed either a deeper understanding of the chemical and physical processes that are at the basis of light-induced on-surface reactions[32,33] and led to the covalent stabilization of specific molecular networks[14,34,35] which can find technological applications in surface nanopatterning[36] and organic electronics.[37]

On-surface photochemical activation of chemical reactions can lead to unusual molecular reactivity, as the close proximity of surface atoms favors the transfer of energy and charge between the substrate and molecules and induces variations in the energy level positioning of the latter. Despite this provides new reaction pathways[192] and potentially favors the formation of the long-range ordered covalent framework, on the other hand it makes the on-surface photochemistry a complex subject with hardly predictable outcomes. The desirable scenarios that follow the photon absorption may be a selective bond cleavage and an efficient molecular recombination. Characteristic dissociation times are in the range 10^{-13} to 10^{-14} s and are competitive with other relaxation processes, that occur within time scales of 10^{-15}-10^{-13} s.[193]

Localized electron systems of organic 2D aggregates in contact with metallic surfaces interacts with intrinsically delocalized metal bands at the interface,[194] hence, following photon absorption both the excitation of the adsorbate, of the adsorbate-substrate complex, and of the

substrate can occur. When the adsorbate alone is involved in the photon absorption and the reaction products are generated by intra- or intermolecular reactions, the process is recognized as “direct” excitation. It differs from the “indirect” excitation, where an initial excitation of the substrate surface states populates unoccupied molecular states. Depending on the bonding or antibonding character of the orbital where the incoming electron resides, these intermediates can either dissociate or remain bound. Radical photodissociation are commonly employed in on-surface photochemistry and indirect transitions mediated by metal absorption is commonly exploited when the molecules are weakly adsorbed on the surface. In general, the latter reactions take place at longer wavelength when compared with the gas phase counterpart.[193]

Alkynes are perfect candidates for this kind of studies, since various coupling and photo-polymerization processes are induced by exposing self-assembled monolayers to UV or visible radiations. This is the case investigated by Gao et al. in which the formerly described Glaser coupling of diethynyl π-system on the Ag(111) surface occurs photochemically.[55] In this case, the formation of aryl alkyne dimers could be induced by UV irradiation at 375 nm, which is far from the molecular UV absorption band maximum, and is an indication that, the coupling reaction is possibly induced by an indirect (substrate mediated) excitation path. This photochemical aryl alkyne dimerization occurred also on Cu(111), but with a significantly reduced efficiency, while on Au(111) it did not occur.[55] This corroborates the hypothesis of a catalytic role of the Ag(111) substrate in the photochemical path towards on-surface alkyne homocoupling. Within this study, DFT simulations indicate why the Ag surface is more efficient than Au: the interactions of the latter with the alkyne moiety results in a reduced mobility of the molecules and in a higher probability that the substrate-coupled intermediates undergo branching reactions.

On-Surface Photochemistry of Pre-Ordered 1-methyl-2-phenyl-acetylenes: Photoselective C-H Bond Activation and Intermolecular Coupling on HOPG

On-surface photochemical synthesis involving the coupling of alkynes affords the production of covalent organic assemblies, which are promising in the production of functional interfaces. Generally, the coupling of alkynes takes place by thermal activation of molecular precursors on metal surfaces. However, the interaction of alkynes with surface metal atoms often induces unwanted reaction pathways when thermal energy is provided to the system.

In this personal contribution the focus is on the light-induced metal-free coupling of propynyl-benzene precursors performed with an in-house experiment on highly oriented pyrolitic graphite (HOPG). The reaction occurred with high efficiency and selectivity within a self-assembled monolayer and led to the generation of covalently coupled dimeric derivatives. Such photochemical uncatalyzed pathway represents an original approach in the field of topological C-C coupling at the solid/liquid interface.

A small π-system, namely 2,5-didodecyl-1,4-di-1-propynylbenzene (ppBz), was used in order to attempt an on-surface photochemical coupling within its self-assembled monolayer at a non-metallic interface and in various environments. With respect to the example proposed in the former section, the terminal alkyne (···C≡C-H) has been substituted with a methyl-terminated alkyne, i.e. propynyl- or methyl-acetylene group (···C≡C-CH_3). It was found that the photoexcitation of a 1-methyl-2-phenyl-acetylenes core induces a C-H dissociation and a site-specific C-C coupling between two neighboring methyl-acetylene terminals. The experiment was performed in a metal-free environment and the 2D confinement of the starting material tailored specific head/tail coupling of the methyl-acetylene moieties. The proximity of the UV-sensitive substituents within a pre-organized monomer layer guaranteed a favorable coupling reaction and, by the analysis of the

reaction products, the UV-induced reaction pathway was correlated with the fission of a methyl C-H bond of the methyl-acetylene group. A propargylic-like recombination[195–197] was eventually suggested.

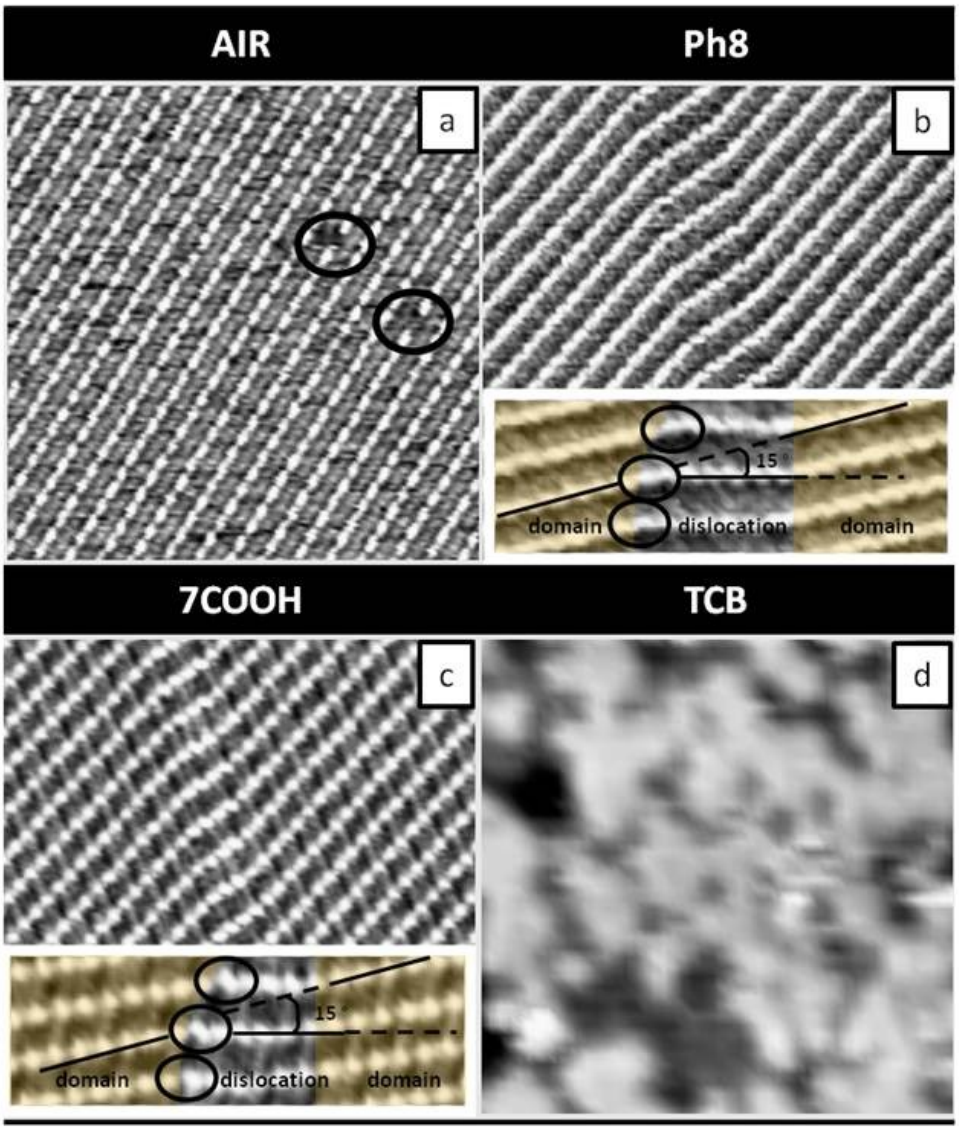

Figure 14. (a) Topographic STM images of the self-assembled structures of ppBz at various interfaces (a) HOPG /air interface (30 nm × 30 nm), (b) HOPG/Ph8 interface (30nm × 30nm, insert: 20nm × 7nm), (c) HOPG/7COOH interface (30nm × 30nm, insert: 20nm × 7nm), (d) HOPG/TCB interface (30nm × 30nm).

This study also shows that the complex recombination chemistry of the starting material and the detection and characterization of the reaction products is strongly affected by the environment in which the reaction takes place. The necessary molecular resolution for this study has been provided by STM operating both at the solid/air and solid/liquid interfaces.

In Figure 14, representative images of the self-assembled phase of the ppBz molecules at various interfaces are shown. Upon deposition of a solution of ppBz on the HOPG substrate, extended lamellar structures emerge, irrespective of the solid/air vs solid/liquid interface, characterized by distinct bright and dim contrast features. At the HOPG/TCB interface the self-assembly did not occur. To account for the higher electronic density on the aromatic core, the bright regions have been attributed to the aryl-alkyne cores,[198] while the dark contrast regions have been attributed to the dodecyl- alkyl chains (see Figure 14a for results at the HOPG/air interface, Figure 14b for the HOPG/Ph8 interface, Figure 14c for the HOPG/7COOH interface and Figure 14d the HOPG/TCB interface).

Differences between 2D racemic solid/air and solid/liquid interfaces emerge from the comparison between STM images: the solid/air interface is characterized by point defects, i.e. molecular vacancies, that side with an irreversible island-degradation upon a raster scanning protracted over the same region. On the other hand, the overflowing solution within the liquid environment ensures the self-healing of the physisorbed monolayer affording a continuous dissolution-precipitation equilibrium.[56]

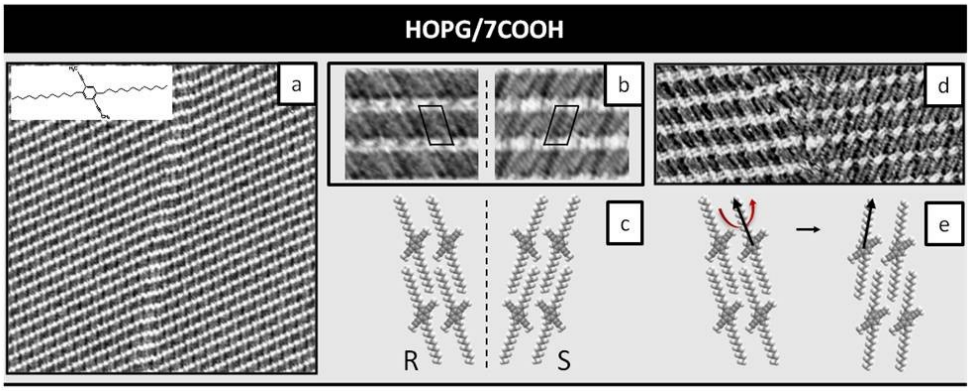

Figure 15. (a) STM image (50 nm × 50 nm) of the self-assembled monolayers of ppBz at the HOPG/7COOH interface. (b) STM images (5 nm × 7 nm) of two homochiral domains of "R" and "S", the chiral packing structures in the SAMs mostly encountered for ppBz at this interface. (c) tentative models for the packing of the "R" and "S" domains (d) STM images (15 nm × 25 nm) of two ppBz domains which differ for the orientation of the alkyl chains. (e) tentative models for the packing of the domains found in (d).

The stretch-marks that occasionally emerge on the lamellar superstructure (see Figure 14 and 15a) are believed to develop from the conglomeration of molecular units with different absorption geometries, resulting in tilts along the close packed directions at both the solid/liquid interfaces.

Unusual absorption geometries were observed only at the HOPG/liquid interface. They are reported in Figure 15 with tentative models. They have been classified as homochiral packing structures (Figure 15b and tentative molecular models in Figure 15c) and orientational isomers, i.e. ppBz domains which differ for the orientation of the alkyl chains reported in Figure 15d (tentative molecular models in Figure 15e).

PpBz island which assemble in homochiral packing structures, namely "R" and "S" domains are displayed in Figure 15b, and aggregate in extended 2D layers (>200 nm × 200 nm), oriented along the main directions of the underlying HOPG. Their dimensions are generally limited by the extension of the substrate terraces, therefore domain boundaries are difficult to observe. An even number of carbon atoms within the alkyl chains generally promotes the formation of 2D

racemates upon adsorption.[199–201] Indeed, 1,4-propynyl-benzene mostly absorb via the same enantiotopic face.

By means of high resolution STM imaging it was possible to establish that the monomers absorb planarly along the lamella. As already encountered for analogous molecules,[202–204] the main stabilizing interactions of the ppBz layers are the registry requirements with the underlying HOPG.[205] The match between an all-trans alkyl chain (zig-zag inter-metylene distance: 0.258 nm) and the HOPG in-plane lattice constant (0.246 nm), has been largely demonstrated to dictate the lateral packing of alkyl chains.[206,207] The registry demands their lateral separation at a distance of 0.42 nm[207] and in our case we obtain a value of 0.45 nm, which is in good agreement with this requirement.

The exact calibration of the overlayer unit cells has been obtained by means of high resolution STM images in which both the substrate and the overlayer are present. These images allow one to calibrate the molecular unit cell, once the size of the HOPG lattice is known. The latter acts as an internal ruler and the molecular parameters are scaled by means of a superposition matrix to the value of 0.246 nm for the in-plane lattice constant of HOPG. The parameters for the unit cell containing one molecule for the ppBz overlayer at the HOPG/air, HOPG/Ph8 and HOPG/7COOH interfaces (highlighted in black in Figure 16a, 16b, 16c, respectively) were extracted directly from the autocorrelation measurements show in Figure 16d, 16e, 16f. The closer commensurate unit cell that best fits the experimental ppBz is reproduced by the epitaxial matrix (3 9 , -5 5), which corresponds to the unit cell whose parameters are a=1.23 nm, b=2.66 nm and an angle of 74°. These values are given without uncertainty, as they are the most reliable representation of the closest unit-cell of the overlayer commensurate with the underlying substrate.

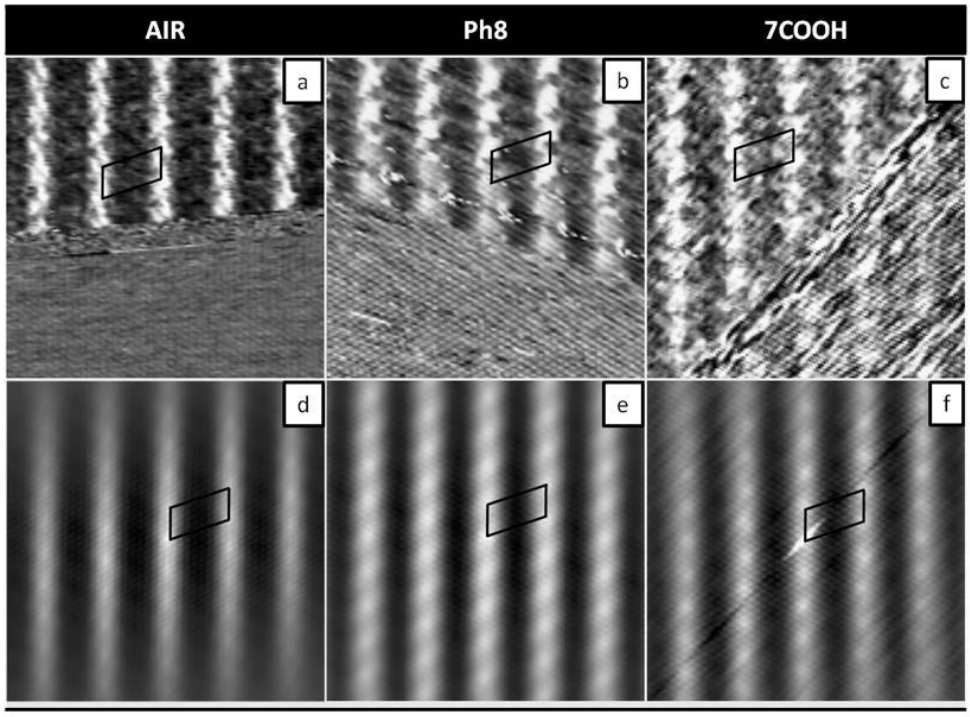

Figure 16. (top panel) STM images showing the ppBz structure (top) and the substrate (bottom) in the same frame (a) for the HOPG/air interface (-0.70 v, 25 pa (overlayer); -0.20 v, 95 pa (substrate), 10 nm × 10 nm), for the HOPG/ph8 interface (-0.50 v, 45 pa (overlayer); -0.15 v, 145 pa (substrate), 10 nm × 10 nm) (b) and for the HOPG/7cooh interface (-0.30 v, 15 pa (overlayer); -0.20 v, 115 pa (substrate), 10 nm × 10 nm). The corresponding autocorrelation images are shown in the bottom panel (d), (e) and (f), respectively.

The UV-Vis spectrum of ppBz in methanol solution, reported in Figure 17a, shows an absorption band in the 250-350 nm region with a maximum at 296 nm. This band is attributed to $\pi^* \leftarrow \pi$ transitions of the propynyl benzene core.[208] Separate studies on the photolysis of simple organic molecules in the gas phase, e.g. propyne ($H\text{-}C\equiv C\text{-}CH_3$),[197] demonstrated that UV photolysis occurs at the methylic C-H bonds[196,209] and the recombination of propargyl radicals ($H\text{-}C\equiv C\text{-}CH_2^{\cdot}$) was proposed as a possible reaction path with 1,5-hexadiyne (15HD) as a reaction product.[195,210]

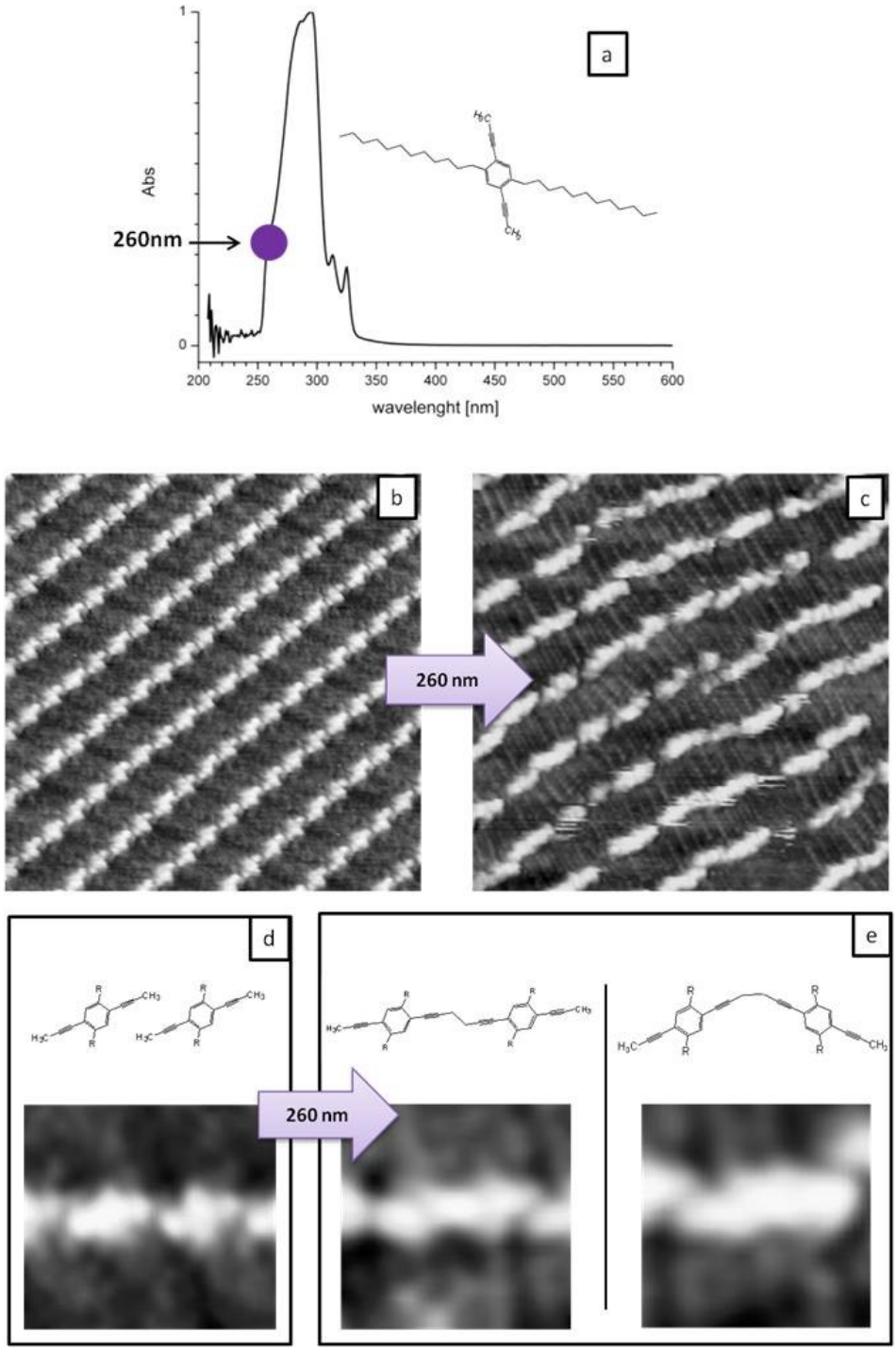

Figure 17. (a) UV-Vis absorption spectrum in methanol solution of the ppBz molecule (the 260 nm wavelength is highlighted with a purple dot) and high resolution zoom images of the ppBz overlayer before and after the UV irradiation at the HOPG/7cooh interface. (b) as deposited, self-assembled structure of ppBz at the 7cooh/HOPG interface (15nm × 15nm) and (c) photochemical recombination after 30 min. Irradiation at 260 nm (15nm × 15nm). (d, e) tentative models and magnification of selected molecules, before (d) and after (e) the irradiation.

Previous reports show that monomer solutions of aromatic acetylenes undergo UV-induced polymerization and coupling reactions that occur in low yield and with low specificity.[211] Aryl-alkyne derivatives also undergo UV-mediated coupling when the irradiation is performed on a 2D preorganized overlayers.[54,55] It was therefore hypothesized that by taking advantage of the 2D confinement of neighboring propynyl-benzene cores a higher reaction selectivity could be obtained in a photoinduced coupling. In this view, the proximity of the propynyl groups (interdistance 0.41±0.05 nm) in the self-assembled ppBz monolayer (Figure 17b) would favor the photochemical coupling of the methyl-acetylene radical groups into 15HD interconnecting groups, a result due to the fact that reactive species generated by photolysis are energetically driven to bond under topochemical control.[195]

In the case of the HOPG/7COOH interface, after an UV-laser irradiation is performed on the ppBz monolayer, the STM imaging produced a clear proof of the on-surface photochemical C-C coupling (see Figure 17d, e). At the HOPG/air interface, the reaction did not occur efficiently. Following the initial formation of ppBz dimers, mostly degradation and desorption occurred after the UV irradiation. In this case oxygen-mediated reactions are likely to occur[212] on the photo-activated monolayer and unwanted photo-oxidation necessarily hampers the desired intermolecular C-C coupling. On the other hand, at the HOPG/liquid interfaces, although low rate oxygen-mediated reactions are also known to occur,[65] a larger amount of coupling-reaction products were obtained, characterized by a wavy aggregation pattern on the large scale (see Figure 17c). The overflowing liquid therefore ensures a low rate of side photo-oxidation reactions and simultaneously acts as a reservoir of monomers for possible error correction within the ppBz layer. Indeed, only the STM imaging at the HOPG/liquid interfaces produced a clear proof of the on-surface photochemical C-C coupling. Ultimately the HOPG/7COOH interface resulted as the best environment for the photo-induced reaction. In this case, the solvent is transparent

to the 260 nm radiation and the reaction occurs relatively fast, hence minimizing the ambient contamination of the sample.

It was observed that after the irradiation, dimers diffuse freely on-surface as a single unit already at the early stages of the overlayer conversion. The covalently linked products are not fully planar, as 15HD interconnections have sp^3- carbons, hence their dimensions derived from STM images may be affected by out-of-plane surface accommodations. Nonetheless, after the UV irradiation, different configurations, namely cis and trans isomers, have been observed and tentative models are proposed in Figure 17 d, e. Dimers have an inter-core distance equal to 1.19±0.05 (trans isomer, Figure 17e, left panel) and 1.05±0.05 nm (cis isomer, Figure 17e, right panel), that is contracted with respect to the inter-monomer distance: 1.23±0.05 nm, as a further proof of the covalent coupling among the precursors.

To explore a possible thermal activation path for the coupling of the ppBz monomers, thermal annealing treatments were performed both at the HOPG/air and HOPG/liquid interfacial systems. Unfortunately, neither direct thermal activation nor synergic thermal and UV irradiation resulted in a successful intermolecular coupling. In the case of the HOPG/air interface, the thermal annealing was protracted up to 450 K, which represented the thermal degradation threshold of the monolayer, presumably because of the activation of air-induced oxidation reactions. Simultaneous thermal and UV irradiation induced desorption of the monolayer. For both the HOPG/liquid interfaces, providing thermal energy, with or without UV irradiation, resulted in the desorption of the ordered monolayer in favor of disordered and poorly resolved adsorbates.

Taking into account that thermal activation is unfavorable in the case of thermally sensitive molecules, the photochemical activation affords higher selectivity over the product distribution even at shorter reaction times. Moreover the photochemical activation gives a better control

over the C-C bond formation when proper pre-assembly conditions are met.

In conclusion, this experiment demonstrates that on-surface photochemical coupling can be activated at the solid/liquid interface providing similar results to analogous systems studied under more stringent and metal-surface catalyzed UHV conditions.[55] Alkyl-chains in orto-positions with respect to the photoactive groups demonstrated to simultaneously offer a good stabilization of the 2D aggregates via cumulative supramolecular interaction networks, and also allowed the proper alignment of the molecular building blocks towards a topochemically favored coupling. As a drawback, this level of stabilization hindered a proper alignment of higher-order coupled precursors and the product distribution was limited to dimers. Finally, the coupling was triggered by direct molecular UV excitation and the reaction occurred in a catalyst- or cofactor- free environment, as occurs for alkyne homocoupling at the HOPG/liquid interface.[54] This substantiate the importance of a proper topological pre-organization as an alternative to a potentially more complex reaction scenario offered by the metal catalysis, in order to exploit the molecular reactivity via the non-thermal, photochemical, approach.

METAL-FREE ON-SURFACE PHOTOCHEMICAL HOMOCOUPLING OF TERMINAL ALKYNES[54]

Within this work, the investigation on the photoactive terminal alkynes groups was mostly performed in-house at the solid/liquid interface. In particular, an uncatalyzed and highly selective dehydrogenative homocoupling was obtained, under topochemical control, by light triggering in a metal- and cofactors-free environment. The terminal alkyne of interest is the small π-system PEBA. STM analysis at the

solid/liquid interface has been carried out by preliminarily dissolving the reagent molecules in 7COOH at a concentration of 2.0 mg/g.

Drop-casting of a solution of PEBA in 7COOH on the HOPG surface produces a self-assembled and stable monolayer. Figure 18a shows a representative image of a 2D ordered aggregate of PEBA molecules. Islands, whose dimensions vary in the range of 20-40 nm, are organized in symmetry-equivalent domains, according to the main directions of the underlying substrate and show close-packed molecular building blocks. By high resolution STM imaging (Figure 18b), it is possible to observe that the superstructure is dominated by apparently dimeric species formed by two ring-like pairs interconnected by a bright feature (outlined by the dashed line in Figure 18b). However, the labeling of the functional groups of the dimers remains not trivial. Figure 18c shows how the supramolecular order of PEBA molecules can be explained in terms of intermolecular hydrogen-bond (HB) networks: two collinear hydrogen-bonded carboxylic groups (highlighted in red) and their cooperative interactions with the nearest neighbor (NN) aromatic systems,[213,214] provide a necessarily stabilizing interaction mesh. On the other hand, the collinear accommodation of the terminal alkynes (highlighted in blue) is maintained by the stabilizing interaction of parallel alkyne groups involved in a two-fold cyclic HB (C≡C–H•••C≡C, double-dotted lines in Figure 18c),[49,130] that adds to the intermolecular interaction with their NN aromatic systems (dotted lines in Figure 18c). The observed dimers are composed by intact and flat-lying physisorbed PEBA molecules, with ring features corresponding to the benzene rings.[215] The dark area between the two rings has been attributed to the HB between the collinear carboxylic groups (Figure 18d), while the bright feature is ascribed to the alkyne end-groups approaching in a quasi-linear fashion (Figure 18e).

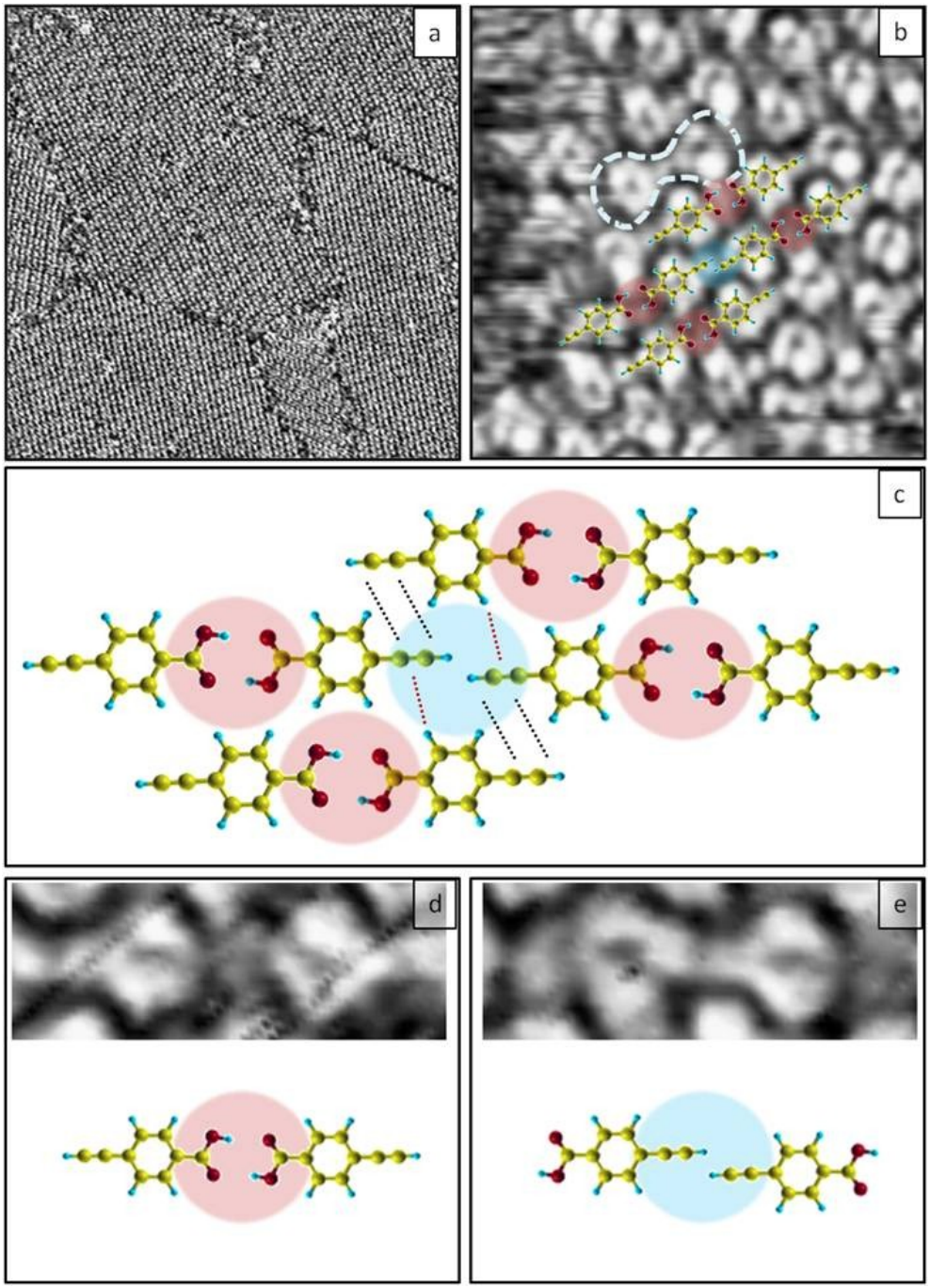

Figure 18. (a) Topographic and (b) high resolution STM image of the self-assembled structure of PEBA; (c) proposed ball and stick model of the PEBA supramolecular interaction network; (d) small-scale STM images of the carboxylic HB interaction and its corresponding proposed ball and stick model; (e) collinear alkyne interaction contrast feature and its corresponding proposed ball and stick model.

In Figure 19a a high resolution image of ordered HB-dimers is shown: short black arrows, pointing towards the alkyne groups, have been used to indicate molecular orientations. The ordered overlayer is reproduced by a unit-cell containing two molecules, whose parameters are a=0.74 ± 0.05 nm, b=1.89 ± 0.05 nm and α=55 ± 1°. These values have been obtained by averaging the real space measurements on five STM images, while by high resolution imaging wherein both the substrate and the overlayer are present (see SI of ref. 54), the exact calibration of the molecular unit cell based on the known size of the substrate lattice (0.264 nm) resulted in a=0.74 nm, b=1.86 nm and α=53°.

Along the overlayer vector b, (see Figure 19a) a distance of 0.95 ± 0.05 nm is obtained as center-to-center distance for two phenyl rings interacting by carboxylic-HBs, while the distance between neighboring alkyne edges is 0.91 ± 0.05 nm. The former is consistent with the 0.96 ± 0.01 nm value found experimentally for the center-to-center distance between two NN terephtalic acid (TPA) molecules,[56] Noteworthy, also vector a is reasonably consistent with the intermolecular distances found for TPA along the same packing direction (0.78 ± 0.01 nm). The NN alkyne-alkyne distance is also in reasonable agreement with the literature value of 0.80 ± 0.10 nm found experimentally for the 1,4-diethynylbenzene SAM on Cu.[49]

Alongside with the ordered 2D aggregates, also randomly oriented monomers have been observed (Figure 19b). These coexist in the PEBA SAM in a dynamic-exchange equilibrium. Both tip-induced perturbations and the liquid environment can provide the driving forces for energetically accessible libration modes and discrete azimuthal rotations. These phenomena are reported in Figure 19c, and a tentative modelization is reported in figure 19d, as successive cartoon-clips (the alkyne end-groups have been highlighted in blue and a grid has been added as a guide for the easy detection of the alkyne positions in different clips).

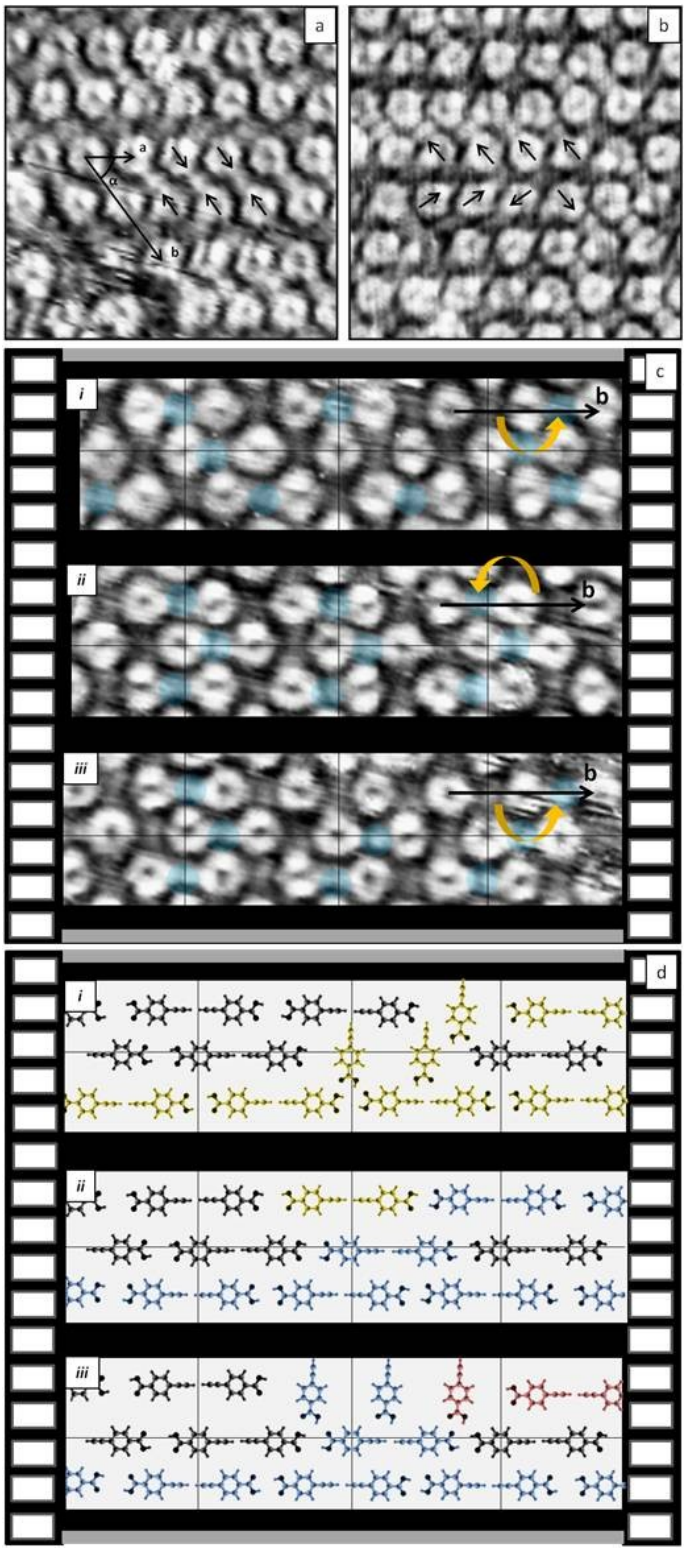

Figure 19. (a) STM image of an ordered aggregate of PEBA. (b) high resolution STM image of a disordered aggregate of PEBA. (c) representative cartoon-clips for the observed on-surface dynamics over a selected area. Arrows and blue highlights are guides for the eye. (d) color-marked model depicting molecular reorientations observed experimentally

Incidentally, also the complete rotation (two successive 180° on-site leaps) of a PEBA monomer has been detected (see yellow arrow in Figure 19c i, ii, iii). Interestingly, if vector b is selected in the starting frame, its direction and length never change during the rotation of the central molecule (see Figure 19c for the original images and the tentative dynamical modelization in Figure 19d).

Dynamic phenomena at the solid/liquid interface are generally associated with the vertical mobility of adsorbed molecules, as the supernatant liquid is responsible for a substantial lowering of the desorption barrier with respect to the vacuum barrier, also in analogous systems.[56] The on-surface dynamic processes observed within the PEBA superstructure imply that the underlying substrate does not strongly influence the aggregation pattern of the absorbed monolayer, although both adsorption/desorption processes and pattern rearrangements are energetically accessible at RT.

Crystalline PEBA reveals thermal and UV-induced reactivity. In the solid state, the photo-polymerization reaction is topochemically promoted by the proximity of adjacent molecules within the crystal lattice.[153] Therefore, it was assumed that by taking advantage of the collinear displacement of neighboring alkynes on the HOPG surface, a topochemical homocoupling could be promoted photochemically. According to the UV-Vis spectrum of a solution of PEBA, the absorption band of the aromatic core is in the 240-270 nm range (see SI of ref. 54 for further details). In order to maximize the photon absorption events, the 260 nm wavelength, which is a local maximum in the absorption curve, has been selected for irradiation. Direct exposure of the liquid cell to the laser beam for relatively short times (5-10 min) induced a nearly complete and irreversible conversion of the PEBA monolayer, resulting in a new molecular building block organized in a new ordered superstructure.

Figure 20a, b and inserts report large and small scale images of the HOPG-supported monolayer before and after the light treatment. On the

large scale it is evident that after the illumination, the SAM is characterized by a new superstructure formed by ordered rows of dimeric species that organize in alternating, symmetrically equivalent domains. After the UV irradiation, except for a few isolated unreacted monomers, almost all the molecular building blocks are constituted by dimers that, in contrast with the pristine HB-dimers, show no on-site rotations, suggesting the possible photo-induced stabilization of the molecular units with a chemical bond in the proposed butadiynyl derivative 4,4'-di-(1,4-buta-1,3-diynyl)-benzoic acid, BUBA.

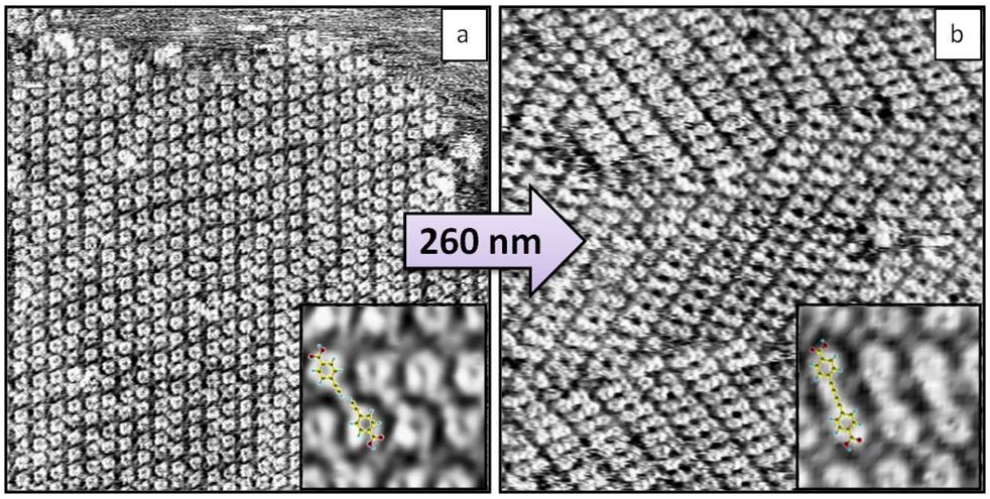

Figure 20. (a) Topographic STM image and (b) high resolution STM image after 5 min. irradiation at 260 nm of the self-assembled PEBA superstructure. Inserts are 2.5 nm × 2.5 nm close-ups of high-resolution images.

In the high resolution inserts of Figure 20b it is also evident that the phenyl rings of BUBA are now connected by an intensified electronic density and the nodal plane observed in the pristine HB-dimers disappears. The center-to-center distance between the phenyl rings within an individual BUBA is 0.95 ± 0.05 nm, which is close to the distance found in the starting system, but nonetheless compatible with the 0.96 nm value obtained experimentally[55,185] and computationally[147]

by other authors for various aryl-butadiynyl derivatives, and supports the occurrence of a photo-induced metal-free homocoupling reaction between terminal alkynes. The presence of few unreacted PEBA monomers, constrained within ordered rows of the BUBA layer (see superposition models in Figure 21), allowed to clearly compare the initial HB-interacting PEBA dimers with the photo-coupled covalent dimers. The photocoupling involving the decarboxylation is unlikely to occur, since it would produce bis-phenyl species whose center-to-center distance is 0.43 nm, as found for oligo p-phenylene derivatives.[216,217]

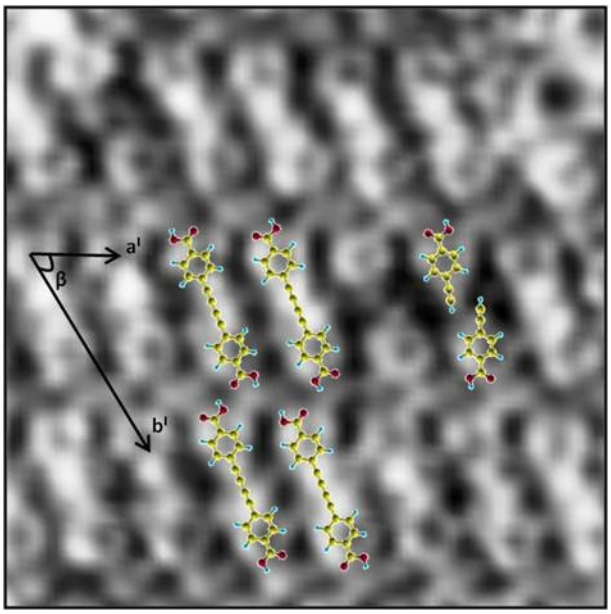

Figure 21. High-resolution STM image (5 nm × 5 nm) of the photo-reaction product and unreacted PEBA monomers.

BUBA molecules have been observed to aggregate adopting specific schemes of carboxylic HB lateral interactions. Particular HB networks have been previously described[218] for this highly adaptable butadiynyl derivative. In this case, a bridging HB (representative unit cell and molecular models are shown in Figure 21) has been observed. The

superstructure is characterized by aggregates, whose arrangement is periodic and described by the unit cell: a^I=0.68±0.05 nm, b^I=1.71±0.05 nm and an angle β=65±1°. For comparison, the exact and closest-commensurate unit-cell with the HOPG is a^I=0.65 nm, b^I=1.77 nm and β = 65° (see SI of ref. 54 for details). If this phase is compared to the initial system (a=0.70 ± 0.05 nm, b=1.89 ± 0.05 nm and α=55 ± 1°), its orientation with respect to the underlying HOPG changes (see SI of ref. 54 for details) and the unit cells become smaller, noticeably along the alkyne axis, compatibly with a photoinduced hydrogen dissociation and C-C coupling.

Previous reports show that monomer solutions of aromatic acetylenes undergo UV-induced polymerization and coupling reactions that occur in low yield and with low specificity.[211] A test was performed in order to exclude the occurrence of the homocoupling reaction in solution (Figure 22). A solution of PEBA in 7COOH was irradiated ex-situ at 260 nm for 10 minutes and then checked at the STM. UV irradiations were performed both on relatively large volumes (500 µl) in a polypropylene (PP) vial, as a generic support and in control environments in which the same liquid-cell used for the irradiations on HOPG was equipped with generic soda-lime glass or PP to support the solution (15 µl) during the irradiation. The solution was checked with STM on HOPG before (Figure 22 middle panel, top) and after (Figure 22 middle panel, bottom) the irradiation. Only the irradiations performed on PP supports produced solutions suitable for the STM imaging, since considerable amounts of impurities made the imaging impossible when glass was used. In conclusion, after the ex situ UV treatment mostly PEBA molecules were observed (Figure 22 middle panel, bottom).

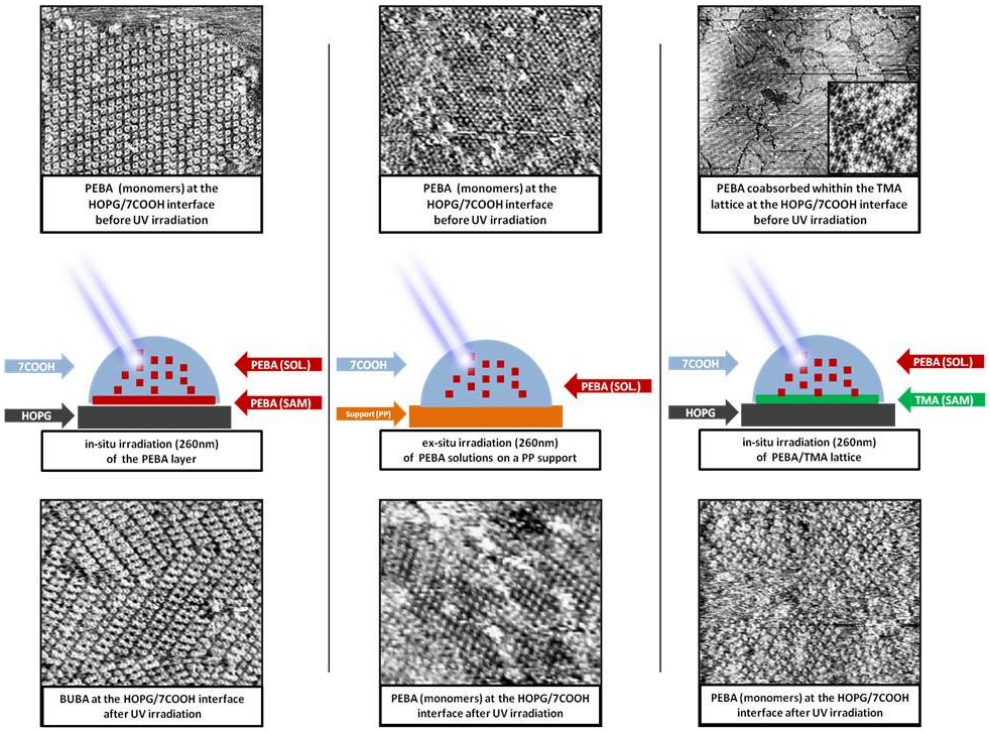

Figure 22. Schematic representation of the experiment in which a SAM of PEBA is irradiated on HOPG with a laser beam tuned at 260 nm (left), a sample in which PEBA solution is irradiated ex-situ (center) and a sample in which the UV irradiation is performed on a SAM of PEBA and TMA coadsorbed on HOPG (right). STM images: (left panel) topographic image of the as-deposited PEBA (top left, 20 nm × 20 nm) and after 5 min irradiation at 260 nm (bottom left, 20 nm × 20 nm); (middle panel) topographic image of the PEBA SAM at the HOPG/7COOH interface before the ex-situ irradiation of the solution (top center, 30 nm × 30 nm) and after the ex-situ irradiation (bottom center, 20 nm × 20 nm); (right panel) topographic image of the HOPG surface pre-covered with a TMA monolayer in co-deposition with PEBA (top right, 200 nm × 200 nm, insert depicts the TMA host-guest activity towards PEBA) and after 5 min irradiation at 260 nm (bottom right 20 nm × 20 nm).

The topochemical control of the HOPG-supported alkyne homocoupling was further corroborated by performing an experiment where the laser irradiation of a solution of PEBA (approx. 40 mM) occurred on the HOPG surface pre-covered with the porous benzene-1,3,5-tricarboxylic acid (TMA, approx 1 mM) monolayer (see Figure 22, right panel). In this system, the aforementioned pre-organization of PEBA is missing, as this molecule is less competitive toward the adsorption with respect to the tricarboxylic species. The codeposition of a solution of PEBA and TMA

in 7COOH favors TMA as the dominant on-surface aggregate. In this system the PEBA is mostly confined in solution, however, the TMA monolayer forms the well-known "chickenwire" and "honeycomb" networks,[78,100,118,119] both capable of host-guest activity towards PEBA molecules or other TMA in solution (see STM image in Figure 22 right panel, top, and bright spots in the chickenwire network, insert in Figure 22 right panel, top). PEBA is less competitive toward adsorption with respect to the tricarboxylic species, although small clusters could be observed among the boundaries of extended TMA domains (dark-regions in STM image in Figure 22 right panel, top). After the irradiation at 260 nm of this system (Figure 22 right panel, bottom), mostly PEBA molecules were observed at the interface. Dimers conversion was estimated to be less than 10%, while photo-induced degradation of the TMA monolayer occurred. Noteworthy, TMA has a non-zero absorbance at 260 nm[219] and its superstructure degradation presumably occurs by dissipating the absorbed energy. Finally, the coupling reaction occurred far less efficiently within an irradiated solution where the proper topological pre-organization of the monomers was missing or otherwise compromised, as when PEBA molecules are coadsorbed within the TMA lattice.

Other tests were also performed with 220, 240, 280, 300 nm on the preformed PEBA SAM (see results in SI of ref 54). Below 260 nm the system appeared disordered, presumably due to UV-induced degradation of both the organic solution and the overlayer. Above 260 nm the system was only partially affected, and most starting material could be found unaltered. In conclusion, the reaction was less efficient in terms of sample quality and product yield over time at wavelengths far from the maximum of the absorption peak, indicating that a direct molecular excitation is needed for the coupling activation. Once the proper reaction conditions were established, the irradiation at 260 nm showed the highest rate and quality of product conversion with high reproducibility.

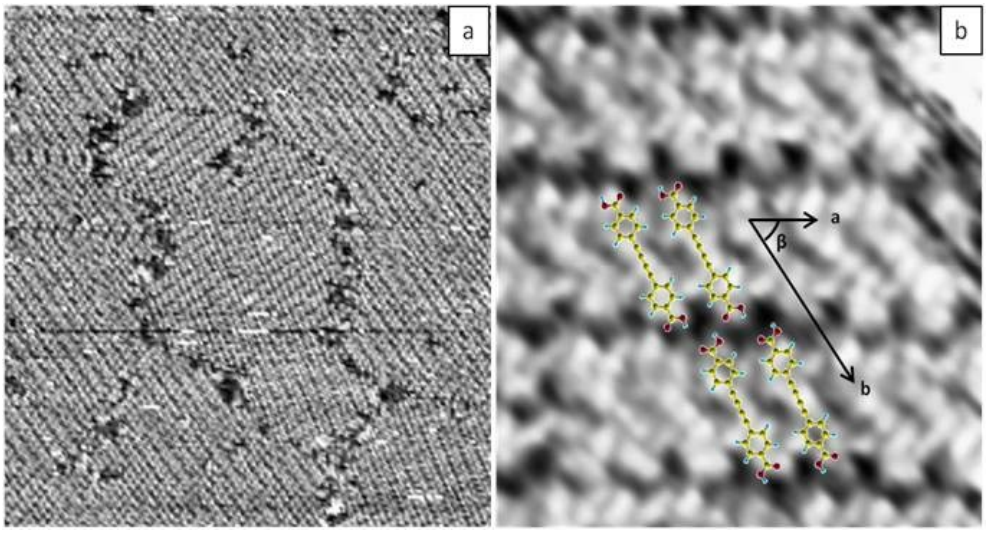

Figure 23. (a) Topographic STM image (50 nm × 50 nm) of the self assembled structure of the ex situ synthesized bis-acetylenic dimer. (b) high resolution STM image (5nm × 5nm) of the self assembled structure of the ex situ synthesized PEBA dimer.

To further corroborate the successful photo-induced reaction, the bis-acetylenic dimer has been synthesized ex-situ with a Cu-catalyzed solution-reaction (see synthesis in SI of ref 54). Synthetic dimers have been dissolved in 7COOH and deposited on the HOPG surface. By STM imaging in the same conditions, the synthetic products aggregated in islands whose dimensions were measured in the range 20-50 nm (Figure 23a). By high-resolution imaging, (Figure 23b) unit cell parameters could be obtained by averaging real-space measurements on five images. Vectors a = 0.67 ± 0.05 nm, b = 1.78 ± 0.05 nm, β = 63 ± 2° resulted similar to the BUBA SAM obtained in-situ. Finally, the wet-reaction product clearly showed the same STM contrast at the molecular level, resulting from a similar carboxylic-HB bridging phase, as it was found for the photochemically coupled PEBA products.

In conclusion, it is demonstrated that metal-free photochemical homocoupling occurs between terminal alkynes at the HOPG/liquid interface. This is obtained within a PEBA monomer SAM by exploiting

its pre-organization, i.e. the topological activation of the photochemical alkyne homocoupling.

The comparison of the self-assembly patterns produced by in-situ photo-reacted monomers and ex-situ synthesized dimers allowed to confirm the chemical nature of the photoreaction product. Also, the in-situ photochemical conversion proved to be faster and cleaner with respect to the wet synthesis (5 minutes versus days and several purification steps, for a complete synthetic route) and the reaction selectivity showed up in monodispersity, which is noteworthy, given the many by-products observed in various metal-catalyzed Glaser coupling reported so far and referenced above.

The successful C-C covalent stabilization is triggered by UV-light, it occurs catalyst-free and the substrate acts only as a template, favoring the proper molecular orientation upon the photon absorption event. The photo-induced mechanism occurred only with absorption-resonant irradiation, which in comparison with the metal-supported layer scenario[55] points toward a direct molecular excitation, in accordance with a weak coupling with the underlying substrate. Photochemical activation on the weakly interacting HOPG thus proves to yield higher reaction selectivity when compared with thermal activation mechanisms observed on metal substrates, which induce disordered intermolecular interactions and broaden the product distribution.

CONCLUSION AND OUTLOOK

In this work, the production and characterization of various on-surface supramolecular networks and of low-dimensional materials has been performed. The bottom-up fabrication of such surface-supported nanostructures allowed to detail their structure and dynamics with molecular precision. The study included the control over single and multiple-component pattern formation of molecules at surfaces by exploiting non-covalent interactions and metal coordination chemistry. The synthesis of such supramolecular systems confirmed that controlled self-assembly allows the production of predictable and well defined architectures which are highly interesting for nanotechnological applications such as catalysis, organic electronics and surface functionalization via nanopatterning.

Scanning Tunneling Microscopy (STM) and various other surface analysis techniques provided the necessary resolution for this studies in various conditions, including solid/liquid or air interfaces and Ultra High Vacuum (UHV). While the latter environment allowed a better control over the surface coverage and temperature, the solid/liquid interface proved to be the ideal environment for extended self-assembly under thermodynamic conditions. Particular attention has been devoted to the role of the substrate and to the medium from which the molecules have been absorbed on-surface. The proper design of the molecular building blocks allowed the spontaneous aggregation and the on-surface synthesis of organic and metal-organic molecular scaffolds by activating the precursors' reactivity by means of thermal energy and UV radiation.

Despite the increased activity in surface photochemistry in the last few decades,[25–28] much effort is still necessary to fully understand the intricate network of mechanisms that govern the interactions between light, the adsorbate and the substrate. Numerous experimental

advances in this field notwithstanding, predictive theories remain a challenge because of conceptual and numerical difficulties in describing accurately the dynamics of the excited states, although important advances are being made.[194] In any case, it is incontestable that by means of surface photochemistry it is possible to develop and fabricate new materials and chemicals, since photo-activated reactions open up new reaction pathways that are not accessible by other techniques. In addition, the dynamics of surface-supported photoreactions is interesting even on fundamental science grounds.

A major effort has been put on the photochemical excitation of different kinds of surface-supported precursors. In particular, direct photochemical excitation of aryl-alkynes, i.e. propynyl-benzene and ethynyl-benzoic acid derivatives,[54] in a HOPG-supported SAM both of which induced a C-H bond dissociation and site-specific C-C coupling between two neighboring molecules. The preferential methyl coupling in the first case is a consequence of a recombination of highly excited electronic states on the aryl-alkyne core, attaining an UV-induced propargylic-like pathway. In the second case, a straightforward metal-free terminal alkyne homocoupling is obtained between the monomers by exploiting the photochemical activation of pre-organized building blocks.

Despite this field of research still in its infancy, the study of the self-assembly properties of properly designed precursor molecules featuring alkyne groups proved to be a powerful approach for the production of covalent architectures and novel carbon-based nanomaterials. Nonetheless, the evidences for various possible reaction pathways open exciting routes towards the atom-precise fabrication of functional organic scaffolds mixing sp- to sp^3 -hybridized carbonaceous materials.

In order to understand and control the coupling mechanisms and possible side reactions it was mandatory to obtain high-quality starting scaffolds and much effort has been done in order to understand their

interfacial behavior. Given the successful demonstration of surface-templated or otherwise tailored reactions, it is possible to anticipate that coupling of terminal alkynes will emerge as an important reaction towards the fabrication of advanced covalent architectures, suitable for nanotechnological devices with tunable functional properties in the near future.

REFERENCES

(1) Ertl, G. Reactions at Surfaces: From Atoms to Complexity http://www.nobelprize.org/nobel_prizes/chemistry/laureates/2007/ertl-lecture.html.
(2) Christmann, K. *Surf. Sci. Rep.* **1988**, *9* (1–3), 1.
(3) Memmel, N. *Surf. Sci. Rep.* **1998**, *32* (3–4), 91.
(4) Lehn, J. M. *Angew. Chem. Int. Ed. Engl.* **1990**, *29* (11), 1304.
(5) Binning, G.; Rohrer, H.; Gerber, C.; Weibel, E. *Phys. Rev. Lett.* **1982**, *49* (1), 57.
(6) Furukawa, S.; De Feyter, S. *Top. Curr. Chem.* **2009**, *287*, 87.
(7) Elemans, J. A. A. W.; Lei, S.; De Feyter, S. *Angewandte Chemie - International Edition*. WILEY-VCH Verlag September 21, 2009, pp 7298–7333.
(8) Elemans, J. A. A. W.; Lei, S.; De Feyter, S. *Angewandte Chemie - International Edition*. 2009, pp 7298–7333.
(9) Hulsken, B.; Van Hameren, R.; Gerritsen, J. W.; Khoury, T.; Thordarson, P.; Crossley, M. J.; Rowan, A. E.; Nolte, R. J. M.; Elemans, J. A. A. W.; Speller, S. *Nat. Nanotechnol.* **2007**, *2* (5), 285.
(10) Yang, Y.; Wang, C. *Chem. Soc. Rev.* **2009**, *38* (9), 2576.
(11) Adisoejoso, J.; Tahara, K.; Lei, S.; Szabelski, P.; Rzysko, W.; Inukai, K.; Blunt, M. O.; Tobe, Y.; De Feyter, S. *ACS Nano* **2012**, *6* (1), 897.
(12) Marschall, M.; Reichert, J.; Weber-Bargioni, A.; Seufert, K.; Auwärter, W.; Klyatskaya, S.; Zoppellaro, G.; Ruben, M.; Barth, J. V. *Nat. Chem.* **2010**, *2* (2), 131.
(13) Lafferentz, L.; Eberhardt, V.; Dri, C.; Africh, C.; Comelli, G.; Esch, F.; Hecht, S.; Grill, L. *Nat. Chem.* **2012**, *4* (3), 215.
(14) Basagni, A.; Ferrighi, L.; Cattelan, M.; Nicolas, L.; Handrup, K.; Vaghi, L.; Papagni, A.; Sedona, F.; Valentin, C. Di; Agnoli, S.; Sambi, M. *Chem. Commun.* **2015**, *51* (63), 12593.
(15) Guan, C.-Z.; Wang, D.; Wan, L.-J. *Chem. Commun.* **2012**, *48* (24), 2943.
(16) Kissel, P.; Erni, R.; Schweizer, W. B.; Rossell, M. D.; King, B. T.; Bauer, T.; Götzinger, S.; Schlüter, A. D.; Sakamoto, J. *Nat. Chem.* **2012**, *4* (4), 287.
(17) Sakamoto, J.; Van Heijst, J.; Lukin, O.; Schlüter, A. D. *Angewandte Chemie - International Edition*. 2009, pp 1030–1069.
(18) Otero, G.; Biddau, G.; Sánchez-Sánchez, C.; Caillard, R.; López, M. F.; Rogero, C.; Palomares, F. J.; Cabello, N.; Basanta, M. A.; Ortega, J.; Méndez, J.; Echavarren, A. M.; Pérez, R.; Gómez-Lor, B.; Martín-Gago, J. A. *Nature* **2008**, *454* (7206), 865.
(19) Basagni, A.; Sedona, F.; Pignedoli, C. A.; Cattelan, M.; Nicolas, L.; Casarin, M.; Sambi, M. *J. Am. Chem. Soc.* **2015**, *137* (5), 1802.
(20) Sun, Q.; Cai, L.; Ma, H.; Yuan, C.; Xu, W. *ACS Nano* **2016**, *10* (7), 7023.

(21) Lafferentz, L.; Eberhardt, V.; Dri, C.; Africh, C.; Comelli, G.; Esch, F.; Hecht, S.; Grill, L. *Nat. Chem.* **2012**, *4* (3), 215.
(22) Ciesielski, A.; El Garah, M.; Haar, S.; Kovaříček, P.; Lehn, J.-M.; Samorì, P. *Nat. Chem.* **2014**, *6* (11), 1017.
(23) Marele, A. C.; Mas-Ballesté, R.; Terracciano, L.; Rodríguez-Fernández, J.; Berlanga, I.; Alexandre, S. S.; Otero, R.; Gallego, J. M.; Zamora, F.; Gómez-Rodríguez, J. M. *Chem. Commun. (Camb).* **2012**, *48* (54), 6779.
(24) Sedona, F.; Di Marino, M.; Sambi, M.; Carofiglio, T.; Lubian, E.; Casarin, M.; Tondello, E. *ACS Nano* **2010**, *4* (9), 5147.
(25) Roop, B. *J. Vac. Sci. Technol. A Vacuum, Surfaces, Film.* **1989**, *7* (3), 2121.
(26) Deming, T. J.; Novak, B. M. *J. Am. Chem. Soc.* **1992**, *114* (20), 7926.
(27) Guo, H.; Saalfrank, P.; Seideman, T. *Prog. Surf. Sci.* **1999**, *62* (7), 239.
(28) Zhu, X.-Y. *Surf. Sci.* **1997**, *390* (1), 224.
(29) Tahara, K.; Inukai, K.; Adisoejoso, J.; Yamaga, H.; Balandina, T.; Blunt, M. O.; De Feyter, S.; Tobe, Y. *Angew. Chemie Int. Ed.* **2013**, *52* (32), 8373.
(30) Browne, W. R.; Feringa, B. L. *Annu. Rev. Phys. Chem.* **2009**, *60*, 407.
(31) Ramamurthy, V.; Mondal, B. *J. Photochem. Photobiol. C Photochem. Rev.* **2015**, *23*, 68.
(32) van Delden, R. A.; ter Wiel, M. K. J.; Pollard, M. M.; Vicario, J.; Koumura, N.; Feringa, B. L. *Nature* **2005**, *437* (7063), 1337.
(33) Friend, C. M. *Chem. Rec.* **2014**, *14* (5), 944.
(34) Petrik, N. G.; Henderson, M. A.; Kimmel, G. A. *J. Phys. Chem. C* **2015**, *119* (22), 12273.
(35) Basagni, A.; Colazzo, L.; Sedona, F.; DiMarino, M.; Carofiglio, T.; Lubian, E.; Forrer, D.; Vittadini, A.; Casarin, M.; Verdini, A.; Cossaro, A.; Floreano, L.; Sambi, M. *Chemistry* **2014**, *20* (44), 14296.
(36) Deshpande, A.; Sham, C. H.; Alaboson, J. M. P.; Mullin, J. M.; Schatz, G. C.; Hersam, M. C. *J. Am. Chem. Soc.* **2012**, *134* (40), 16759.
(37) Zang, L.; Che, Y.; Moore, J. S. *Acc. Chem. Res.* **2008**, *41* (12), 1596.
(38) In't Veld, M.; Iavicoli, P.; Haq, S.; Amabilino, D. B.; Raval, R. *Chem. Commun.* **2008**, *15* (13), 1536.
(39) Sun, Q.; Cai, L.; Ma, H.; Yuan, C.; Xu, W. *Chem. Commun.* **2016**, *52* (35), 6009.
(40) Floris, A.; Haq, S.; In't Veld, M.; Amabilino, D. B.; Raval, R.; Kantorovich, L. *J. Am. Chem. Soc.* **2016**, *138* (18), 5837.
(41) Zhong, D.; Franke, J.-H.; Podiyanachari, S. K.; Blömker, T.; Zhang, H.; Kehr, G.; Erker, G.; Fuchs, H.; Chi, L. *Science* **2011**, *334* (6053), 213.
(42) Gao, H.-Y.; Wagner, H.; Zhong, D.; Franke, J.-H.; Studer, A.; Fuchs, H. *Angew. Chemie Int. Ed.* **2013**.
(43) Haley, M. M.; Brand, S. C.; Pak, J. J. *Angew. Chemie Int. Ed. English* **1997**, *36* (8), 836.

(44) Baughman, R. H.; Eckhardt, H.; Kertesz, M. *J. Chem. Phys.* **1987**, *87* (11), 6687.
(45) Li, Z.; Smeu, M.; Rives, A.; Maraval, V.; Chauvin, R.; Ratner, M. A.; Borguet, E. *Nat. Commun.* **2015**, *6*, 6321.
(46) Bieri, M.; Treier, M.; Cai, J.; Aït-Mansour, K.; Ruffieux, P.; Gröning, O.; Gröning, P.; Kastler, M.; Rieger, R.; Feng, X.; Müllen, K.; Fasel, R. *Chem. Commun. (Camb).* **2009**, No. 45, 6919.
(47) Zhang, Y.-Q.; Björk, J.; Weber, P.; Hellwig, R.; Diller, K.; Papageorgiou, A. C.; Oh, S. C.; Fischer, S.; Allegretti, F.; Klyatskaya, S.; Ruben, M.; Barth, J. V.; Klappenberger, F. *J. Phys. Chem. C* **2015**, *119* (17), 9669.
(48) Björk, J.; Zhang, Y. Q.; Klappenberger, F.; Barth, J. V.; Stafström, S. *J. Phys. Chem. C* **2014**, *118* (6), 3181.
(49) Eichhorn, J.; Heckl, W. M.; Lackinger, M. *Chem. Commun. (Camb).* **2013**, *49* (28), 2900.
(50) Liu, J.; Ruffieux, P.; Feng, X.; Müllen, K.; Fasel, R. *Chem. Commun. (Camb).* **2014**, *50* (76), 11200.
(51) Liu, J.; Chen, Q.; Xiao, L.; Shang, J.; Zhou, X.; Zhang, Y.; Wang, Y.; Shao, X.; Li, J.; Chen, W.; Xu, G. Q.; Tang, H.; Zhao, D.; Wu, K. *ACS Nano* **2015**, 150522152745007.
(52) Cirera, B.; Zhang, Y.-Q.; Klyatskaya, S.; Ruben, M.; Klappenberger, F.; Barth, J. V. *ChemCatChem* **2013**, *5* (11), 3281.
(53) Gao, H.-Y.; Wagner, H.; Zhong, D.; Franke, J.-H.; Studer, A.; Fuchs, H. *Angew. Chem. Int. Ed. Engl.* **2013**, *52* (14), 4024.
(54) Colazzo, L.; Sedona, F.; Moretto, A.; Casarin, M.; Sambi, M. *J. Am. Chem. Soc.* **2016**, *138* (32), 10151.
(55) Gao, H. Y.; Zhong, D.; Mönig, H.; Wagner, H.; Held, P. A.; Timmer, A.; Studer, A.; Fuchs, H. *J. Phys. Chem. C* **2014**, *118* (12), 6272.
(56) Song, W.; Martsinovich, N.; Heckl, W. M.; Lackinger, M. *J. Am. Chem. Soc.* **2013**, *135* (39), 14854.
(57) Favaro, M.; Ferrighi, L.; Fazio, G.; Colazzo, L.; Di Valentin, C.; Durante, C.; Sedona, F.; Gennaro, A.; Agnoli, S.; Granozzi, G. *ACS Catal.* **2015**, *5* (1), 129.
(58) El Habra, N.; Visentin, F.; Gerbasi, R.; Favaro, M.; Natile, M. M.; Colazzo, L.; Sambi, M. *Phys. status solidi* **2015**, *212* (7), 1588.
(59) Zanatta, M.; Calvillo, L.; Zheng, J.; Rizzi, G. A.; Durante, C.; Giallongo, G.; Chirkov, D.; Colazzo, L.; Marega, C.; Gennaro, A.; Granozzi, G. *Thin Solid Films* **2016**, *603*, 193.
(60) Favaro, M.; Carraro, F.; Cattelan, M.; Colazzo, L.; Durante, C.; Sambi, M.; Gennaro, A.; Agnoli, S.; Granozzi, G. *J. Mater. Chem. A* **2015**, *3* (27), 14334.
(61) Sedona, F.; Di Marino, M.; Basagni, A.; Colazzo, L.; Sambi, M. *J. Phys. Chem. C* **2014**, *118* (3), 1587.
(62) Horcas, I.; Fernández, R.; Gómez-Rodríguez, J. M.; Colchero, J.; Gómez-Herrero, J.; Baro, A. M. *Rev. Sci. Instrum.* **2007**, *78* (1), 13705.
(63) Geim, A. K.; Novoselov, K. S. *Nat. Mater.* **2007**, *6* (3), 183.
(64) Teyssandier, J.; Battaglini, N.; Seydou, M.; Anquetin, G.; Diawara,

B.; Sun, X.; Maurel, F.; Lang, P. *J. Phys. Chem. C* **2013**, *117* (17), 8737.
(65) den Boer, D.; Li, M.; Habets, T.; Iavicoli, P.; Rowan, A. E.; Nolte, R. J. M.; Speller, S.; Amabilino, D. B.; De Feyter, S.; Elemans, J. A. A. W. *Nat. Chem.* **2013**, *5* (7), 621.
(66) Floreano, L.; Naletto, G.; Cvetko, D.; Gotter, R.; Malvezzi, M.; Marassi, L.; Morgante, A.; Santaniello, A.; Verdini, A.; Tommasini, F.; Tondello, G. *Rev. Sci. Instrum.* **1999**, *70* (10), 3855.
(67) Jona, F.; Marcus, P. M. Springer Berlin Heidelberg, 1988; pp 90–99.
(68) Brune, H. *Surf. Sci. Rep.* **1998**, *31* (4–6), 125.
(69) Brune, H.; Romainczyk, C.; Röder, H.; Kern, K. *Nature* **1994**, *369* (6480), 469.
(70) Röder, H.; Hahn, E.; Brune, H.; Bucher, J.-P.; Kern, K. *Nature* **1993**, *366* (6451), 141.
(71) Venables, J. A.; Spiller, G. D. T.; Hanbucken, M. *Reports Prog. Phys.* **1984**, *47* (4), 399.
(72) Klappenberger, F.; Cañas-Ventura, M. E.; Clair, S.; Pons, S.; Schlickum, U.; Qu, Z. R.; Strunskus, T.; Comisso, A.; Wöll, C.; Brune, H.; Kern, K.; De Vita, A.; Ruben, M.; Barth, J. V. *ChemPhysChem* **2008**, *9* (17), 2522.
(73) Bieri, M.; Nguyen, M. T.; Gröning, O.; Cai, J.; Treier, M.; Aït-Mansour, K.; Ruffieux, P.; Pignedoli, C. A.; Passerone, D.; Kastler, M.; Müllen, K.; Fasel, R. *J. Am. Chem. Soc.* **2010**, *132* (46), 16669.
(74) Ramoino, L.; Von Arx, M.; Schintke, S.; Baratoff, A.; Güntherodt, H. J.; Jung, T. A. *Chem. Phys. Lett.* **2006**, *417* (1–3), 22.
(75) Ahmad Zebari, A. A.; Kolmer, M.; Prauzner-Bechcicki, J. S. *Appl. Surf. Sci.* **2015**, *332*, 403.
(76) Wagner, S. R.; Huang, B.; Park, C.; Feng, J.; Yoon, M.; Zhang, P. *Phys. Rev. Lett.* **2015**, *115* (9), 96101.
(77) Sirtl, T.; Song, W.; Eder, G.; Neogi, S.; Schmittel, M.; Heckl, W. M.; Lackinger, M. *ACS Nano* **2013**, *7* (8), 6711.
(78) Kampschulte, L.; Lackinger, M.; Maier, A.-K.; Kishore, R. S. K.; Griessl, S.; Schmittel, M.; Heckl, W. M. *J. Phys. Chem. B* **2006**, *110* (22), 10829.
(79) Cincotti, S.; Rabe, J. P. *Appl. Phys. Lett.* **1993**, *62* (26), 3531.
(80) McGonigal, G. C.; Bernhardt, R. H.; Thomson, D. J. *Appl. Phys. Lett.* **1990**, *57* (1), 28.
(81) Hamers, R. J.; Tromp, R. M.; Demuth, J. E. *Phys. Rev. B* **1986**, *34* (8), 5343.
(82) Mitsui, T.; Takayanagi, K. *Phys. Rev. B - Condens. Matter Mater. Phys.* **2000**, *62* (24), R16251.
(83) Giesen, M. *Prog. Surf. Sci.* **2001**, *68* (1–3), 1.
(84) Barth, J. V. *Surf. Sci. Rep.* **2000**, *40* (3), 75.
(85) Rost, M. J.; Crama, L.; Schakel, P.; Van Tol, E.; Van Velzen-Williams, G. B. E. M.; Overgauw, C. F.; Ter Horst, H.; Dekker, H.; Okhuijsen, B.; Seynen, M.; Vijftigschild, A.; Han, P.; Katan, A. J.; Schoots, K.; Schumm, R.; Van Loo, W.; Oosterkamp, T. H.; Frenken, J. W. M. *Rev. Sci. Instrum.* **2005**, *76* (5), 53710.

(86) Eigler, D. M. *Nature* **1991**, *352*.
(87) Schaffert, J.; Cottin, M. C.; Sonntag, A.; Karacuban, H.; Bobisch, C. A.; Lorente, N.; Gauyacq, J.-P.; Möller, R. *Nat. Mater.* **2012**, *12* (3), 223.
(88) Feng, M.; Petek, H.; Shi, Y.; Sun, H.; Zhao, J.; Calaza, F.; Sterrer, M.; Freund, H.-J. *ACS Nano* **2015**.
(89) Ulman, A. *Chem. Rev.* **1996**, *96* (4), 1533.
(90) Tully, J. C.; Muhlhausen, C. W.; Ruby, L. R. *Berichte der Bunsengesellschaft für Phys. Chemie* **1982**, *86* (5), 433.
(91) Kindt, J. T.; Tully, J. C.; Head-Gordon, M.; Gomez, M. A. *J. Chem. Phys.* **1998**, *109* (9), 3629.
(92) Nourtier, A. *J. Phys.* **1985**, *46* (1), 55.
(93) Sols, F.; García, N.; Flores, F. *Surf. Sci.* **1984**, *146* (2), L577.
(94) Tully, J. C. *Surf. Sci.* **1994**, *299*, 667.
(95) and, C. T. R.; Auerbach*, D. J.; Tully, J. C.; Kleyn, A. W. **1996**.
(96) Harris, J.; Kasemo, B. *Surf. Sci.* **1981**, *105* (2), L281.
(97) Tully, J. C. *Surf. Sci.* **1981**, *111* (3), 461.
(98) Head-Gordon, M.; Tully, J. C.; Rettner, C. T.; Mullins, C. B.; Auerbach, D. J. *J. Chem. Phys.* **1991**, *94* (2), 1516.
(99) Bagus, P. S.; Hermann, K.; Wöll, C. *J. Chem. Phys.* **2005**, *123* (18), 184109.
(100) MacLeod, J. M.; Lipton-Duffin, J. A.; Cui, D.; De Feyter, S.; Rosei, F. *Langmuir* **2015**, *31* (25), 7016.
(101) Di Marino, M.; Sedona, F.; Sambi, M.; Carofiglio, T.; Lubian, E.; Casarin, M.; Tondello, E. *Langmuir* **2010**, *26* (4), 2466.
(102) Brede, J.; Linares, M.; Kuck, S.; Schwöbel, J.; Scarfato, A.; Chang, S.-H.; Hoffmann, G.; Wiesendanger, R.; Lensen, R.; Kouwer, P. H. J.; Hoogboom, J.; Rowan, A. E.; Bröring, M.; Funk, M.; Stafström, S.; Zerbetto, F.; Lazzaroni, R. *Nanotechnology* **2009**, *20* (27), 275602.
(103) Buchner, F.; Kellner, I.; Hieringer, W.; Görling, A.; Steinrück, H.-P.; Marbach, H. *Phys. Chem. Chem. Phys.* **2010**, *12* (40), 13082.
(104) King, G. A.; Oliver, T. A. A.; Ashfold, M. N. R. *J. Chem. Phys.* **2010**, *132* (21), 214307.
(105) Hatch, S. R.; Zhu, X.-Y.; White, J. M.; Campion, A. *J. Chem. Phys.* **1990**, *92* (4), 2681.
(106) Gadzuk, J. W. *J. Chem. Phys.* **2012**, *137* (9), 91703.
(107) Basagni, A.; Colazzo, L.; Sedona, F.; DiMarino, M.; Carofiglio, T.; Lubian, E.; Forrer, D.; Vittadini, A.; Casarin, M.; Verdini, A.; Cossaro, A.; Floreano, L.; Sambi, M. *Chem. - A Eur. J.* **2014**, *20* (44), 14296.
(108) Lloyd, J. A.; Papageorgiou, A. C.; Fischer, S.; Oh, S. C.; Sa‡lam, Ö.; Diller, K.; Duncan, D. A.; Allegretti, F.; Klappenberger, F.; Stöhr, M.; Maurer, R. J.; Reuter, K.; Reichert, J.; Barth, J. V. *Nano Lett.* **2016**, *16* (3), 1884.
(109) de Jonge, J. J.; Ratner, M. a.; de Leeuw, S. W.; Simonis, R. O. *J. Phys. Chem. B* **2004**, *108*, 2666.
(110) Écija, D.; Auwärter, W.; Vijayaraghavan, S.; Seufert, K.; Bischoff,

F.; Tashiro, K.; Barth, J. V. *Angew. Chemie - Int. Ed.* **2011**, *50* (17), 3872.
(111) Browne, W. R.; Feringa, B. L. *Nat. Nanotechnol.* **2006**, *1* (1), 25.
(112) Balzani, V.; Credi, A.; Venturi, M. *ChemPhysChem*. WILEY-VCH Verlag February 1, 2008, pp 202–220.
(113) Wintjes, N.; Bonifazi, D.; Cheng, F.; Kiebele, A.; Stöhr, M.; Jung, T.; Spillmann, H.; Diederich, F. *Angew. Chemie - Int. Ed.* **2007**, *46* (22), 4089.
(114) Kudernac, T.; Lei, S.; Elemans, J. A. A. W.; De Feyter, S. *Chem. Soc. Rev.* **2009**, *38* (2), 402.
(115) Elemans, J. a a W.; Lei, S.; De Feyter, S. *Angew. Chem. Int. Ed. Engl.* **2009**, *48* (40), 7298.
(116) Kühne, D.; Klappenberger, F.; Krenner, W.; Klyatskaya, S.; Ruben, M.; Barth, J. V. *Proc. Natl. Acad. Sci. U. S. A.* **2010**, *107* (50), 21332.
(117) Klappenberger, F.; Zhang, Y.-Q.; Björk, J.; Klyatskaya, S.; Ruben, M.; Barth, J. V. *Acc. Chem. Res.* **2015**, *48* (7), 2140.
(118) Lackinger, M.; Griessl, S.; Heckl, W. M.; Hietschold, M.; Flynn, G. W. *Langmuir* **2005**, *21* (11), 4984.
(119) Griessl, S. J. H.; Lackinger, M.; Jamitzky, F.; Markert, T.; Hietschold, M.; Heckl, W. M. *J. Phys. Chem. B* **2004**, *108* (31), 11556.
(120) Schultz, M. J.; Zhang, X.; Unarunotai, S.; Khang, D.-Y.; Cao, Q.; Wang, C.; Lei, C.; MacLaren, S.; Soares, J. A. N. T.; Petrov, I.; Moore, J. S.; Rogers, J. A. *Proc. Natl. Acad. Sci. U. S. A.* **2008**, *105* (21), 7353.
(121) den Boer, D.; Han, G. D.; Swager, T. M. *Langmuir* **2014**, *30* (3), 762.
(122) Yang, Y.; Wang, C. *Curr. Opin. Colloid Interface Sci.* **2009**, *14* (2), 135.
(123) De Feyter, S.; Xu, H.; Mali, K. *Chimia (Aarau).* **2012**, *66* (1–2), 38.
(124) Thi Ngoc Ha, N.; Gopakumar, T. G.; Hietschold, M. *J. Phys. Chem. C* **2011**, *115* (44), 21743.
(125) Mali, K. S.; Schwab, M. G.; Feng, X.; Müllen, K.; De Feyter, S. *Phys. Chem. Chem. Phys.* **2013**, *15* (30), 12495.
(126) Klappenberger, F. *Prog. Surf. Sci.* **2014**, *89* (1), 1.
(127) Hwang, E.; Jung, S. J.; Kim, S.; Kim, D. H. *J. Phys. Chem. C* **2016**, *120* (27), 14742.
(128) Rochefort, A.; Wuest, J. D. *Langmuir* **2009**, *25* (1), 210.
(129) Vu, T. H.; Wandlowski, T. *J. Electroanal. Chem.* **2016**, *776*, 40.
(130) Steiner, T. *J. Chem. Soc. Perkin Trans. 2* **1995**, No. 7, 1315.
(131) Li, H.-Q.; Roscoe, S. G.; Lipkowski, J. *J. Solution Chem.* **2000**, *29* (10), 987.
(132) Li, H.-Q.; Roscoe, S. G.; Lipkowski, J. *J. Electroanal. Chem.* **1999**, *478* (1), 67.
(133) Kwon, Y. J.; Son, D. H.; Ahn, S. J.; Kim, M. S.; Kim, K. *J. Phys. Chem.* **1994**, *98* (34), 8481.
(134) Zelenay, P.; Waszczuk, P.; Dobrowolska, K.; Sobkowski, J. *Electrochim. Acta* **1994**, *39* (5), 655.
(135) Ikezawa, Y.; Sekiguchi, R.; Kitazume, T. *Electrochim. Acta* **1999**, *45*

(7), 1089.
(136) Lackinger, M.; Griessl, S.; Markert, T.; Jamitzky, F.; Heckl, W. M. *J. Phys. Chem. B* **2004**, *108* (36), 13652.
(137) Beyer, T.; Price, S. L. *J. Phys. Chem. B* **2000**, *104* (12), 2647.
(138) Ha, N. T. N.; Gopakumar, T. G.; Gutzler, R.; Lackinger, M.; Tang, H.; Hietschold, M. *J. Phys. Chem. C* **2010**, *114* (8), 3531.
(139) MacLeod, J. M.; Ivasenko, O.; Perepichka, D. F.; Rosei, F. *Nanotechnology* **2007**, *18* (42), 424031.
(140) Florio, G. M.; Stiso, K. A.; Campanelli, J. S. *J. Phys. Chem. C* **2012**, *116* (34), 18160.
(141) Dienstmaier, J. F.; Mahata, K.; Walch, H.; Heckl, W. M.; Schmittel, M.; Lackinger, M. *Langmuir* **2010**, *26* (13), 10708.
(142) Kittelmann, M.; Nimmrich, M.; Neff, J. L.; Rahe, P.; Greń, W.; Bouju, X.; Gourdon, A.; Kühnle, A. *J. Phys. Chem. C* **2013**, *117* (45), 23868.
(143) Hauke, C. M.; Bechstein, R.; Kittelmann, M.; Storz, C.; Kilbinger, A. F. M.; Rahe, P.; Kühnle, A. *ACS Nano* **2013**, *7* (6), 5491.
(144) Rahe, P.; Kittelmann, M.; Neff, J. L.; Nimmrich, M.; Reichling, M.; Maass, P.; Kühnle, A. *Adv. Mater.* **2013**, *25* (29), 3948.
(145) Sim, G. A.; Robertson, J. M.; Goodwin, T. H. *Acta Crystallogr.* **1955**, *8* (3), 157.
(146) Chen, Q.; Perry, C. C.; Frederick, B. G.; Murray, P. W.; Haq, S.; Richardson, N. V. *Surf. Sci.* **2000**, *446* (1–2), 63.
(147) Zhang, Y.-Q.; Kepčija, N.; Kleinschrodt, M.; Diller, K.; Fischer, S.; Papageorgiou, A. C.; Allegretti, F.; Björk, J.; Klyatskaya, S.; Klappenberger, F.; Ruben, M.; Barth, J. V. *Nat. Commun.* **2012**, *3*, 1286.
(148) Stepanow, S.; Strunskus, T.; Lingenfelder, M.; Dmitriev, A.; Spillmann, H.; Lin, N.; Barth, J. V.; Wöll, C.; Kern, K. *J. Phys. Chem. B* **2004**, *108* (50), 19392.
(149) McDonagh, A. M.; Zareie, H. M.; Ford, M. J.; Barton, C. S.; Ginic-Markovic, M.; Matisons, J. G. *J. Am. Chem. Soc.* **2007**, *129* (12), 3533.
(150) Wallart, X.; Henry de Villeneuve, C.; Allongue, P. *J. Am. Chem. Soc.* **2005**, *127* (21), 7871.
(151) Felter, T. E.; Weinberg, W. H.; Lastushkina, G. Y.; Boronin, A. I.; Zhdan, P. A.; Boreskov, G. K.; Hrbek, J. *Surf. Sci.* **1982**, *118* (3), 369.
(152) Arras, E.; Seitsonen, A. P.; Klappenberger, F.; Barth, J. V. *Phys. Chem. Chem. Phys.* **2012**, *14* (46), 15995.
(153) Njus, J. M.; Sandman, D. J.; Yang, L.; Foxman, B. M. *Macromolecules* **2005**, *38* (18), 7645.
(154) De Feyter, S.; Abdel-Mottaleb, M. M. S.; Schuurmans, N.; Verkuijl, B. J. V.; van Esch, J. H.; Feringa, B. L.; De Schryver, F. C. *Chem. - A Eur. J.* **2004**, *10* (5), 1124.
(155) Surin, M.; Samorì, P.; Jouaiti, A.; Kyritsakas, N.; Hosseini, M. W. *Angew. Chemie - Int. Ed.* **2007**, *46* (1–2), 245.
(156) Ciesielski, A.; Piot, L.; Samorì, P.; Jouaiti, A.; Hosseini, M. W. *Adv.*

Mater. **2009**, *21* (10–11), 1131.
(157) Mourran, A.; Ziener, U.; Möller, M.; Breuning, E.; Ohkita, M.; Lehn, J.-M. *Eur. J. Inorg. Chem.* **2005**, *2005* (13), 2641.
(158) Langner, A.; Tait, S. L.; Lin, N.; Rajadurai, C.; Ruben, M.; Kern, K. *Proc. Natl. Acad. Sci. U. S. A.* **2007**, *104* (46), 17927.
(159) Stepanow, S.; Strunskus, T.; Lingenfelder, M.; Dmitriev, A.; Spillmann, H.; Lin, N.; Barth, J. V.; Wöll, C.; Kern, K. *J. Phys. Chem. B* **2004**, *108* (50), 19392.
(160) Stepanow, S.; Lin, N.; Barth, J. V.; Kern, K. *J. Phys. Chem. B* **2006**, *110* (46), 23472.
(161) Tseng, T.-C.; Lin, C.; Shi, X.; Tait, S.; Liu, X.; Starke, U.; Lin, N.; Zhang, R.; Minot, C.; Van Hove, M.; Cerdá, J.; Kern, K. *Phys. Rev. B* **2009**, *80* (100), 1.
(162) Tersoff, J. *Phys. Rev. B* **1985**, *31* (2), 805.
(163) Giovanelli, L.; Ourdjini, O.; Abel, M.; Pawlak, R.; Fujii, J.; Porte, L.; Themlin, J.-M.; Clair, S. *J. Phys. Chem. C* **2014**, *118* (27), 14899.
(164) Bebensee, F.; Svane, K.; Bombis, C.; Masini, F.; Klyatskaya, S.; Besenbacher, F.; Ruben, M.; Hammer, B.; Linderoth, T. R. *Angew. Chemie Int. Ed.* **2014**, *53* (47), 12955.
(165) Bebensee, F.; Svane, K.; Bombis, C.; Masini, F.; Klyatskaya, S.; Besenbacher, F.; Ruben, M.; Hammer, B.; Linderoth, T. *Chem. Commun.* **2013**, *49* (81), 9308.
(166) Francis, J. T.; Hitchcock, A. P. *J. Phys. Chem.* **1992**, *96* (16), 6598.
(167) Lehmann, J.; Liang, B.; Solomon, D.; Lerotic, M.; Luizão, F.; Kinyangi, J.; Schäfer, T.; Wirick, S.; Jacobsen, C. *Global Biogeochem. Cycles* **2005**, *19* (1), n/a.
(168) Bebensee, F.; Svane, K.; Bombis, C.; Masini, F.; Klyatskaya, S.; Besenbacher, F.; Ruben, M.; Hammer, B.; Linderoth, T. *Chem. Commun.* **2013**, *49* (81), 9308.
(169) Abel, M.; Oison, V.; Koudia, M.; Porte, L. *Phys. Rev. B* **2008**, *77* (8), 85410.
(170) Liu, C.; Yang, B.; Tyo, E.; Seifert, S.; DeBartolo, J.; von Issendorff, B.; Zapol, P.; Vajda, S.; Curtiss, L. A. *J. Am. Chem. Soc.* **2015**, *137* (27), 8676.
(171) Schlickum, U.; Decker, R.; Klappenberger, F.; Zoppellaro, G.; Klyatskaya, S.; Ruben, M.; Silanes, I.; Arnau, A.; Kern, K.; Brune, H.; Barth, J. V. *Nano Lett.* **2007**, *7* (12), 3813.
(172) Stepanow, S.; Lin, N.; Payer, D.; Schlickum, U.; Klappenberger, F.; Zoppellaro, G.; Ruben, M.; Brune, H.; Barth, J. V.; Kern, K. *Angew. Chemie - Int. Ed.* **2007**, *46* (5), 710.
(173) Gambardella, P.; Stepanow, S.; Dmitriev, A.; Honolka, J.; de Groot, F. M. F.; Lingenfelder, M.; Gupta, S. Sen; Sarma, D. D.; Bencok, P.; Stanescu, S.; Clair, S.; Pons, S.; Lin, N.; Seitsonen, A. P.; Brune, H.; Barth, J. V.; Kern, K. *Nat. Mater.* **2009**, *8* (3), 189.
(174) Lewis, E. A.; Murphy, C. J.; Liriano, M. L.; Sykes, E. C. H. *Chem. Commun.* **2014**, *50* (8), 1006.
(175) Xi, M.; Bent, B. E. *J. Am. Chem. Soc.* **1993**, *115* (16), 7426.
(176) Fan, Q.; Wang, C.; Han, Y.; Zhu, J.; Hieringer, W.; Kuttner, J.; Hilt,

G.; Gottfried, J. M. *Angew. Chemie - Int. Ed.* **2013**, *52* (17), 4668.
(177) Grill, L.; Dyer, M.; Lafferentz, L.; Persson, M.; Peters, M. V.; Hecht, S. *Nat. Nanotechnol.* **2007**, *2* (11), 687.
(178) Lafferentz, L.; Eberhardt, V.; Dri, C.; Africh, C.; Comelli, G.; Esch, F.; Hecht, S.; Grill, L. *Nature Chemistry*. 2012, pp 215–220.
(179) Shi, K. J.; Yuan, D. W.; Wang, C. X.; Shu, C. H.; Li, D. Y.; Shi, Z. L.; Wu, X. Y.; Liu, P. N. *Org. Lett.* **2016**, *18* (6), 1282.
(180) Kittelmann, M.; Nimmrich, M.; Lindner, R.; Gourdon, A.; Kühnle, A. *ACS Nano* **2013**, *7* (6), 5614.
(181) Basagni, A.; Vasseur, G.; Pignedoli, C. A.; Vilas-Varela, M.; Peña, D.; Nicolas, L.; Vitali, L.; Lobo-Checa, J.; de Oteyza, D. G.; Sedona, F.; Casarin, M.; Ortega, J. E.; Sambi, M. *ACS Nano* **2016**, *10* (2), 2644.
(182) Vasseur, G.; Fagot-Revurat, Y.; Sicot, M.; Kierren, B.; Moreau, L.; Malterre, D.; Cardenas, L.; Galeotti, G.; Lipton-Duffin, J.; Rosei, F.; Di Giovannantonio, M.; Contini, G.; Fèvre, P. Le; Bertran, F.; Liang, L.; Meunier, V.; Perepichka, D. F. **2015**.
(183) Wang, S.; Wang, W.; Lin, N. *Phys. Rev. Lett.* **2011**, *106* (20), 206803.
(184) Glaser, C. *Berichte der Dtsch. Chem. Gesellschaft* **1869**, *2* (1), 422.
(185) Gao, H. Y.; Franke, J. H.; Wagner, H.; Zhong, D.; Held, P. A.; Studer, A.; Fuchs, H. *J. Phys. Chem. C* **2013**, *117* (36), 18595.
(186) Klappenberger, F.; Zhang, Y.-Q.; Björk, J.; Klyatskaya, S.; Ruben, M.; Barth, J. V. *Acc. Chem. Res.* **2015**, *48* (7), 2140.
(187) Li, Q.; Owens, J. R.; Han, C.; Sumpter, B. G.; Lu, W.; Bernholc, J.; Meunier, V.; Maksymovych, P.; Fuentes-Cabrera, M.; Pan, M. *Sci. Rep.* **2013**, *3*, 2102.
(188) Gao, H.-Y.; Wagner, H.; Zhong, D.; Franke, J.; Studer, A.; Fuchs, H. *Angew. Chemie Int. Ed.* **2013**, *52* (111), 4024.
(189) Gao, H. Y.; Franke, J. H.; Wagner, H.; Zhong, D.; Held, P. A.; Studer, A.; Fuchs, H. *J. Phys. Chem. C* **2013**, *117* (36), 18595.
(190) Gao, H. Y.; Held, P. A.; Knor, M.; Mück-Lichtenfeld, C.; Neugebauer, J.; Studer, A.; Fuchs, H. *J. Am. Chem. Soc.* **2014**, *136* (27), 9658.
(191) Cirera, B.; Zhang, Y. Q.; Björk, J.; Klyatskaya, S.; Chen, Z.; Ruben, M.; Barth, J. V.; Klappenberger, F. *Nano Lett.* **2014**, *14* (4), 1891.
(192) Zhu, X.-Y.; White, J. M. *J. Chem. Phys.* **1991**, *94* (2), 1555.
(193) Zhou, X.-L.; Zhu, X.-Y.; White, J. M. *Surf. Sci. Rep.* **1991**, *13* (3–6), 73.
(194) Tognolini, S.; Ponzoni, S.; Sedona, F.; Sambi, M.; Pagliara, S. *J. Phys. Chem. Lett.* **2015**, *6* (18), 3632.
(195) Stein, S. E.; Walker, J. A.; Suryan, M. M.; Fahr, A. *Symp. Combust.* **1991**, *23* (1), 85.
(196) Tang, W.; Tranter, R. S.; Brezinsky, K. *J. Phys. Chem. A* **2005**, *109* (27), 6056.
(197) Ni, C.-K.; Huang, J. D.; Chen, Y. T.; Kung, A. H.; Jackson, W. M. *J. Chem. Phys.* **1999**, *110* (7), 3320.
(198) Mali, K. S.; Lava, K.; Binnemans, K.; De Feyter, S. *Chem. - A Eur. J.*

2010, *16* (48), 14447.
(199) Zhang, H.; Gong, Z.; Sun, K.; Duan, R.; Ji, P.; Li, L.; Li, C.; Müllen, K.; Chi, L. *J. Am. Chem. Soc.* **2016**, jacs. 6b05597.
(200) Wei, Y.; Kannappan, K.; Flynn, G. W.; Zimmt, M. B. *J. Am. Chem. Soc.* **2004**, *126* (16), 5318.
(201) Elemans, J. A. A. W.; De Cat, I.; Xu, H.; De Feyter, S. *Chem. Soc. Rev.* **2009**, *38* (3), 722.
(202) Taki, S.; Kadotani, T.; Kai, S. *J. Phys. Soc. Japan* **1999**, *68* (4), 1286.
(203) Tahara, K.; Furukawa, S.; Uji-i, H.; Uchino, T.; Ichikawa, T.; Zhang, J.; Mamdouh, W.; Sonoda, M.; De Schryver, F. C.; De Feyter, S.; Tobe, Y. *J. Am. Chem. Soc.* **2006**, *128* (51), 16613.
(204) Taki, S.; Okabe, H.; Kai, S. *Jpn. J. Appl. Phys.* **2003**, *42* (Part 1, No. 11), 7053.
(205) Smith, D. P. E.; Hörber, J. K. H.; Binnig, G.; Nejoh, H. *Nature* **1990**, *344* (6267), 641.
(206) Ilan, B.; Florio, G. M.; Hybertsen, M. S.; Berne, B. J.; Flynn, G. W. *Nano Lett.* **2008**, *8* (10), 3160.
(207) Groszek, A. J. *Proc. R. Soc. A Math. Phys. Eng. Sci.* **1970**, *314* (1519), 473.
(208) Ishii, F.; Matsunami, S.; Shibata, M.; Kakuchi, T. *Polym. J.* **1999**, *31* (1), 84.
(209) Qadiri, R. H.; Feltham, E. J.; Hendrik Nahler, N.; Pérez García, R.; Ashfold, M. N. R. *J. Chem. Phys.* **2003**, *119* (24), 12842.
(210) Miller, J. A.; Klippenstein, S. J. *J. Phys. Chem. A* **2003**, *107* (39), 7783.
(211) Rohde, O.; Wegner, G. *Die Makromol. Chemie* **1978**, *179* (8), 2013.
(212) Sohn, Y.; Wei, W.; White, J. M. *J. Phys. Chem. C* **2008**, *112* (47), 18531.
(213) Suzuki, H.; Yamada, T.; Kamikado, T.; Okuno, Y.; Mashiko, S. *J. Phys. Chem. B* **2005**, *109* (27), 13296.
(214) Arras, E.; Seitsonen, A. P.; Klappenberger, F.; Barth, J. V. *Phys. Chem. Chem. Phys.* **2012**, *14* (46), 15995.
(215) MacLeod, J. M.; Lipton-Duffin, J. A.; Cui, D.; De Feyter, S.; Rosei, F. *Langmuir* **2015**, *31* (25), 7016.
(216) Lipton-Duffin, J. A.; Ivasenko, O.; Perepichka, D. F.; Rosei, F. *Small* **2009**, *5* (5), 592.
(217) Baker, K. N.; Fratini, A. V.; Resch, T.; Knachel, H. C.; Adams, W. W.; Socci, E. P.; Farmer, B. L. *Polymer (Guildf).* **1993**, *34* (8), 1571.
(218) Kley, C. S.; Čechal, J.; Kumagai, T.; Schramm, F.; Ruben, M.; Stepanow, S.; Kern, K. *J. Am. Chem. Soc.* **2012**, *134* (14), 6072.
(219) Lawrence, F. A. *Anal. Chem.* **1951**, *23* (12), 1882.

COMMUNICATIONS AT CONFERENCES

Colazzo L., Sedona F., Moretto A., Casarin M., Sambi M.
XLIV Congresso Nazionale di Chimica Inorganica
Padova, Italy , September 14-17, 2016
Metal-Free Photochemical Homocoupling of HOPG-Supported Terminal Alkynes (oral communication)

Colazzo L., Sedona F., Moretto A., Casarin M., Sambi M.
On-Surface Synthesis: International workshop
San Sebastian, Spain , June 27-30, 2016
Metal-Free Photochemical Glaser Coupling of HOPG-Supported Terminal Alkynes (oral communication)

Basagni A., Colazzo L., Sedona F., di Marino M., Carofiglio T., Lubian E., Forrer D., Vittadin A., Casarin M., Verdini A., Cossaro A., Floreano L, Sambi M.
2nd Workshop on Surfaces, Interfaces and Functionalization Processes in Organic Compounds and Applications - SINFO II
Trieste, Italy June 25-27 2014
Laser induced covalent stabilization of Tetraphenylporphyrin derivatives on Ag(110) at the sub-monolayer level

Basagni A., Colazzo L., SedonaF.,di Marino M., Carofiglio T., Lubian E., Forrer D., Vittadin A., Casarin M., Verdini A., Cossaro A., Floreano L., Sambi M.
International Workshop "On-Surface Synthesis"
Ecole de Physique des Houches, France, May 25-30 2014
Laser induced covalent stabilization of Tetraphenylporphyrin derivatives on Ag(110) at the sub-monolayer level.

PUBLICATIONS

Colazzo L., Sedona F., Moretto A., Casarin M., Sambi M. On-surface photochemistry of pre-ordered 1-methyl-2-phenyl-acetylenes: photo-selective C-H bond activation and intermolecular coupling on HOPG (in preparation)

Merino-Diez N., Carbonell-Sanromà E., Corso M., Peña D., Colazzo L., Sedona F., Sambi M., Pascual J.I., de Oteyza D.G., Width-dependent energy gap in armchair graphene nanoribbons (in preparation)

Lo Cicero M., Della Pia A., Riello M., Colazzo L., Sedona F., Betti M. G, Sambi M., De Vita A., Mariani C. Copper tetrameric units embedded in a metal-organic structure on surfaces (submitted)

Colazzo L., Sedona F., Moretto A., Casarin M., Sambi M. Metal-Free on-Surface Photochemical Homocoupling of Terminal Alkynes. J. Am. Chem. Soc., 2016, 138, 10151–10156

Zanatta M., Calvillo L., Zheng J., Rizzi G.A., Durante C., Giallongo G., Chirkov D., Colazzo L., Marega C., Gennaro A., Granozzi G. Cu_2O/TiO_2 heterostructures on a DVD as easy&cheap photoelectrochemical sensors. Thin Solid Films, 2016, 603, 193-201

Favaro M., Carraro F., Cattelan M., Colazzo L., Durante C., Sambi M., Gennaro A., Agnoli S., Granozzi G. Multiple doping in graphene oxide foams and quantum dots: new switchable systems for oxygen reduction and water remediation. J. Mater. Chem. A, 2015, 3, 14334-14347

El Habra N., Visentin F., Gerbasi R., Favaro M., Natile M. M., Colazzo L., Sambi M. Co_3O_4/TiO_2 heterostructures obtained by hybrid method. Physica Status Solidi (a), 2015, 212, 7, 1588–1598

Favaro M., Ferrighi L., Fazio G., Colazzo L., Di Valentin C., Durante C., Sedona F., Gennaro A., Agnoli S., Granozzi G. Single and Multiple Doping in Graphene Quantum Dots: Unraveling the Origin of Selectivity in the Oxygen Reduction Reaction ACS Catal., 2015, 5 (1), 129–144

Basagni A., Colazzo L., Sedona F., Di Marino M., Carofiglio T., Lubian E., Forrer D., Vittadini A., Casarin M., Verdini A., Cossaro A., Floreano L., Sambi M.; StereoselectivePhotopolymerization of TetraphenylporphyrinDerivatives on Ag(110) at the Sub-Monolayer Level. Chem. Eur. J. 2014 20, 44, 14296–14304

Sedona F., Di Marino M., Basagni A., Colazzo L., Sambi M.; Structurally Tunable Self-Assembled 2D Cocrystals of C60 andPorphyrins on the Ag (110) Surface. J. Phys. Chem. C 2014, 118, 1587–1593

TEACHING EXPERIENCES

University of Padua, Italy, 2015-2016. Tutoring service (Courses and Lab. Assistant)

University of Padua, Italy, 2014-2015. Tutoring service (Courses and Lab. Assistant)

University of Padua, Italy, 2013-2014. Tutoring service (Lab. Assistant)

Progetto Lauree Scientifiche (PLS): 19-20/06/2014

SELECTED PUBLICATIONS

This section is dedicated the publications concerning the project of on-surface activation of chemical reaction performed during my Ph.D.. The first work is in advanced phase of preparation and is reported here only with its abstract. Most of its parts have been discussed in the main text of this thesis work.

On-surface photochemistry of pre-ordered 1-methyl-2-phenyl-acetylenes: photo-selective C-H bond activation and intermolecular coupling on HOPG

Luciano Colazzo,[*†‖] *Francesco Sedona,*[†] *Maurizio Casarin,*[†‖] *Mauro Sambi*[†§]

† Dipartimento di Scienze Chimiche, Università di Padova, Via Marzolo 1, 35131 Padova (Italy)

‖ CNR-IENI, Via Marzolo 1, 35131 Padova (Italy)

§ Consorzio INSTM, Unità di Ricerca di Padova, Via Marzolo 1, 35131 Padova (Italy)

ABSTRACT

On-surface photochemical synthesis involving the coupling of alkynes affords the production of covalent organic assemblies, which are promising in the production of functional interfaces. Generally, the coupling of alkynes takes place by thermal activation of molecular precursors on metal surfaces. However, the interaction of alkynes with surface metal atoms often induces unwanted reaction pathways when thermal energy is provided to the system. In this contribution we report about light-induced metal-free coupling of propynylbenzene molecular units on highly oriented pyrolitic graphite (HOPG). The reaction occurs with high efficiency and selectivity within the self-assembled monolayer and leads to the generation of covalently coupled 1,5-hexadiyne derivatives. Such photochemical uncatalysed pathway represents an original approach in the field of topological C-C coupling at the solid/liquid interface

JACS
JOURNAL OF THE AMERICAN CHEMICAL SOCIETY

Article

pubs.acs.org/JACS

Metal-Free on-Surface Photochemical Homocoupling of Terminal Alkynes

Luciano Colazzo,[*,†,‡] Francesco Sedona,[*,†] Alessandro Moretto,[†] Maurizio Casarin,[†,‡] and Mauro Sambi[†,§]

[†]Dipartimento di Scienze Chimiche, Università di Padova, Via Marzolo 1, 35131 Padova, Italy

[‡]CNR-ICMATE, Via Marzolo 1, 35131 Padova, Italy

[§]Consorzio INSTM, Unità di Ricerca di Padova, Via Marzolo 1, 35131 Padova, Italy

Supporting Information

ABSTRACT: On-surface synthesis involving the homocoupling of aryl-alkynes affords the buildup of bisacetylene derivatives directly at surfaces, which in turn may be further used as ingredients for the production of novel functional materials. Generally, homocoupling of terminal alkynes takes place by thermal activation of molecular precursors on metal surfaces. However, the interaction of alkynes with surface metal atoms often induces unwanted reaction pathways when thermal energy is provided to the system. In this contribution we report about light-induced metal-free homocoupling of terminal alkynes on highly oriented pyrolitic graphite (HOPG). The reaction occurred with high efficiency and selectivity within a self-assembled monolayer (SAM) of aryl-alkynes and led to the generation of large domains of ordered butadiynyl derivatives. Such a photochemical uncatalyzed pathway represents an original approach in the field of topological C−C coupling at the solid/liquid interface.

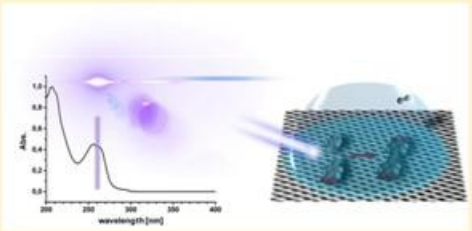

INTRODUCTION

On-surface coupling of simple molecular precursors has been widely exploited for the production of molecular superstructures with tunable electronic and mechanical properties.[1−4] Several chemical reactions have been tested on different surfaces, mostly metal substrates, that have shown catalytic activity for reactions that hardly take place in solution.[5,6] Ullman coupling of aryl-halides,[4,7] dehydration of boronic acid,[8] C−H bond activation processes,[9] and azyde-alkyne cycloaddition[10] are only a few examples of the extended literature on this matter.

Recently, on-surface terminal alkyne homocoupling, commonly (if somewhat improperly) referred to as Glaser coupling,[11,12] gained growing interest as a result of its exploitation to produce sp- and sp^2-hybridized nanomaterials.[13−15] Alkyne homocoupling is a well-known chemical reaction taking place both in solution, by metals-catalysis,[16−20] and on-surface. As far as the on-surface synthesis is concerned, it is well-known that this reaction occurs on low Miller index Cu,[21] Ag,[22] and Au[23] surfaces by providing heat to the organic monolayers. However, the strong adsorbate−substrate interaction often induces unwanted side-reactions (cyclotrimerizations,[23,24] generation of metal−organic species,[25] and oligomers cross-linking[26]), which accompany the homocoupling.[22] These side-reactions frequently inhibit the production of extended and regular nanostructures so that the real challenge still remains to take control of the many possible reaction pathways. Besides the use of templating substrates[27] or the adoption of steric hindering groups,[22] promising approaches to overcome this limit rely on nonthermal activation processes of supported alkynes. Gao et al.[28] reported the photochemical coupling of aryl-alkynes on Ag(111), aiming at their on-surface photopolymerization. However, after several hours of UV irradiation, they were able to produce only short oligomers; moreover, the high surface diffusion barrier for the heaviest oligomers hindered a favorable intermolecular orientation under UV exposure. Furthermore, the reaction proved to be fairly insensitive to different wavelengths, thus indicating a possible indirect, i.e. substrate-mediated, molecular excitation.[29−32] The interaction between the alkyne group and the metallic substrate[33,34] certainly provides a rationale for this finding. Nevertheless, the actual role played by the substrate, essential for the occurrence and propagation of the on-surface reaction, or able to stray the mechanism from a straightforward C−C coupling into a multistep reaction pathway, has never been tackled from an experimental point of view.

Here we show that the photochemical, metal-free homocoupling of terminal alkynes (Scheme 1) readily occurs on highly oriented pyrolytic graphite (HOPG) with high efficiency and selectivity within a self-assembled monolayer (SAM) of aryl-alkynes. The reaction takes place at the solid/liquid interface

Received: April 7, 2016
Published: July 20, 2016

DOI: 10.1021/jacs.6b03589
J. Am. Chem. Soc. 2016, 138, 10151−10156

Scheme 1. Schematic Representation of the on-Surface Photochemical Homocoupling

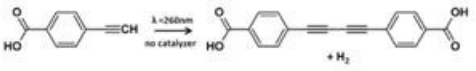

after short-time irradiation at the molecular precursor UV-resonant absorption wavelengths, eventually leading to the specific formation of butadiynyl derivatives.

Within the solid/liquid environment, the low activation barrier for the alkyne on-surface diffusion on the HOPG surface provides interfacial dynamics that possibly favors an appropriate intermolecular orientation upon the photon absorption event. In this view, the reduced or nearly absent photoconversion of the starting material with off-resonant wavelengths (irradiation wavelength out of the molecular UV-absorption band) ultimately testifies a direct molecular photoexcitation rather than a substrate-mediated mechanisms.[35,36] The experimental outcomes herein reported are consistent with a photoinduced topological C−C coupling at the solid/liquid interface. A single reaction product has been isolated and characterized in situ. The successful alkyne homocoupling reaction has been further confirmed by carrying out the same reaction ex-situ (in solution) and comparing the obtained products with the photochemically coupled precursors. Both the initial and the final molecular products and the ex-situ synthesized molecules were imaged by means of scanning tunneling microscopy (STM).

METHODS

In this study, the terminal alkyne of interest is a small π-system, namely 4-ethynylbenzoic (para-ethynylbenzoic) acid, hereafter called PEBA, purchased by Sigma-Aldrich and used without further purification. STM analysis at the solid/liquid interface has been carried out by preliminarily dissolving the reagent molecules in heptanoic acid (hereafter, 7COOH) at a concentration of 2.0 mg/g. A 5−15 μL droplet of solution was used for the observation of the interfacial behavior of the solute at the solid/liquid interface (see SI for further details).

Ex-situ synthesized molecules (4,4′-di(1,4-buta-1,3-diynyl)-benzoic acid (hereafter BUBA; see SI for the synthesis) where prepared for comparison with the photochemical reaction product and were analyzed under the same experimental conditions by using solutions at the same concentration.

Surface preparation was performed by scotch tape cleaving of the HOPG surface, and the surface cleaning was accurately checked prior to each deposition of the PEBA solution. Relatively clean and stable samples were obtained by drop-casting the solution at RT. Samples remained unaltered for several days, albeit, to limit contamination and solvent evaporation, STM investigations were performed just after the completion of the drop-casting process (see SI for further details). By using a tunable laser source we studied the behavior of our system at several wavelengths. The monochromatic light source used in this experiment was a tunable Nd:YAG laser system NT342A-SH (EKSPLA) equipped with an optical parametric oscillator (OPO). The output energy at the 260 nm wavelength was 1.71 mJ, pulse frequency 30 Hz, and pulse width 3.9 ns (see SI for further details).

RESULTS AND DISCUSSION

Drop-casting of a solution of PEBA in 7COOH on the HOPG surface produces a self-assembled and stable monolayer. Figure 1a shows a representative image of a 2D ordered aggregate of PEBA molecules. Islands, whose dimensions vary in the range 20−40 nm, are organized in symmetry-equivalent domains, according to the main directions of the underlying substrate

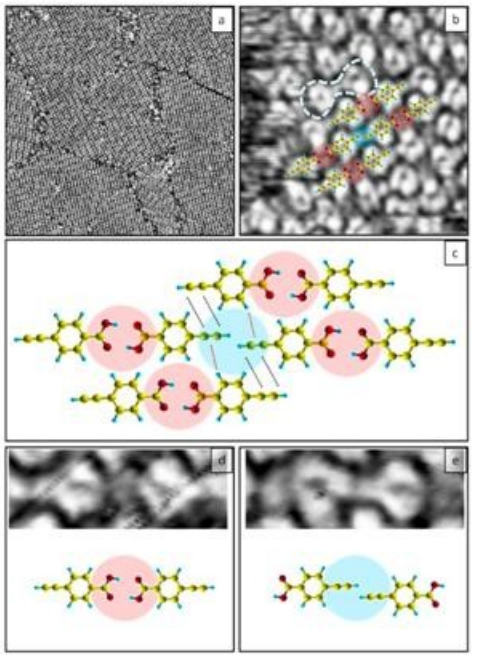

Figure 1. (a) Topographic (−0.70 V, 35 pA, 50 nm × 50 nm) and (b) high resolution STM image (−0.70 V, 35 pA, 5 nm × 5 nm) of the self-assembled structure of PEBA; (c) proposed ball and stick model of the PEBA supramolecular interaction network; (d) small-scale STM images of the carboxylic HB interaction and its corresponding proposed ball and stick model; (e) collinear alkyne interaction contrast feature and its corresponding proposed ball and stick model. See text for dashed and dotted lines and for red-/blue-shaded areas.

and show close-packed molecular building blocks. By high resolution STM imaging (Figure 1b), it is possible to observe that the superstructure is dominated by apparently dimeric species formed by two ring-like pairs interconnected by a bright feature, as outlined by the dashed line in Figure 1b. We propose that the observed dimers are composed of intact and flat-lying physisorbed PEBA molecules, with ring features corresponding to the benzene rings.[37] However, the labeling of the functional groups of the dimers remains not trivial.

PEBA molecules are heterofunctionalized with an ethynyl end-group and a carboxylic group pointing apart on a benzene ring (see superposition models in Figure 1b; shaded areas are a guide for the eye). Figure 1c (cf. shaded areas in Figure 1b) shows how the supramolecular order of PEBA molecules can be explained in terms of intermolecular hydrogen-bond (HB) networks. In more detail, two collinear hydrogen-bonded carboxylic groups (highlighted in red in Figure 1c) and their cooperative interactions with the nearest neighbor (NN) aromatic systems[38,39] provide a necessarily stabilizing interaction mesh. On the other hand, the collinear accommodation of the terminal alkynes (highlighted in blue in Figure 1c) is maintained by the stabilizing interaction of parallel alkyne groups involved in a 2-fold cyclic HB (C≡C−H···C≡C, see double-dotted lines in Figure 1c),[24,40] that sides with the

DOI: 10.1021/jacs.6b03589
J. Am. Chem. Soc. 2016, 138, 10151−10156

intermolecular interaction with their NN aromatic systems (dotted lines in Figure 1c).

According to recent investigations,[41,42] and in comparison with other reports of STM imaging regarding benzene-carboxylic acids,[43−46] the carboxylate groups appear darker with respect to the aromatic core for a combination of topographical and electronic effects around the negatively charged oxygens.[41] On this basis, we tentatively assign the dark area between the two rings to the HB between the collinear carboxylic groups (Figure 1d), while the aforementioned bright interconnection feature is ascribed to the alkyne end-groups approaching in a quasi-linear fashion, as depicted in Figure 1e.

In Figure 2a a high resolution image of ordered HB-dimers is shown: short black arrows, pointing toward the alkyne groups,

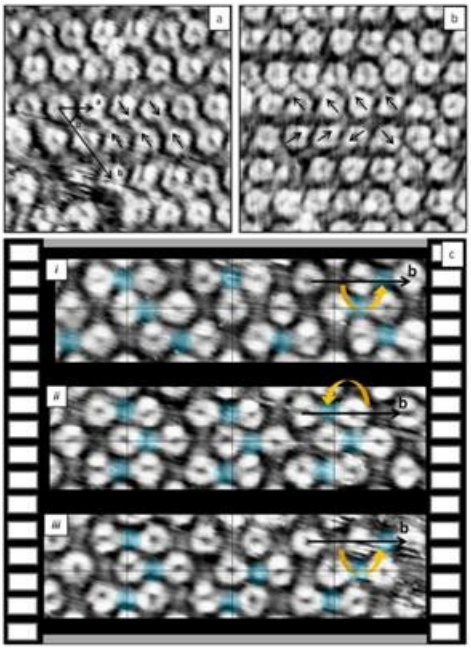

Figure 2. (a) STM image (−0.70 V, 25 pA, 5 nm × 5 nm) of an ordered aggregate of PEBA. (b) High resolution STM image (−0.40 V, 10 pA, 5 nm × 5 nm) of a disordered aggregate of PEBA. (c) Representative cartoon-clips for the observed on-surface dynamics over a selected area. Arrows and blue highlights are guides for the eye.

have been used to indicate molecular orientations. The ordered overlayer is reproduced by a unit-cell containing two molecules, whose parameters are a = 0.74 ± 0.05 nm, b = 1.89 ± 0.05 nm, and α = 55 ± 1°. These values have been obtained by averaging the real space measurements on five STM images, while, by high resolution imaging wherein both the substrate and the overlayer are present (SI, Figure S2a), the exact calibration of the molecular unit-cell based on the known size of the substrate lattice (0.264 nm) resulted in a = 0.74 nm, b = 1.86 nm, and α = 53° (see discussion in SI).

Along the overlayer vector b (see Figure 2a), a distance of 0.95 ± 0.05 nm is obtained as center-to-center distance for two phenyl rings interacting by carboxylic-HBs, while the distance between neighboring alkyne edges is 0.91 ± 0.05 nm. The former is consistent with the 0.96 ± 0.01 nm value found experimentally for the center-to-center distance between two NN terephtalic acid (TPA) molecules.[47] It is noteworthy that also vector a is reasonably consistent with the intermolecular distances found for TPA along the same packing direction (0.78 ± 0.01 nm). The NN alkyne−alkyne distance is also in reasonable agreement with the literature value of 0.80 ± 0.10 nm found experimentally for the 1,4-diethynylbenzene SAM on Cu.[24]

Alongside with the ordered 2D aggregates, also randomly oriented monomers have been observed (Figure 2b). These coexist in the PEBA SAM, where the aforementioned HB interaction network is involved in a dynamic-exchange equilibrium. Both tip-induced perturbations and the liquid environment can provide the driving forces for energetically accessible libration modes and discrete azimuthal rotations. These phenomena are reported in Figure 2c, as successive cartoon-clips (the alkyne end-groups have been highlighted in blue, and a grid has been added as a guide for the easy detection of the alkyne positions in different clips). Incidentally, also the complete rotation (two successive 180° on-site leaps) of a PEBA monomer has been detected (see yellow arrow in Figure 2c(i), (ii), (iii). Interestingly, if vector b is selected in the starting frame, its direction and length never change during the rotation of the central molecule (original images are in SI, Figure S3a, and a tentative modelization is in SI, Figure S3b).

Dynamic phenomena at the solid/liquid interface are generally associated with the vertical mobility of adsorbed molecules, as the supernatant liquid is responsible for a substantial lowering of the desorption barrier with respect to the vacuum barrier.[47] The on-surface dynamic processes observed within the PEBA superstructure imply that the underlying substrate does not strongly influence the aggregation pattern of the absorbed monolayer, although both adsorption/desorption processes and pattern rearrangements are energetically accessible at RT.

Crystalline PEBA reveals thermal and UV-induced reactivity. In the solid state, the photopolymerization reaction is topochemically promoted by the proximity of adjacent molecules within the crystal lattice.[48] We therefore assumed that by taking advantage of the collinear displacement of neighboring alkynes on the HOPG surface, a topochemical homocoupling could be promoted photochemically. According to the UV−vis spectrum of a solution of PEBA, the absorption band of the aromatic core is in the 240−270 nm range (see SI for further details). In order to maximize the photon absorption events, the 260 nm wavelength, which is a local maximum in the absorption curve, has been selected for irradiation. Direct exposure of the liquid cell to the laser beam for relatively short times (5−10 min) induced a nearly complete and irreversible conversion of the PEBA monolayer, resulting in a new molecular building block organized in a new ordered superstructure.

Figure 3a, b and insets report large and small scale images of the HOPG-supported monolayer before and after the light treatment. On the large scale it is evident that, after the illumination, the SAM is characterized by a new superstructure formed by ordered rows of dimeric species that organize in alternating, symmetrically equivalent domains.

After the UV irradiation, except for a few isolated unreacted monomers, almost all the molecular building blocks are constituted by dimers that, in contrast with the pristine HB-

DOI: 10.1021/jacs.6b03589
J. Am. Chem. Soc. 2016, 138, 10151−10156

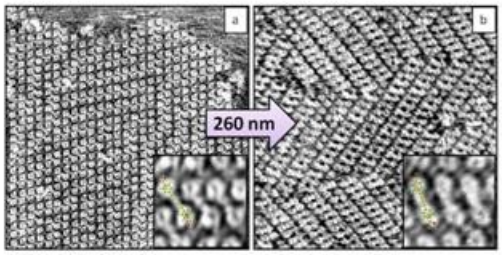

Figure 3. (a) Topographic STM image (−0.45 V, 10 pA, 20 nm × 20 nm) and (b) high resolution STM image (−0.30 V, 35 pA, 20 nm × 20 nm) after 5 min irradiation at 260 nm of the self-assembled PEBA superstructure. Insets are 2.5 nm × 2.5 nm close-ups of high resolution images obtained with similar tunneling conditions.

dimers, show no on-site rotations, suggesting the possible photoinduced stabilization of the molecular units with a chemical bond in the proposed butadiynyl derivative 4,4′-di(1,4-buta-1,3-diynyl)-benzoic acid, BUBA.

In the high resolution insets of Figure 3b it is also evident that the phenyl rings of BUBA are now connected by an intensified electronic density and the nodal plane observed in the pristine HB-dimers disappears. The center-to-center distance between the phenyl rings within an individual BUBA is 0.95 ± 0.05 nm, which is close to the distance found in the starting system, but nonetheless compatible with the 0.96 nm value obtained experimentally[12,28] and computationally[11] by other authors for various aryl-butadiynyl derivatives, and supports the occurrence of a photoinduced metal-free homocoupling reaction between terminal alkynes. The presence of a few unreacted PEBA monomers, constrained within ordered rows of the BUBA layer (see superposition models in Figure 4), allowed us to clearly compare the initial HB-interacting PEBA dimers with the photocoupled covalent dimers. The photocoupling involving the decarboxylation is

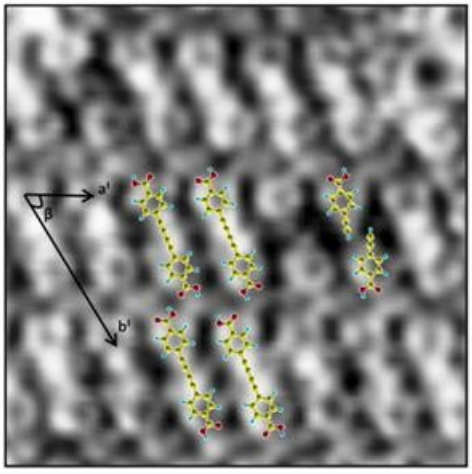

Figure 4. High resolution STM image (−0.30 V, 15 pA, 5 nm × 5 nm) of the photoreaction product and unreacted PEBA monomers.

unlikely to occur, since it would produce bis-phenyl species whose center-to-center distance is 0.43 nm, as found for oligo p-phenylene derivatives.[49,50]

The difference between the ordered SAMs before and after irradiation is more evident if one analyzes the corresponding unit-cells (exact calibration of the unit-cell in SI, Figure S2).

BUBA molecules have been observed to aggregate adopting specific schemes of carboxylic HB lateral interactions. Particular HB networks have been previously described[51] for this highly adaptable butadiynyl derivative. In our case, a bridging HB (representative unit-cell and molecular models are shown in Figure 4) has been observed. The superstructure is characterized by aggregates, whose arrangement is periodic and described by the unit-cell: $a' = 0.68 \pm 0.05$ nm, $b' = 1.71 \pm 0.05$ nm, and an angle $\beta = 65 \pm 1°$. For comparison, the exact and closest-commensurate unit-cell with the HOPG is $a' = 0.65$ nm, $b' = 1.77$ nm, and $\beta = 65°$ (see SI for the unit-cell determination). If this phase is compared to the initial system ($a = 0.70 \pm 0.05$ nm, $b = 1.89 \pm 0.05$ nm, and $\alpha = 55 \pm 1°$), its orientation with respect to the underlying HOPG changes (see Figure S2) and the unit-cells become smaller, noticeably along the alkyne axis, compatible with a photoinduced hydrogen dissociation and C−C coupling.

Previous reports show that monomer solutions of aromatic acetylenes undergo UV-induced polymerization and coupling reactions that occur in low yield and with low specificity.[52] A test was performed in order to exclude the occurrence of the homocoupling reaction in solution (Figure S4). A solution of PEBA in 7COOH was irradiated ex-situ under the same control conditions. Afterward, the UV-irradiated solution was checked with the STM on a clean HOPG substrate. In this case mostly PEBA molecules were observed by STM and, in particular, dimers were nearly absent. To further support the hypothesis of the topochemical control of the homocoupling reaction, we performed another control experiment in which we deposited a solution of excess PEBA and 1,3,5-benzenetribenzoic acid (TMA) (molar ratio PEBA/TMA = 40/1) in 7COOH on HOPG (see SI for experimental details). In this system, the aforementioned preorganization of PEBA is missing, as this molecule is less competitive toward the adsorption with respect to the tricarboxylic species and the preferential formation of the well-known ordered TMA superstructure emerges.[53−56] As a matter of fact, PEBA molecules intercalated within the TMA porous network and also small isolated clusters of PEBA could be observed among the boundaries of the extended TMA superstructure. Within this system, PEBA is mostly confined in solution (see Figure S4). After the irradiation of this system at 260 nm for various time intervals, the coupling reaction was less effective and mostly unreacted PEBA molecules were observed at the interface. Dimers conversion was estimated to be less than 10%. Noteworthy, photoinduced degradation of the TMA monolayer occurred. TMA has a nonzero absorbance at 260 nm,[57] and its superstructure degradation presumably occurs by dissipating the absorbed energy. In conclusion, the coupling reaction occurred far less efficiently within an irradiated solution where the proper topological preorganization of the monomers was missing or otherwise compromised, as when PEBA molecules are coadsorbed within the TMA lattice.

Other tests were also performed with 220, 240, 280, and 300 nm on the preformed PEBA SAM (see results in SI, Figure S6). Below 260 nm the system appeared disordered, presumably due to UV-induced degradation of both the organic solution and the overlayer. Above 260 nm the system was only partially

DOI: 10.1021/jacs.6b03589
J. Am. Chem. Soc. 2016, 138, 10151−10156

affected, and most starting material could be found unaltered. In conclusion, the reaction was less efficient in terms of sample quality and product yield over time at wavelengths far from the maximum of the absorption peak, indicating that a direct molecular excitation is needed for the coupling activation. Once the proper reaction conditions were established, the irradiation at 260 nm showed the highest rate and quality of product conversion with high reproducibility.

To further corroborate the successful photoinduced reaction, the bis-acetylenic dimer has been synthesized ex-situ with a Cu-catalyzed solution-reaction (see synthesis in the SI). Synthetic dimers have been dissolved in 7COOH and deposited on the HOPG surface. By STM imaging under the same conditions, we observed that the synthetic products aggregate in islands whose dimensions were measured in the range 20−50 nm (Figure 5a). By high resolution imaging (Figure 5b), unit-cell

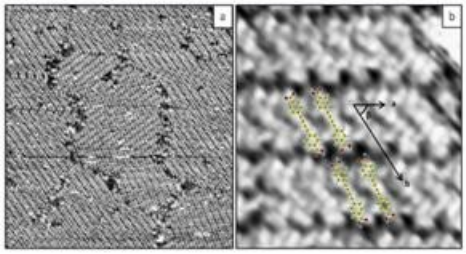

Figure 5. (a) Topographic STM image (−1.10 V, 5 pA, 50 nm × 50 nm) of the self-assembled structure of the ex situ synthesized bis-acetylenic dimer. (b) High resolution STM image (−0.50 V, 25 pA, 5 nm × 5 nm) of the self-assembled structure of the ex situ synthesized PEBA dimer.

parameters could be obtained by averaging real-space measurements on five images. Vectors a = 0.67 ± 0.05 nm, b = 1.78 ± 0.05 nm, and $\beta = 63 \pm 2°$ resulted similar to the BUBA SAM obtained in situ. Finally, the wet-reaction product clearly showed the same STM contrast at the molecular level, resulting from a similar carboxylic-HB bridging phase, as was found for the photochemically coupled PEBA products.

■ CONCLUSION

In this work we demonstrate that metal-free photochemical homocoupling occurs between terminal alkynes at the HOPG/liquid interface. This is obtained within a PEBA monomer SAM by exploiting its preorganization, i.e. the topological activation of the photochemical alkyne homocoupling. The successful C−C covalent stabilization is triggered by UV-light, it occurs catalyst-free, and the substrate acts only as a template, favoring the proper molecular orientation upon the photon absorption event. The comparison of the self-assembly patterns produced by in situ photoreacted monomers and ex-situ synthesized dimers allowed us to confirm the chemical nature of the photoreaction product. Also, the in situ photochemical conversion proved to be faster and cleaner with respect to the wet synthesis (5 min versus days and several purification steps, for a complete synthetic route) and the reaction selectivity showed up in monodispersity, which is noteworthy, given the many byproducts observed in the various metal-catalyzed Glaser couplings reported so far and referenced above.

The photoinduced mechanism occurred only with absorption-resonant irradiation, which in comparison with the metal-supported layers behavior[28] points toward a direct molecular excitation in accordance with a weak coupling with the underlying substrate. Photochemical activation on the weakly interacting HOPG thus proves to yield higher reaction selectivity when compared with thermal activation mechanisms observed on metal substrates, which induce disordered intermolecular interactions and broaden the product distribution.

The simple but heterofunctionalized starting material may eventually provide inspiration, biased by the recent debate on the on-surface reactivity of terminal alkynes, for the construction of more sophisticated superstructures by metal-free protocols and rational design of the molecular building blocks.

■ ASSOCIATED CONTENT

Supporting Information

The Supporting Information is available free of charge on the ACS Publications website at DOI: 10.1021/jacs.6b03589.

Detailed description of sample preparation and characterization (PDF)

■ AUTHOR INFORMATION

Corresponding Authors

*luciano.colazzo@studenti.unipd.it

*francesco.sedona@unipd.it

Notes

The authors declare no competing financial interest.

■ ACKNOWLEDGMENTS

This work was partially funded by MIUR (PRIN 2010/11, Project 2010BNZ3F2: "DESCARTES") and by the University of Padova (Grant CPDA154322, Project AMNES).

■ REFERENCES

(1) Nitzan, A.; Ratner, M. A. *Science* **2003**, *300* (5624), 1384.

(2) Wan, S.; Gándara, F.; Asano, A.; Furukawa, H.; Saeki, A.; Dey, S. K.; Liao, L.; Ambrogio, M. W.; Botros, Y. Y.; Duan, X.; Seki, S.; Stoddart, J. F.; Yaghi, O. M. *Chem. Mater.* **2011**, *23* (18), 4094.

(3) Côté, A. P.; Benin, A. I.; Ockwig, N. W.; O'Keeffe, M.; Matzger, A. J.; Yaghi, O. M. *Science* **2005**, *310* (5751), 1166.

(4) Basagni, A.; Sedona, F.; Pignedoli, C. A.; Cattelan, M.; Nicolas, L.; Casarin, M.; Sambi, M. *J. Am. Chem. Soc.* **2015**, *137* (5), 1802.

(5) Otero, G.; Biddau, G.; Sánchez-Sánchez, C.; Caillard, R.; López, M. F.; Rogero, C.; Palomares, F. J.; Cabello, N.; Basanta, M. A.; Ortega, J.; Méndez, J.; Echavarren, A. M.; Pérez, R.; Gómez-Lor, B.; Martín-Gago, J. A. *Nature* **2008**, *454* (7206), 865.

(6) Sun, Q.; Zhang, C.; Kong, H.; Tan, Q.; Xu, W. *Chem. Commun. (Cambridge, U. K.)* **2014**, *50* (80), 11825.

(7) Basagni, A.; Ferrighi, L.; Cattelan, M.; Nicolas, L.; Handrup, K.; Vaghi, L.; Papagni, A.; Sedona, F.; Valentin, C.; Di Agnoli, S.; Sambi, M. *Chem. Commun.* **2015**, *51* (63), 12593.

(8) Zwaneveld, N. A. A.; Pawlak, R.; Abel, M.; Catalin, D.; Gigmes, D.; Bertin, D.; Porte, L. *J. Am. Chem. Soc.* **2008**, *130* (21), 6678.

(9) Zhong, D.; Franke, J.-H.; Podiyanachari, S. K.; Blömker, T.; Zhang, H.; Kehr, G.; Erker, G.; Fuchs, H.; Chi, L. *Science* **2011**, *334* (6053), 213.

(10) Díaz Arado, O.; Mönig, H.; Wagner, H.; Franke, J. H.; Langewisch, G.; Held, P. A.; Studer, A.; Fuchs, H. *ACS Nano* **2013**, *7* (10), 8509.

(11) Zhang, Y.-Q.; Kepčija, N.; Kleinschrodt, M.; Diller, K.; Fischer, S.; Papageorgiou, A. C.; Allegretti, F.; Björk, J.; Klyatskaya, S.;

DOI: 10.1021/jacs.6b03589
J. Am. Chem. Soc. 2016, 138, 10151−10156

Klappenberger, F.; Ruben, M.; Barth, J. V. *Nat. Commun.* **2012**, *3*, 1286.
(12) Gao, H. Y.; Franke, J. H.; Wagner, H.; Zhong, D.; Held, P. A.; Studer, A.; Fuchs, H. *J. Phys. Chem. C* **2013**, *117* (36), 18595.
(13) Haley, M. M.; Brand, S. C.; Pak, J. J. *Angew. Chem., Int. Ed. Engl.* **1997**, *36* (8), 836.
(14) Baughman, R. H.; Eckhardt, H.; Kertesz, M. *J. Chem. Phys.* **1987**, *87* (11), 6687.
(15) Klappenberger, F.; Zhang, Y.-Q.; Björk, J.; Klyatskaya, S.; Ruben, M.; Barth, J. V. *Acc. Chem. Res.* **2015**, *48* (7), 2140.
(16) Hay, A. S. *J. Org. Chem.* **1962**, *27* (9), 3320.
(17) Mo, G.; Tian, Z.; Li, J.; Wen, G.; Yang, X. *Appl. Organomet. Chem.* **2015**, *29* (4), 231.
(18) Zhu, M.; Ning, M.; Fu, W.; Xu, C.; Zou, G. *Bull. Korean Chem. Soc.* **2012**, *33* (4), 1325.
(19) Chinchilla, R.; Nájera, C. *Chem. Rev.* **2014**, *114* (3), 1783.
(20) Zhang, X.; Liao, L.; Wang, S.; Hu, F.; Wang, C.; Zeng, Q. *Sci. Rep.* **2014**, *4*, 3899.
(21) Li, Q.; Owens, J. R.; Han, C.; Sumpter, B. G.; Lu, W.; Bernholc, J.; Meunier, V.; Maksymovych, P.; Fuentes-Cabrera, M.; Pan, M. *Sci. Rep.* **2013**, *3*, 2102.
(22) Gao, H.-Y.; Wagner, H.; Zhong, D.; Franke, J.-H.; Studer, A.; Fuchs, H. *Angew. Chem., Int. Ed.* **2013**, *52* (14), 4024.
(23) Liu, J.; Ruffieux, P.; Feng, X.; Müllen, K.; Fasel, R. *Chem. Commun. (Cambridge, U. K.)* **2014**, *50* (76), 11200.
(24) Eichhorn, J.; Heckl, W. M.; Lackinger, M. *Chem. Commun. (Cambridge, U. K.)* **2013**, *49* (28), 2900.
(25) Liu, J.; Chen, Q.; Xiao, L.; Shang, J.; Zhou, X.; Zhang, Y.; Wang, Y.; Shao, X.; Li, J.; Chen, W.; Xu, G. Q.; Tang, H.; Zhao, D.; Wu, K. *ACS Nano* **2015**, *9*, 6305.
(26) Cirera, B.; Zhang, Y.-Q.; Klyatskaya, S.; Ruben, M.; Klappenberger, F.; Barth, J. V. *ChemCatChem* **2013**, *5* (11), 3281.
(27) Cirera, B.; Zhang, Y. Q.; Björk, J.; Klyatskaya, S.; Chen, Z.; Ruben, M.; Barth, J. V.; Klappenberger, F. *Nano Lett.* **2014**, *14* (4), 1891.
(28) Gao, H. Y.; Zhong, D.; Mönig, H.; Wagner, H.; Held, P. A.; Timmer, A.; Studer, A.; Fuchs, H. *J. Phys. Chem. C* **2014**, *118* (12), 6272.
(29) Tognolini, S.; Ponzoni, S.; Sedona, F.; Sambi, M.; Pagliara, S. *J. Phys. Chem. Lett.* **2015**, *6* (18), 3632.
(30) Hatch, S. R.; Zhu, X.-Y.; White, J. M.; Campion, A. *J. Chem. Phys.* **1990**, *92* (4), 2681.
(31) Gadzuk, J. W. *J. Chem. Phys.* **2012**, *137* (9), 091703.
(32) Zhu, X.-Y.; White, J. M. *J. Chem. Phys.* **1991**, *94* (2), 1555.
(33) Zhang, Y.-Q.; Björk, J.; Weber, P.; Hellwig, R.; Diller, K.; Papageorgiou, A. C.; Oh, S. C.; Fischer, S.; Allegretti, F.; Klyatskaya, S.; Ruben, M.; Barth, J. V.; Klappenberger, F. *J. Phys. Chem. C* **2015**, *119* (17), 9669.
(34) Björk, J.; Zhang, Y. Q.; Klappenberger, F.; Barth, J. V.; Stafström, S. *J. Phys. Chem. C* **2014**, *118* (6), 3181.
(35) Ishida, Y.; Togashi, T.; Yamamoto, K.; Tanaka, M.; Taniuchi, T.; Kiss, T.; Nakajima, M.; Suemoto, T.; Shin, S. *Sci. Rep.* **2011**, *1*, 64.
(36) Zhou, X.-L.; Zhu, X.-Y.; White, J. M. *Surf. Sci. Rep.* **1991**, *13* (3−6), 73.
(37) MacLeod, J. M.; Lipton-Duffin, J. A.; Cui, D.; De Feyter, S.; Rosei, F. *Langmuir* **2015**, *31* (25), 7016.
(38) Suzuki, H.; Yamada, T.; Kamikado, T.; Okuno, Y.; Mashiko, S. *J. Phys. Chem. B* **2005**, *109* (27), 13296.
(39) Arras, E.; Seitsonen, A. P.; Klappenberger, F.; Barth, J. V. *Phys. Chem. Chem. Phys.* **2012**, *14* (46), 15995.
(40) Steiner, T. *J. Chem. Soc., Perkin Trans. 2* **1995**, No. 7, 1315.
(41) Guo, X.; Marrucci, F.; Price, N.; Stewart, E. L.; Baum, J. C.; Olson, J. A. *J. Phys. Chem. C* **2015**, *119* (44), 24804.
(42) Tan, Q.; Sun, Q.; Cai, L.; Wang, J.; Ding, Y. *J. Phys. Chem. C* **2015**, *119* (23), 12935.
(43) Lackinger, M.; Griessl, S.; Markert, T.; Jamitzky, F.; Heckl, W. M. *J. Phys. Chem. B* **2004**, *108* (36), 13652.
(44) De Feyter, S.; De Schryver, F. C. *J. Phys. Chem. B* **2005**, *109* (10), 4290.
(45) Addou, R.; Batzill, M. *Langmuir* **2013**, *29* (21), 6354.
(46) Florio, G. M.; Stiso, K. A.; Campanelli, J. S. *J. Phys. Chem. C* **2012**, *116* (34), 18160.
(47) Song, W.; Martsinovich, N.; Heckl, W. M.; Lackinger, M. *J. Am. Chem. Soc.* **2013**, *135* (39), 14854.
(48) Njus, J. M.; Sandman, D. J.; Yang, L.; Foxman, B. M. *Macromolecules* **2005**, *38* (18), 7645.
(49) Lipton-Duffin, J. A.; Ivasenko, O.; Perepichka, D. F.; Rosei, F. *Small* **2009**, *5* (5), 592.
(50) Baker, K. N.; Fratini, A. V.; Resch, T.; Knachel, H. C.; Adams, W. W.; Socci, E. P.; Farmer, B. L. *Polymer* **1993**, *34* (8), 1571.
(51) Kley, C. S.; Čechal, J.; Kumagai, T.; Schramm, F.; Ruben, M.; Stepanow, S.; Kern, K. *J. Am. Chem. Soc.* **2012**, *134* (14), 6072.
(52) Rohde, O.; Wegner, G. *Makromol. Chem.* **1978**, *179* (8), 2013.
(53) Lackinger, M.; Griessl, S.; Heckl, W. M.; Hietschold, M.; Flynn, G. W. *Langmuir* **2005**, *21* (11), 4984.
(54) Griessl, S. J. H.; Lackinger, M.; Jamitzky, F.; Markert, T.; Hietschold, M.; Heckl, W. M. *J. Phys. Chem. B* **2004**, *108* (31), 11556.
(55) MacLeod, J. M.; Lipton-Duffin, J. A.; Cui, D.; De Feyter, S.; Rosei, F. *Langmuir* **2015**, *31* (25), 7016.
(56) Kampschulte, L.; Lackinger, M.; Maier, A.-K.; Kishore, R. S. K.; Griessl, S.; Schmittel, M.; Heckl, W. M. *J. Phys. Chem. B* **2006**, *110* (22), 10829.
(57) Lawrence, F. A. *Anal. Chem.* **1951**, *23* (12), 1882.

DOI: 10.1021/jacs.6b03589
J. Am. Chem. Soc. 2016, 138, 10151−10156

SUPPORTING INFORMATION

Metal-Free on-Surface Photochemical Homocoupling Of Terminal Alkynes

Luciano Colazzo,*[,†,‡] Francesco Sedona,*[,†] Alessandro Moretto,[†] Maurizio Casarin,[†,‡] Mauro Sambi[†,§]

[†] Dipartimento di Scienze Chimiche, Università di Padova, Via Marzolo 1, 35131 Padova (Italy)
[‡] CNR-ICMATE, Via Marzolo 1, 35131 Padova (Italy)
[§] Consorzio INSTM, Unità di Ricerca di Padova, Via Marzolo 1, 35131 Padova (Italy)

* luciano.colazzo@studenti.unipd.it
* francesco.sedona@unipd.it

METHODS, SELF ASSEMBLY, AND ASSEMBLY-TRESHOLD

STM measurements were performed in constant-current mode with an Agilent 5500 SPM. Vibration insulation was insured by a bungee system enclosed in a sound-dumping chamber. STM tips were mechanically cut from a Pt/Ir (80:20) wire with a diameter of 0.25 mm. The substrate was HOPG, grade ZYB, 12x12 mm, Surface Preparation Laboratory - SPL, Netherlands. STM measurements were performed at the HOPG/7COOH interface at room temperature (RT). STM data were analyzed with the WSxM software.[1] The topography measurements were background-corrected and rendered with a 3×3 smooth matrix filter. All mentioned bias values correspond to the sample voltage, relative to the grounded tip.

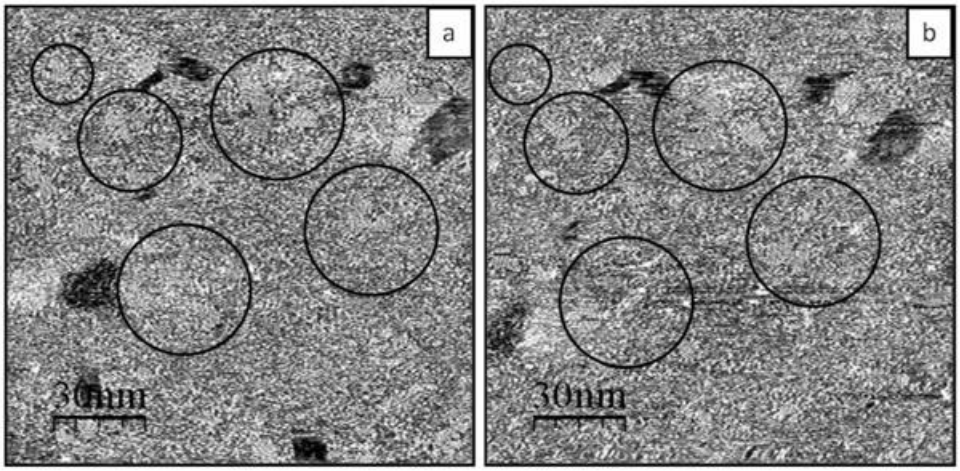

Figure S1: Successive STM images over the same area (a) isolated clusters of PEBA highlighted with solid circles (-0.75 V, 5 pA, 150 nm × 150 nm) and (b) evolution of PEBA clusters after the second scan over the same area (-0.75 V, 5 pA, 150 nm × 150 nm).

In order to obtain a monolayer coverage on the HOPG surface with the highest possible island dimensions, the PEBA solution concentration was adjusted to 2.0 mg/g in 7COOH. Below this concentration value (1.0 mg/g or less, see Figure S1), only small and isolated supramolecular aggregates could be found at the liquid-solid interface, whose STM imaging is difficult because of the high diffusivity of the molecular building blocks on the underlying HOPG surface. In Figure S1, a representative image of the interfacial behaviour of a solution of PEBA at a concentration of 1.0 mg/g is shown. Small and isolated clusters of PEBA have been highlighted with circles. In Figure S1b, cluster evolution is shown. It is observed that the high diffusivity of the molecular building blocks on the underlying HOPG surface causes cluster instability during raster scanning.

SUPRAMOLECULAR PATTERNS

The exact calibration of the overlayer unit cells has been obtained by means of high resolution STM images in which both the substrate and the overlayer are present. These images allow one to calibrate the molecular unit cell, once the size of the HOPG lattice is known. The latter acts as an internal ruler and the molecular parameters are scaled by means of a superposition matrix to the value of 0.246 nm for the in-plane lattice constant of HOPG.

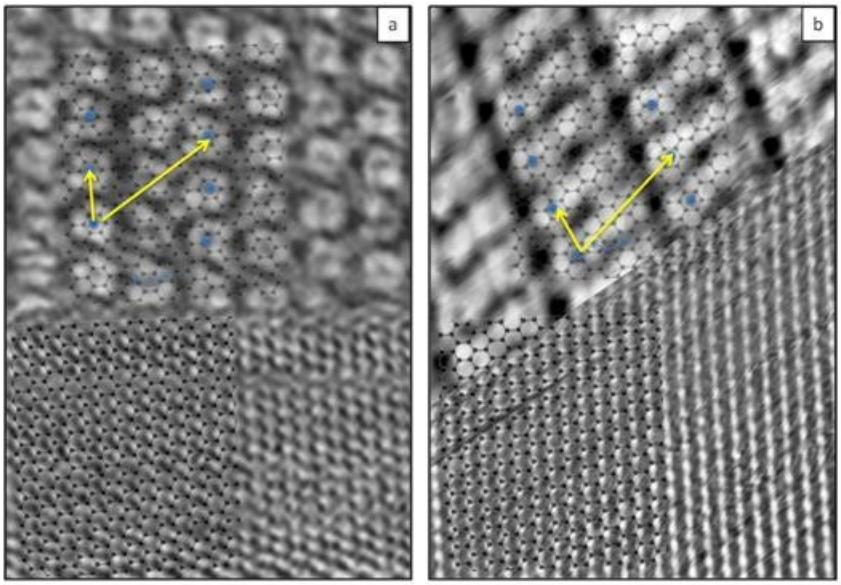

Figure S2: STM images showing the molecular structures (top) and the substrate in the same frame (bottom): (a) HOPG/PEBA (-0.75 V, 25 pA (top), -0.40 V, 230 pA (bottom)): (b) HOPG/BUBA (-0.45 V, 45 pA (top), -0.40 V, 180 pA (bottom)). The orientation of the substrate in the two images is the same.

In Figure S2 it is possible to observe that the overlayer unit-cell changes its orientation with respect to the fixed HOPG lattice upon the UV irradiation (cf. HOPG lattice models of Figure S2a and S2b and epitaxy matrix in the discussion). The closer commensurate unit cell that best fits the experimental PEBA lattice in Figure S2a is reproduced by the epitaxial matrix (8 1, 3 3), which corresponds to the unit cell whose parameters are a=0.74 nm, b=1.86 nm and α=53°. On the other hand, the closer epitaxial matrix for the BUBA dimers in Figure S2b is (8 2, 2 3), which corresponds to the unit cell whose parameters are a^{I}=0.65 nm, b^{I}=1.77 nm and β = 65°. These values are given without uncertainty, as they are the most reliable representation of the closest unit-cell of the overlayer commensurate with the underlying substrate.

SURFACE DYNAMICS

Monomers and HB-dimers coexist in a dynamic-exchange equilibrium. Discrete azimuthal rotations have been detected as single or collective 180° on-site leaps. In Figure S3a i, ii, iii, successive STM images over the same area are reported as cartoon-clips. A grid is added as a guide for the identification of the molecular reorientation throughout the clips. Scanning over these areas took approximately 10 s for each frame.

In Figure S3b i, ii, iii, a color-marked model for the molecular reorientations is proposed. Black-marked molecules have been used to indicate those HB-dimers whose orientation remains unchanged over successive clips. Yellow-marked molecules have been used to indicate those molecules that reorient in the i+1 frame. Blue-marked molecules have been used to indicate those monomers or HB-dimers for which one leap has been observed over the clips (wrt i-1 frame). Red-marked molecules have been used to indicate those monomers or HB-dimers for which a second leap has been observed over the clips.

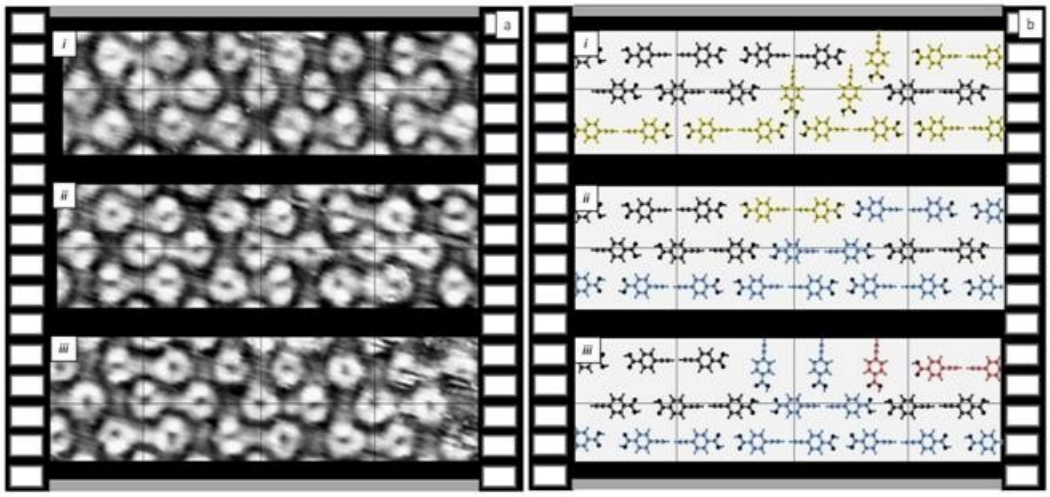

Figure S3: (a) Successive cartoon-clips for the observed on-surface dynamics over the same area. (b) color-marked model depicting molecular reorientations observed experimentally.

EVALUATION OF THE POSSIBLE TOPOLOGICAL CONTRIBUTION TO PHOTOCHEMICAL ACTIVATION

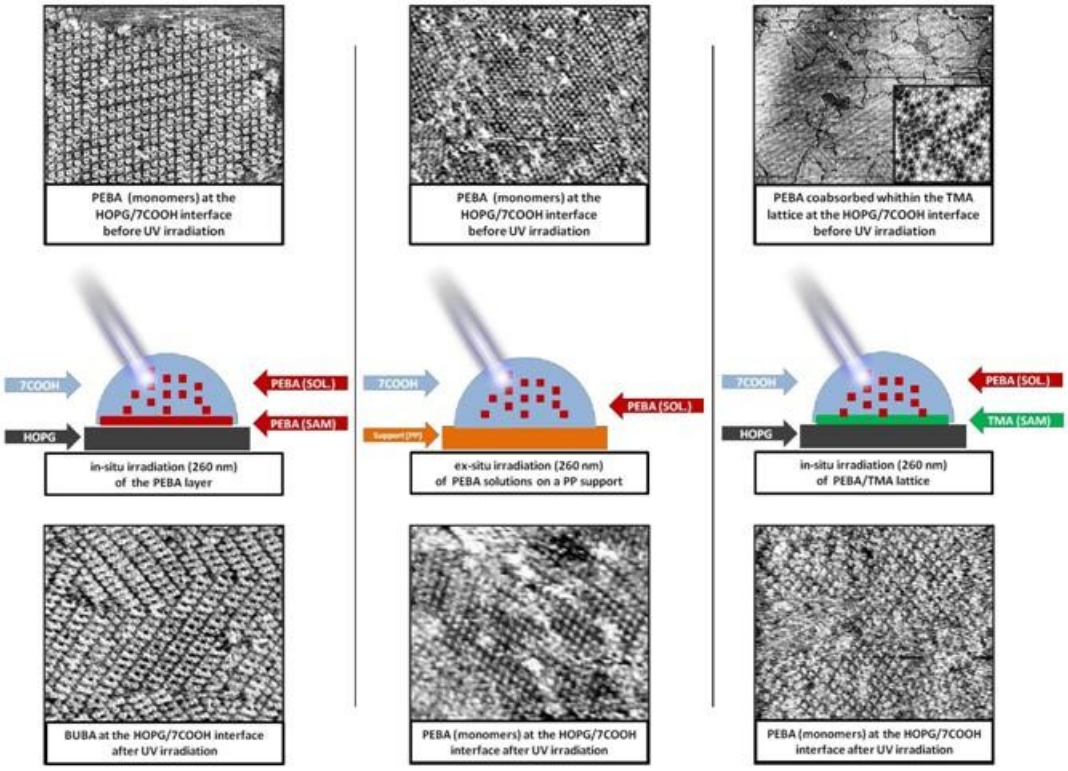

Figure S4: schematic representation of the experiment in which a SAM of PEBA is irradiated on HOPG with a laser beam tuned at 260 nm (left), a sample in which PEBA solution is irradiated ex-situ (center) and a sample in which the UV irradiation is performed on a SAM of PEBA and TMA coadsorbed on HOPG (right). STM images: (left panel) topographic image of the as-deposited PEBA (top left, -0.45 V, 10 pA, 20 nm × 20 nm) and after 5 min irradiation at 260 nm (bottom left, -0.30 V, 35 pA, 20 nm × 20 nm); (middle panel) topographic image of the PEBA SAM at the HOPG/7COOH interface before the ex-situ irradiation of the solution (top center, -0.76 V, 25 pA, 30 nm × 30 nm) and after the ex-situ irradiation (bottom center, -0.80 V, 35 pA, 20 nm × 20 nm); (right panel) topographic image of the HOPG surface pre-covered with a TMA monolayer in co-deposition with PEBA (top right , -0.90 V, 15 pA, 200 nm × 200 nm, inset depicts the TMA host-guest activity towards PEBA) and after 5 min irradiation at 260 nm (bottom right -0.90 V, 20 pA, 20 nm × 20 nm).

To validate the hypothesis of the surface-confined topochemical effect for the activation of the HOPG-supported alkyne homocoupling (Figure S4, left panel), a control test was performed in which the solution of PEBA in 7COOH was irradiated ex-situ at 260 nm for 10 minutes and then checked at the STM. UV irradiations were performed both on relatively large volumes (500 µl) in a polypropylene (PP) vial and in control environments in which the same liquid-cell used for the irradiations on HOPG was equipped with generic soda-lime glass or PP to support the solution (15 µl) during the irradiation. The solution was checked with STM on HOPG before (Figure S4 middle panel, top) and after (Figure S4 middle panel, bottom) the irradiation. Only the irradiations performed on PP supports produced solutions suitable for the STM imaging, since considerable amounts of impurities made the imaging impossible when glass was used. In conclusion, after the ex situ UV treatment mostly PEBA molecules were observed (Figure S4 middle panel, bottom).

The topochemical control of the HOPG-supported alkyne homocoupling was further corroborated by performing an experiment where the laser irradiation of a solution of PEBA (approx. 40 mM) occurred on the HOPG surface pre-covered with the porous benzene-1,3,5-tricarboxylic acid (TMA, approx 1 mM) monolayer (see Figure S4, right panel). The codeposition of a solution of PEBA and TMA in 7COOH favors TMA as the dominant on-surface aggregate. In this system the PEBA is mostly confined in solution, however, the TMA monolayer forms the well-known "chickenwire" and "honeycomb" networks,[2–5] both capable of host-guest activity towards PEBA molecules or other TMA in solution (see STM image in Figure S4 right panel, top, and bright spots in the chickenwire network, inset in Figure S4 right panel, top). PEBA is less competitive toward adsorption with respect to the tricarboxylic species, although small clusters could be observed among the boundaries of extended TMA domains (dark-regions in STM image in Figure S4 right panel, top). After the irradiation at 260 nm of this system (Figure S4 right panel, bottom), mostly PEBA molecules were observed. Only limited dimers formation was observed, while photoinduced degradation of the TMA monolayer occurred.

Both control tests therefore evidence that the photochemical alkyne homocoupling occurred less efficiently from an irradiated solution where the proper topological pre-organization of the monomers was missing or compromised.

REACTIVITY AT VARIOUS WAVELENGHTS

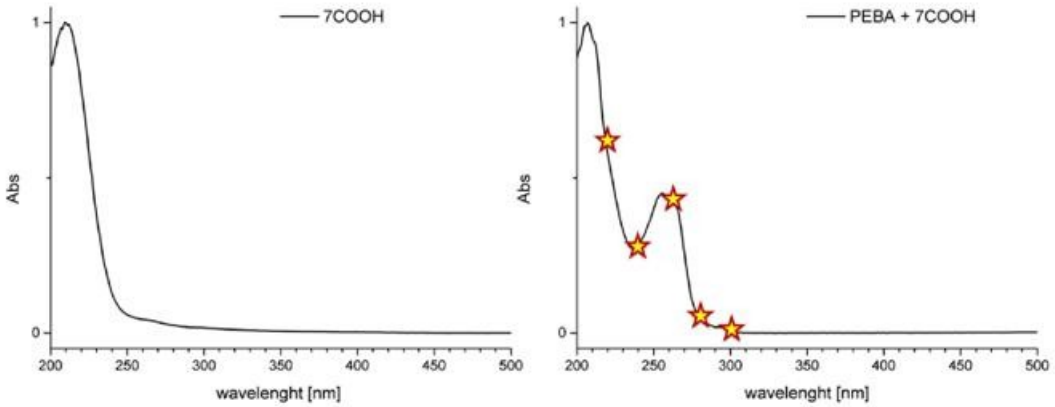

Figure S5: Left, UV/Vis spectrum of 7COOH approximately 1×10^{-3} M in methanol. Right, PEBA/7COOH solution in methanol. The concentration of PEBA is 1×10^{-6} M. The wavelengths 220, 240, 260, 280, 300 nm have been highlighted on the absorption curve.

In order to perform UV irradiation tests, the unfocused output beam (≈ 6 mm diameter, pulse frequency 30 Hz and pulse width 3.9 ns, output energy at 220, 240, 260, 280, 300 nm wavelength was 1.30, 1.82, 1.71, 1.57, 1.24 mJ, respectively), additionally attenuated with an absorptive neutral density (OD1) filter, has been directed perpendicularly to the sample surface and the overlying solution by means of an Al-coated UV mirror. No temperature increase was detected on the sample during the irradiation. The selected attenuation provided a good balance between non-destructive beam intensity and short time of exposure to prevent atmospheric contamination of the sample and beam-induced heating.

The solution of PEBA in 7COOH that has been used for the STM characterization has been initially characterized by means of UV/Vis spectroscopy. The UV-Vis spectrum in Figure S5 (right) is characterized by two components: the PEBA absorption band is located in the 240-270 nm range, while the band centered at 210 nm has been attributed to 7COOH (see Figure S5 (left) for comparison). Within the PEBA absorption band, 260 nm is a local maximum. The irradiation at this wavelength indeed provided good results in terms of high reaction efficiency and low photodegradation. Other tests were performed at the other highlighted wavelengths using the same laser settings and irradiation times. Results are shown in Figure S6: dimers domains are highlighted by means of blue lines. Inset (enlarged images) added in Figure S6 may be helpful for a clearer distinction of monomers and dimers on the large scale, as monomers emerge as dot-like aggregates while dimers appear as prolate objects.

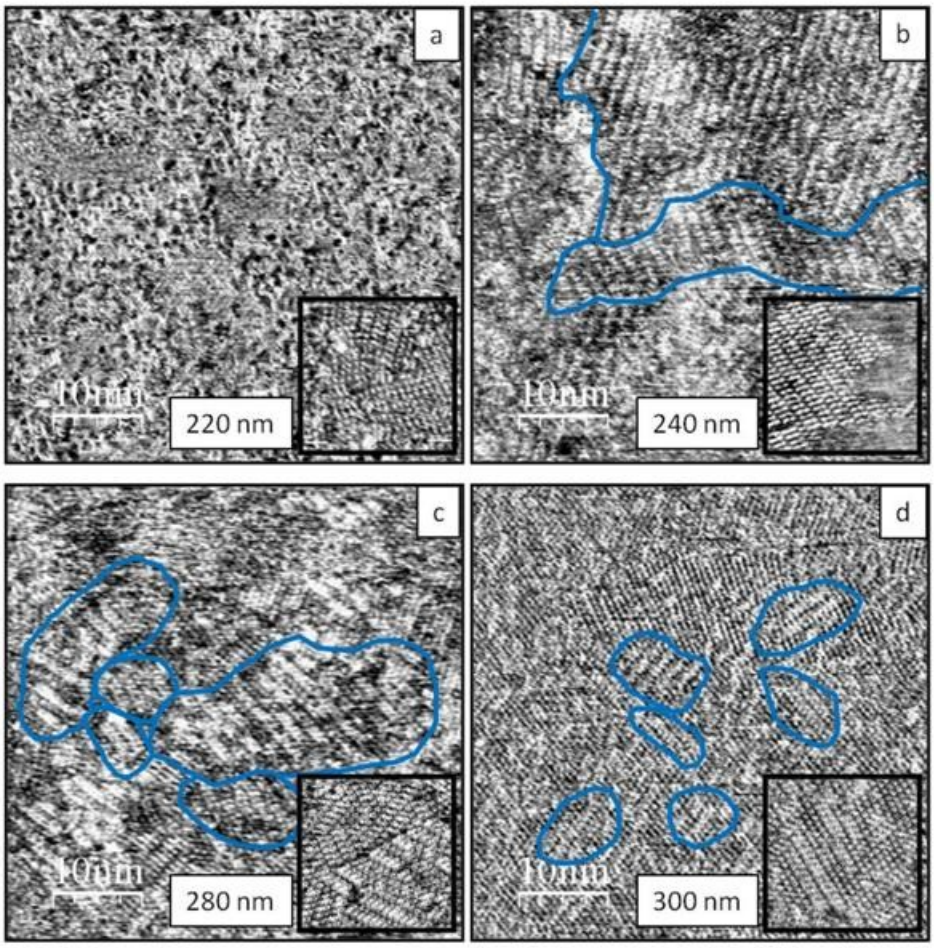

Figure S6 STM images after the irradiation of PEBA at various wavelengths for 10 minutes. Blue lines highlight boundaries among the photocoupled products and both monomers and photodegradation products (a) 220 nm (-0.95 V, 5 pA, 50 nm × 50 nm), inset: (-0.80 V, 5 pA, 15 nm × 15 nm). (b) 240 nm (-0.65 V, 15 pA, 50 nm × 50 nm), inset: (-0.80 V, 15 pA, 15 nm × 15 nm). (c) 280 nm (-0.60 V, 25 pA, 50 nm × 50 nm) , inset: (-0.65 V, 15 pA, 15 nm × 15 nm). (d) 300 nm (-0.65 V, 35 pA, 50 nm × 50 nm) , inset: (-0.50 V, 10 pA, 15 nm × 15 nm).

We found that 220 nm (Figure S6a) mostly induced degradation of the system; after the irradiation at this wavelength, only small islands (5-10 nm in diameter) could be found on the surface, characterized by reacted and unreacted starting material (see inset of Figure S6a). At 240 nm (Figure S6b, blue lines highlight the domain boundaries of the dimer domains) we found a relevant amount of photoconverted starting material (see inset of Figure S6b), but imaging was made difficult because of a moderate sample degradation. At 280 nm the photoinduced covalent transformation occurred less efficiently (Figure S6c, isolated and disordered domains of photocoupled dimer are highlighted with blue lines) and a relevant amount of unreacted PEBA could be found unaltered (see inset of Figure S6c). At 300 (Figure S6d) nm only isolated clusters of covalent dimer could be found within the aggregates of unreacted PEBA (see inset of Figure S6c).

CHEMICAL DIMERIZATION OF 4-ETHYNYL BENZOIC ACID[6]

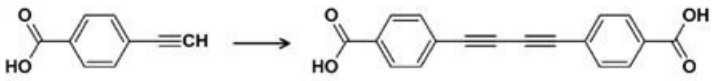

4-ethynyl benzoic acid 4,4'-di-(1,4-buta-1,3-diynyl)-benzoic acid

CuI (5 mol%) and $NiCl_2 \cdot H_2O$ (5 mol%) were dissolved in 500 µL of THF, then TMEDA (20 mol%) was added. This solution was stirred at RT under air for 2 min. 4-Ethynyl benzoic acid (300 mg, 2.05 mmol) was dissolved in 3 mL of THF, added to the previous solution, and the resulting mixture was stirred under air for 48 hours at room temperature. The solvent was removed under reduced pressure and the residue was purified by flash chromatography on silica gel (CH_2Cl_2/MeOH/acetic acid = 92/6/1, v/v). The product was recovered as a solid in 19 % yield (60 mg) and it was further purified (to run STM) by crystallization cycles, using hot methanol, mp 231-233°C. HRMS (ESI+): m/z calcd. 290.0579, found 291.0746 [M+H]+. 1H NMR (400 MHz, DMSO) δ ppm: 10.32 (br, 2H), 7.98 (d, 4 H), 7.76 (d, 4 H). 13C NMR (75 MHz, DMSO): δ ppm: 76.9, 82.5 (CC), 126.5, 130.4, 131.6, 133.2 (ArC), 169.2 (CO). Anal. Calcd for C18H10O4: C, 74.48; H, 3.47. Found: C, 74.50; H, 3.52.

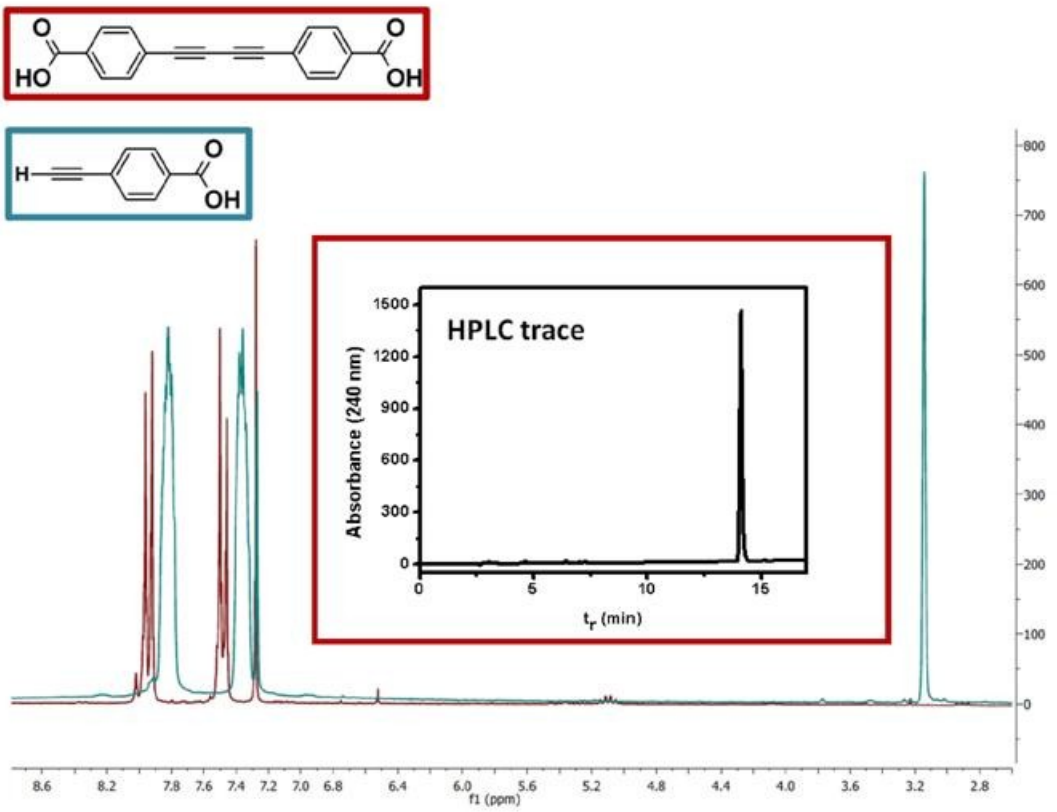

Figure S7 H-NMR spectra recorded for: PEBA monomer (blue) and BUBA dimer (red). Inset: HPLC trace recorded for the BUBA dimer

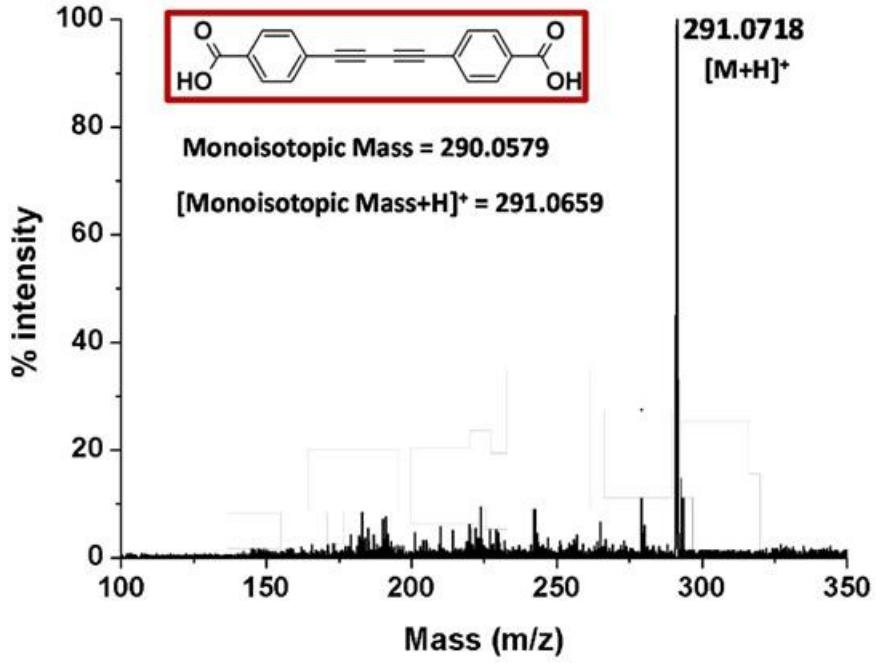

Figure S8 HRMS (ESI+) recorded for the dimer

ChemPubSoc Europe

DOI: 10.1002/chem.201403208

CHEMISTRY
A European Journal
Full Paper

Surface Photochemistry |Hot Paper|

Stereoselective Photopolymerization of Tetraphenylporphyrin Derivatives on Ag(110) at the Sub-Monolayer Level

Andrea Basagni,*[a] Luciano Colazzo,[a] Francesco Sedona,*[a] Marco Di Marino,[a] Tommaso Carofiglio,[a] Elisa Lubian,[a] Daniel Forrer,[b, c] Andrea Vittadini,[b, c] Maurizio Casarin,[a, b, c] Alberto Verdini,[d] Albano Cossaro,[d] Luca Floreano,[d] and Mauro Sambi[a, b]

Abstract: We explore a photochemical approach to achieve an ordered polymeric structure at the sub-monolayer level on a metal substrate. In particular, a tetraphenylporphyrin derivative carrying *para*-amino-phenyl functional groups is used to obtain extended and highly ordered molecular wires on Ag(110). Scanning tunneling microscopy and density functional theory calculations reveal that porphyrin building blocks are joined through azo bridges, mainly as *cis* isomers. The observed highly stereoselective growth is the result of adsorbate/surface interactions, as indicated by X-ray photoelectron spectroscopy. At variance with previous studies, we tailor the formation of long-range ordered structures by the separate control of the surface molecular diffusion through sample heating, and of the reaction initiation through light absorption. This previously unreported approach shows that the photo-induced covalent stabilization of self-assembled molecular monolayers to obtain highly ordered surface covalent organic frameworks is viable by a careful choice of the precursors and reaction conditions.

Introduction

Over the past few years, synthesis of organic surface-supported covalent nanostructures has gained substantial interest for the preparation of low-dimensional materials.[1,2] These are highly interesting from a basic science perspective, but also for nanotechnological applications such as template-assisted nanopatterning[3] and organic electronics.[4] Molecular self-assembly is a widely applied tool for creating ordered organic structures on surfaces and indeed many arrangements have been produced in ultrahigh-vacuum (UHV) conditions, ranging from wirelike structures[5] and two dimensional layers[6] to more complex architectures such as host-guest networks.[7–9] Formation and stabilization of self-assembled structures can be driven by intermolecular interactions such as metal-ligand coordination[10–12] and hydrogen bonding,[13–17] but also by the weaker and non-directional van der Waals interactions.[18–20] The weakness of these interactions makes the network formation reversible, which, on one hand, favors defect correction, and, ultimately, the formation of long-range ordered structures. On the other hand, instability is a severe limitation for ex situ applications in ambient environment.

In recent years, direct on-substrate synthesis in UHV has been exploited as a promising strategy to obtain thermally and chemically stable structures by covalent bonding of suitable precursors.[21] The 2D confinement of molecular precursors has many advantages over 3D solution chemistry, such as the possibility of preparing large molecules impossible to synthesize in solution owing to their low solubility, better control of the system architecture through the use of a pretemplating substrate, and finally access to new reaction pathways, thanks to the catalytic role of the substrate.[22,23] Usually, covalent linking of organic molecules onto metal and bulk insulator surfaces is carried out thermally: the energy supplied to the system promotes substitution reactions[24–27] or activates the precursors by C–Br or C–I homolytic dissociation.[28–32] These approaches, however, perform monomer assembly and polymerization simultaneously under dynamic-bond-forming conditions, and usually provide polymers with many defects and only short-range order.[33] A reversible reaction environment might improve the surface covalent organic frameworks (SCOF) quality,[34–36] but typically thermodynamic equilibrium conditions cannot be achieved in UHV.

[a] A. Basagni, L. Colazzo, F. Sedona, M. Di Marino, Prof. T. Carofiglio, E. Lubian, Prof. M. Casarin, Prof. M. Sambi
Dipartimento di Scienze Chimiche
Università di Padova
Via Marzolo 1, 35131, Padova (Italy)
E-mail: andrea.basagni@studenti.unipd.it
francesco.sedona@unipd.it

[b] D. Forrer, A. Vittadini, Prof. M. Casarin, Prof. M. Sambi
Consorzio INSTM
Via Marzolo 1, 35131 Padova (Italy)

[c] D. Forrer, A. Vittadini, Prof. M. Casarin
CNR-IENI
Via Marzolo 1, 35131 Padova (Italy)

[d] A. Verdini, A. Cossaro, L. Floreano
Laboratorio Nazionale TASC
Area Science Park
S. S. 14, km 163.5, 34149 Trieste (Italy)

Photochemically activated reactions, instead, have proven to be a powerful tool to stabilize the self-organized structures without disrupting the long-range order.[37–39] However, covalent interlinking of molecules by light triggering on metal substrates poses additional challenges. First of all, the high quenching rate of electronically excited species on metal surfaces inhibits the photophysical processes commonly observed in the gas phase and in solution.[40] Moreover, the presence of the surface can also provide new relaxation pathways, such as photodesorption,[41,42] and new charge-transfer-mediated photochemistry.[43,44] As a result, the surface photochemistry of a given molecule is considerably different from what would be anticipated for a gas-phase or solution environment. These are some of the reasons why light-driven on-surface synthesis is not as developed as it is in solution.

Herein, we present the covalent coupling of a tetraphenyl porphyrin derivative, namely 5,15-bis(4-aminophenyl)-10,20-diphenylporphyrin (hereafter, *trans*-TPP(NH_2)$_2$). The aniline moiety is known to adsorb on and interact with a silver substrate much like phenol[45] and both molecules display similar photophysical behavior in the gas phase.[46,47] In particular, the N–H bond photodissociation threshold was estimated at 4.61 eV, that is approximately 0.4 eV lower than the O–H analogue in phenol—we therefore expect that aniline residues can form radicals on the silver surface, as reported for phenol.[48,49] Here, the anilino radical formation is employed to covalently bond *trans*-TPP(NH_2)$_2$ monomers by a radical coupling reaction. Our results indicate that porphyrins form nanowires extending along the substrate [1$\bar{1}$0] direction and that the monomers are joined by N=N (azo) links. N 1s X-ray photoelectron spectroscopy (XPS) measurements show that the substrate takes an active part in the stabilization of the formed bond and in its stereochemistry.

The interest for such a prototype reaction is tightly linked to the use of radical photodissociation reactions between organic chromophores as a tool for the covalent stabilization of highly ordered surface supramolecular structures. Moreover, light-induced topochemical processes exploiting small fragments ($H^{\bullet}$ or $CH_3^{\bullet}$ radicals) as leaving groups, not directly involved in the self-assembly process, are expected to induce minor conformational rearrangements, thus minimizing the probability of generating structural defects.

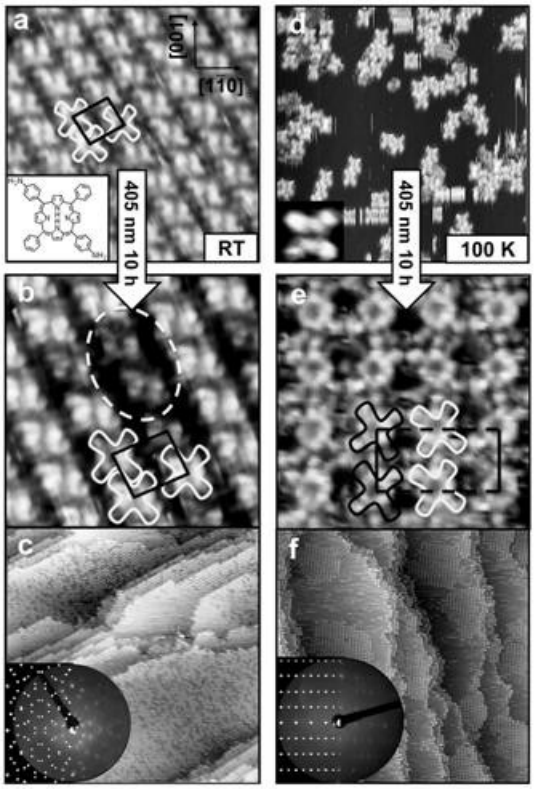

Figure 1. a) STM image of the oblique (5 ± 2, ∓2 3) self-assembled *trans*-TPP(NH_2)$_2$ superstructure on Ag(110) at RT with the corresponding molecular structural formula (13×13 nm^2, $V_{bias}=0.58$ V, $I=15.20$ nA). b) Small- (7×7 nm^2, $V_{bias}=0.45$ V, $I=3.20$ nA), and c) large-scale (150×150 nm^2, $V_{bias}=1.00$ V, $I=1.00$ nA) STM images and LEED pattern with superimposed simulation of the oblique structure illuminated for 10 h at RT. d) STM image of *trans*-TPP(NH_2)$_2$ on Ag(110) at 100 K (30×30 nm^2, $V_{bias}=0.30$ V, $I=1.00$ nA; inset 2.4×2.4 nm^2, $V_{bias}=-0.95$ V, $I=1.94$ nA). e) Small- (8×8 nm^2, $V_{bias}=-1.00$ V, $I=17.37$ nA) and f) large-scale (150×150 nm^2, $V_{bias}=1.00$ V, $I=1.00$ nA) STM images and LEED pattern with superimposed simulation of the rectangular p(12×4) structure obtained by the two-step procedure as described in the text. The superimposed porphyrin shapes highlight the different azimuthal orientation of the molecules in the rectangular phase, which gives rise to the glide symmetry line (dashed line). In all the STM images, the directions lie as indicated in (a).

Results and Discussion

As reported in previous studies,[8,9] *trans*-TPP(NH_2)$_2$ molecules deposited on Ag(110) at room temperature (RT) self-organize in an ordered structure, Figure 1a. This is characterized by an oblique unit cell, which is commensurate with the substrate, and described by the epitaxial matrices (5 ± 2, ∓2 3), hereafter referred to as "oblique phase".

We first checked the effects of 10 h of irradiation at $\lambda=$ 405 nm on 0.5 monolayer (ML) *trans*-TPP(NH_2)$_2$ deposited on Ag(110) at RT. As shown in Figure 1c, the low-energy electron diffraction (LEED) pattern still displays the same (5 ± 2, ∓2 3) symmetry observed before irradiation. Nevertheless, within the sample illuminated area, some porphyrins exhibit a decrease of their apparent height by 0.5 ± 0.1 Å, as highlighted by the dashed oval in Figure 1b; the irradiated molecules also show a reduced mobility over the terraces at RT. These molecular changes (in conformation and mobility) disappear after one hour at 410 K, thus highlighting the metastable nature of the molecular state produced by irradiation.

We found an efficient photoreaction pathway by depositing different amounts of *trans*-TPP(NH_2)$_2$ on Ag(110) maintained at 100 K. The sample was then illuminated at 405 nm during a linear heating ramp up to RT over approximately 10 h. With this two-step procedure, the formation of a new extended su-

perstructure is observed for coverage lower than about 0.5 ML (Figure 1 f). At higher coverage, the oblique structure develops, whereas at very low coverage, step decoration occurs. As shown in Figure 1 d, porphyrin molecules deposited at 100 K are randomly distributed owing to the low mobility, and are mostly aggregated as disordered small clusters. The new superstructure only develops when molecules are irradiated during the slow heating ramp up to RT, that is, during the self-assembly process. Conversely, if molecules are first exposed to the light at 100 K and then heated to RT in the dark, they organize into the known oblique structure.

Figure 1 e and f show small- and large-scale STM images of the new photo-induced phase, together with the corresponding measured and simulated LEED patterns that are consistent with a commensurate p(12×4) superstructure, hereafter referred to as "rectangular phase". The systematic absence of the $(2n+1, 0)$ diffraction spots in LEED patterns indicates the presence of a glide line symmetry operation parallel to the b_2 unit vector. The STM images reveal a rectangular unit cell, in agreement with the LEED pattern, Figure 1 e, where it is also evident that two adjacent porphyrins along the [1$\bar{1}$0] direction display a mirror-like azimuthal orientation. This alternation is the origin of the observed glide line symmetry, represented in Figure 1 e by a dashed line. The reported unit cell contains two molecules, so that the surface density (ρ_S) in the rectangular structure is 0.37 nm^{-2}, 16% lower than in the oblique phase (0.44 nm^{-2}). The large-scale STM image in Figure 1 f shows that the new rectangular phase forms extended domains on terraces within the illuminated area.

As observed in several self-organized structures of TPP derivatives,[50,51] the self-assembly driving force generating the oblique structure is the T interaction between *meso*-phenyl rings (where the H atom of one ring points toward the center of the adjacent ring, as shown in the model of the oblique phase in Figure 2, bottom).

However, geometrical constraints associated with the rectangular phase prevent a full exploitation of these interactions. As a matter of fact, the distances between the phenyl centroids of nearest neighbor (NN) molecules are estimated to be approximately 7.2 and 9.5 Å along the [1$\bar{1}$0] direction, segments 1 and 3 respectively, and about 7.8 Å along [1$\bar{1}$2], segment 2, see Figure 2. All these distances are significantly longer than those suitable for T interactions (~5 Å), as well as for direct stacking (3.3–3.6 Å) between adjacent benzene rings.[52–54]

Taking into account the lower ρ_S of the rectangular phase with respect to the oblique one, the stability of this superstructure requires the onset of a highly uni-directional interaction between monomers, stronger than T interaction, such as a covalent bond. As an alternative, a different intramolecular structure (either a conformational change or a structural change due to light-induced intramolecular reactions) could lead to a different organization, for example, owing to changes in the molecular recognition interactions governing the self-assembly process, as well to changes in the molecular size and/or shape.[55] To get a comparative insight into the structure of oblique and rectangular phases under the same tunneling conditions, we made a RT deposition of *trans*-TPP$(NH_2)_2$ on a sample partially precovered by the rectangular phase, as shown in Figure 3.

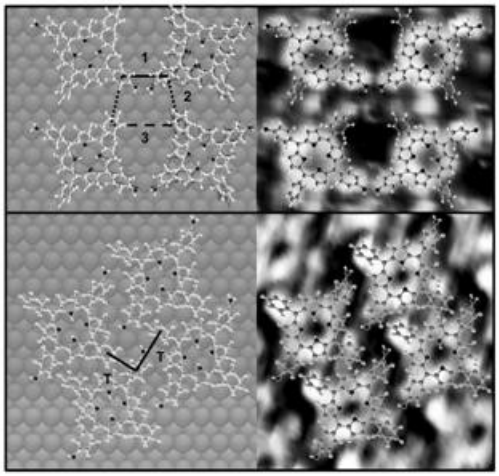

Figure 2. Overlay of STM images and the ball-sticks models of the rectangular (top) and oblique (bottom) structures on the Ag(110) surface. Four segments in the rectangular structure indicate the distances between the phenyl centroids: 1) 0.72 nm, 2) 0.78 nm, 3) 0.95 nm. In the oblique structure, two segments highlight the T interaction between adjacent molecules. The Ag(110) lattice is illustrated by the underlying spheres. The relative positions of the adsorbate and the substrate are chosen arbitrarily. The tunneling parameters are $V_{bias} = -1.00$ V, $I = 17.37$ nA and $V_{bias} = 1.00$ V, $I = 3.47$ nA for the top and bottom images, respectively.

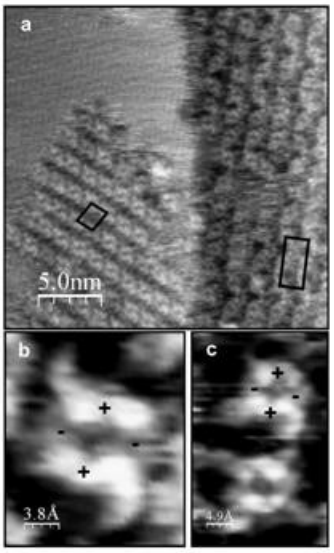

Figure 3. a) STM image (20×20 nm^2) of the rectangular and oblique structures coexisting on a silver terrace. b) Small-scale image of non-illuminated (1.5×1.5 nm^2) and c) illuminated TPP$(NH_2)_2$ (1.9×3.8 nm^2), the signs "+" and "−" indicate the elevated and depressed macrocycle positions, respectively ($V_{bias} = -0.51$ V, $I = 4.72$ nA for all three images).

The comparison of the small-scale images shows that in both phases the molecules display the so-called saddle shape, a characteristic contrast of the metal-free porphyrin macrocycle.[56,57] A quantitative analysis of the intramolecular contrast reveals that the difference between the apparent height of up and down pyrrole rings (marked by plus (+) and minus (−) signs in Figure 3) is very similar ($\Delta h_{oblique} = 0.4 \pm 0.1$ Å and $\Delta h_{rectangular} = 0.5 \pm 0.1$ Å) and perfectly in agreement with former reports for TPP on Ag.[51] In addition, there is no difference in the apparent porphyrin height with respect to the substrate. The strong similarity of molecules in the rectangular phase with those in the oblique one suggests that no significant change of the central macrocycle structure takes place upon irradiation.

As a direct probe of the *trans*-TPP$(NH_2)_2$ positioning and molecular unoccupied electronic structure, we compared the near-edge X-ray absorption fine structure (NEXAFS) spectra of the two phases, Figure 4 a and b, at different orientations of the surface with respect to the electric field direction.

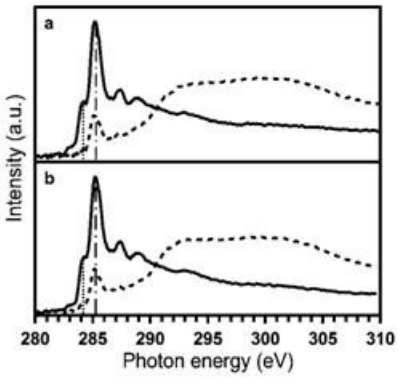

Figure 4. NEXAFS spectra measured by partial electron yield at the C K-edge of oblique (a) and rectangular (b) structures. Two spectra are reported for each sample corresponding to transverse magnetic (solid line) and transverse electric polarization (dashed line). The peaks at 284.1 and 285.2 eV are marked with a dotted and dot-dashed line, respectively.

The C K-edge NEXAFS spectra of the oblique phase are equivalent to those reported for the monolayer phase of H_2-TPP on Ag(111) deposited at RT.[58] Transverse-magnetic (TM) spectra are dominated by the feature at approximately 285.2 eV (dot-dashed line), mainly generated by C^{Ph}-based $1s \rightarrow \pi^*$ electronic transitions,[59] and the evident shoulder on its lower excitation energy side at approximately 284.1 eV (dotted line), associated with $1s \rightarrow \pi^*$ excitations involving macrocycle carbon atoms.[59] Additional resonances in the 286–290 eV range correspond to a mix of higher order π^*-symmetry molecular orbitals (MOs) localized on the aromatic atoms and σ^*-symmetry MOs associated with C–H bonds. The intensity variation of the NEXAFS resonances observed upon changing the orientation from TM to transverse-electric (TE) (polar dichroism) confirms the preferential orientation of the molecules and the intensity ratio allows us to determine the average molecular orientation. In particular, we find that the resonance at 284.1 eV vanishes in TE polarization, an observation that implies that the macrocycle is parallel to the surface, whereas the large residual intensity measured in TE polarization at 285.2 eV indicates that the phenyl rings are oriented off the surface with a tilt angle in the range of 30–35°.

The NEXAFS spectra measured in the rectangular phase preserve approximately the same polar dichroism of the oblique phase, thus confirming the absence of significant conformational change upon irradiation.

To understand whether the rectangular phase is a metastable structure rather than the product of a chemical reaction, we studied its thermal stability. Figure 5 shows the comparison between the thermal behavior of the as-deposited *trans*-TPP$(NH_2)_2$ and of the rectangular phase (a–c and d–f, respectively).

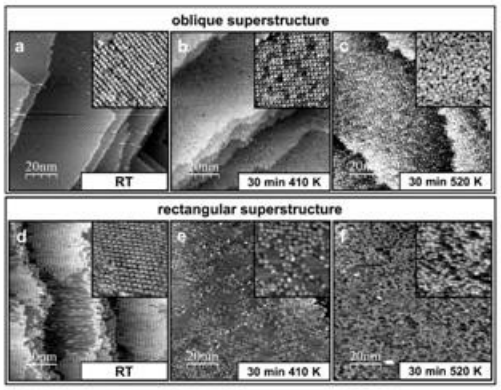

Figure 5. Comparison between the thermal stability of the oblique (a–c) and rectangular (d–f) phases. The temperatures and the annealing times are shown in the figures. All the images have been acquired at RT. Large images: 100×100 nm^2; insets: 30×30 nm^2. a) $V_{bias} = 1.80$ V, $I = 0.07$ nA; inset $V_{bias} = -0.74$ V, $I = 1.71$ nA; b) $V_{bias} = -1.00$ V, $I = 1.00$ nA; inset $V_{bias} = 0.65$ V, $I = 10.00$ nA; c) $V_{bias} = -0.24$ V, $I = 3.66$ nA; inset $V_{bias} = -0.15$ V, $I = 2.00$ nA; d) $V_{bias} = 1.00$ V, $I = 1.00$ nA; inset $V_{bias} = 0.47$ V, $I = 13.05$ nA; e) $V_{bias} = 0.53$ V, $I = 7.36$ nA; inset $V_{bias} = 1.00$ V, $I = 1.88$ nA; f) $V_{bias} = 1.00$ V, $I = 2.58$ nA; inset $V_{bias} = 0.77$ V, $I = 7.36$ nA.

As far as the oblique structure is concerned, the results of many experiments carried out at the sub-monolayer level are consistent with data reported in ref. [55]. There, it is shown that high-temperature annealing induces a flat molecular conformation as a consequence of the generation of new aryl–aryl carbon bonds between the phenyl rings and the macrocycle. The sequence a–c shown in Figure 5 clearly indicates that, in addition to the total loss of molecular order and mobility, the treatment at 520 K induces changes affecting both the molecular shape (which becomes more rectangular) and the apparent height (molecules appear flattened). On the other hand, annealing at lower temperatures (410 K) promotes the surface ordering of this phase, which therefore appears to be the thermodynamically most stable arrangement before thermal deg-

radation. The rectangular structure instead shows molecular disordering and domain fragmentation already at 410 K (Figure 5e). This excludes the rectangular phase to be a kinetically frozen intermediate stage of the self-assembly mechanism leading to the formation of the oblique phase. The irradiation protocol is thus associated with an irreversible chemical reaction that brings the system into a different thermodynamic path.

The estimated distances between facing *meso*-groups along the [1$\bar{1}$0] direction indicate that the amino residues might interact when the NN is either a nonfunctionalized phenyl ($d_{NC} \approx 2.9$ Å) or another amino group ($d_{NN} \approx 2$ Å).

To obtain indications on the nature of this interaction, several polymerization schemes of porphyrin monomers have been modelled by referring to the possible nitrogen oxidation states. In Figure 6, we compare the STM images acquired at

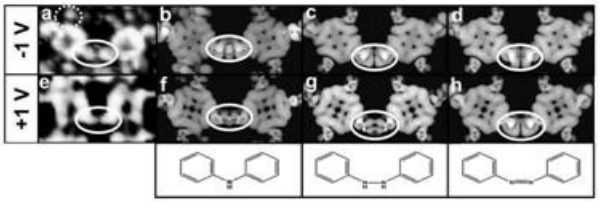

Figure 6. Experimental (a, e) and calculated (b–d), (f–h) STM images of the rectangular superstructure with sketched models of the simulated bonds. The simulated images represent the integrated local density of states between E_f and -1.5 eV (b–d) and between E_f and $+1.5$ eV (f–h), respectively (see Experimental Section). From left to right: the simulations of polyaniline- (b, f), 1,2-diphenylhydrazine- (c, g) and azobenzene-like bonds (d, h) are shown. The white ovals highlight the bond between the units, which are to be compared with the experimentally observed nodal plane structure. The dotted circle marks the cushion effect. (a): 4.3×2.4 nm^2, $V_{bias} = -1.00$ V, $I = 17.37$ nA; (e): 4.16×2.59 nm^2, $V_{bias} = +1.00$ V, $I = 6.70$ nA.

-1 V ($+1$ V) with the simulated STM images of three different models: Figure 6b (6f) shows a polyaniline-like structure with an amino bridge (Ph–NH–Ph)[60] between the porphyrinic units, whereas both Figure 6c (6g) and 6d (6h) imply the coupling of nitrogen atoms with the formation of a Ph-NH–NH-Ph or a Ph-N=N-Ph group, respectively, which are structurally related either to 1,2-diphenylhydrazine (Figure 6c, g), or to azobenzene (Figure 6d, h). Irrespective of the applied bias, the STM image is characterized by a spread of the integrated density of states over the whole molecule except for the area highlighted with a white oval. In this region, a nodal plane parallel to the [001] substrate direction is clearly visible. In addition, some regular circular bright tunneling features are identifiable between TPP units (dotted circle) only at negative bias. These features have been already observed by some of us[61] and ascribed to the so-called "cushion effect". This consists in electron density build-ups in the intermolecular interstices owing to the interaction between the surface and the adsorbate electron clouds.[62]

It appears that the amino bridge, at both positive and negative bias (Figure 6b and f), does not match the experimental observation, both because the azimuthal orientation of TPP units differs by several degrees from the experimental evidence and because the nodal plane crossing the bond is missing. Although at negative bias, Figure 6c and d, it is not possible to distinguish between a Ph-NH–NH-Ph and a Ph-N=N-Ph bond, the images simulated at positive bias display some differences. Even if in both models reported in Figure 6g and h TPP units have the correct azimuthal orientation, only the azo group in Figure 6h exhibits a nodal plane crossing the N=N bond as in the experimental STM images. Thus, the azobenzene-like polymeric structure fits best with the real system.

Having accepted this model, it remains to be explained why azobenzene-like structures are almost exclusively in a *cis* configuration, while *trans* structures amount to less than 4% of the surface coverage.

These are observed as linear defects within the rectangular structure and are identifiable by a wavelike pattern, Figure 7. In these regions, the *trans*-TPP$(NH_2)_2$ units are shifted by half a lattice parameter along the [001] direction and the position and the mutual orientation of molecules facing each other at the linear defect are compatible with the presence of a *trans* azo bond between the porphyrins, as sketched in Figure 7. Explaining the strong stereoselectivity of the polymerization reaction requires understanding the details of the polymerization mechanism. XPS data give valuable, albeit indirect, information in this respect.

The N1s XPS spectrum from as-deposited *trans*-TPP$(NH_2)_2$ at RT (Figure 8a) shows two main peaks whose area ratio (R) is 2. As the molecule has three pairs of inequivalent nitrogen atoms (iminic, pyrrolic, and aminic), it is clear that the aminic signal partially

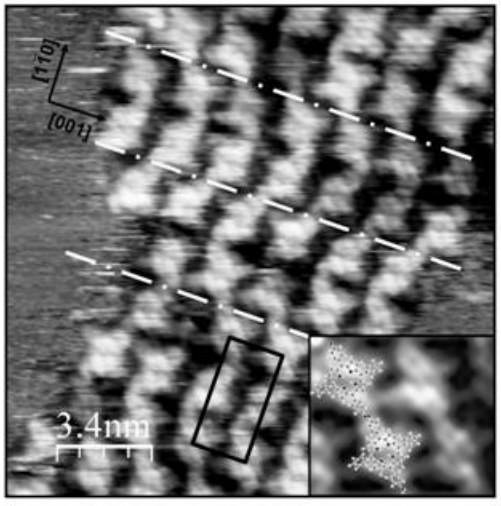

Figure 7. STM image of the linear defects occasionally found within the rectangular structure compatible with the presence of the *trans*-azo geometrical isomer (17×17 nm^2 $V_{bias} = 0.09$ V, $I = 5.71$ nA). Inset: Small-scale STM image of a linear defect with superimposed model (4.94×4.24 nm^2, $V_{bias} = 0.09$ V, $I = 5.71$ nA).

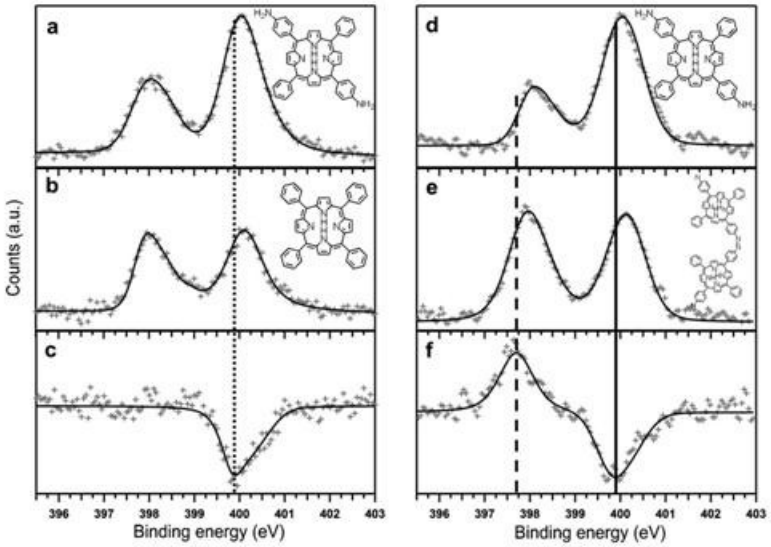

Figure 8. The left panel shows the N 1s XP signals from as-deposited *trans*-TPP(NH_2)$_2$ (a) and H_2-TPP (b) at RT with the corresponding difference spectrum (c). The right panel shows the N 1s XP spectra from as-deposited *trans*-TPP(NH_2)$_2$ at 130 K (d) and the rectangular phase (e) acquired on the same sample of (d) after the reaction protocol. The (d)−(e) difference spectrum is shown in (f). The molecular models are superimposed for clarity and the lines mark the positions of the peaks determined by difference.

overlaps with the pyrrolic one, so its position can be determined by difference, Figure 8c, with the spectrum originated from tetraphenylporphyrin (H_2-TPP), Figure 8b. According to this analysis, the pyrrolic peak (–NH–) is found at a binding energy (BE) of 400.1 ± 0.05 eV, the aminic N (–NH_2) at BE = 399.9 ± 0.05 eV, and the iminic N (–N=) at BE = 398.0 ± 0.05 eV; these values are in agreement with previous studies on monolayer phases on Ag.[63] The effects of the reaction protocol on *trans*-TPP(NH_2)$_2$ were observed on the same sample by measuring the N 1s XP signals before and after irradiation, Figure 8d and e, respectively. After reaction, the peak area at high BE decreases and is associated with the increase by the same amount of the peak at lower BE, as shown in the difference spectrum in Figure 8f and marked by the solid and dashed lines, respectively. In particular, a new N species arises at 397.7 ± 0.05 eV at the expense of the species at 399.9 eV, previously associated with the amino groups. Although these arguments, supported by literature data that confirm the Ag-supported photocatalyzed formation of azo bonds from primary amines,[64–68] would suggest a straightforward association of this new component to the azo nitrogen, we note that the expected BE for a simply physisorbed azo group should be higher than the observed one.[69–72] Chemisorption on metal surfaces generally induces a BE redshift[73] as consequence of the electron donation from the surface.[74] In particular, chemisorption through the central azo bridge at the metal surface[75] can reduce the observed binding energy to 398 eV.[76] Our results show a new species at 397.7 eV, which can be interpreted as nitrogen azo atoms chemisorbed on silver, in agreement with the BE observed for diazonium salts grafted on several metal surfaces (397.5 eV).[77,78] Moreover, the complete dissociation of the azo center can be ruled out because metal-N-Ar nitrogen species exhibit lower binding energy values (397–395 eV).[76,77] In summary, the resulting reaction scenario includes the formation of covalent bonds between the *trans*-TPP(NH_2)$_2$ through N=N bonds that chemisorb associatively on the silver surface. In turn, this interaction likely promotes the preferential formation of the *cis* isomer.

It appears, then, reasonable to imagine an active role of the substrate in the observed reactivity.

Several photochemical studies[40,44,79,80] have shown that the absorption of light by metallic substrates produces a hot electron distribution able to populate an adsorbate empty state. Such a mechanism is known as an indirect excitation process and it may be responsible for photochemical reactions occurring at a noncovalently interacting molecule–metal interfacial system. Besides triggering a reaction through the population of an adsorbate excited state, an indirect excitation may also activate photodissociation processes at longer wavelengths (λ) than those observed in molecular beams. For instance, gas-phase measurements on phenol[46] indicate that the phenoxyl radical (O–H dissociation) is formed by photoexcitations at $\lambda <$ 275 nm, whereas at sub-monolayer coverage on Ag(111) photodissociation takes place at $\lambda = 355$ nm.[48] Aniline in the gas phase undergoes N–H bond breaking at wavelengths in the range $193.3 \leq \lambda \leq 269.5$ nm, with a photophysical electronic mechanism equivalent to that observed for phenol.[47]

To our knowledge, no two-photon-photoemission results pertaining to aniline on Ag single-crystal surfaces are available, but it is plausible that irradiation at 405 nm (3.06 eV) could trigger the N–H photodissociation also in *trans*-TPP(NH_2)$_2$. Within such an assumption, a direct transformation of the oblique phase into the rectangular phase would imply a significant in-plane expansion of the superstructure, which would require a simultaneous highly ordered long-range mass transport with a contextual reorientation of the monomers. However, this only partly explains why the reaction does not proceed at RT. In fact, given the estimated deposition flux (see Experimental Section), the local instantaneous ρ_S is low during deposition. Nevertheless, direct illumination during growth at RT is not efficient in promoting the photoreaction, but it rather leads to the same oblique phase obtained in dark conditions. The role

of the substrate temperature, therefore, proves to be of critical importance in its own right. In the first place, our two-step protocol (low-temperature deposition followed by illumination during slow annealing to RT) provides a separate control of the local density ρ_S (low-density frozen molecules, see Figure 1 d) and of the diffusion anisotropy (by preferentially quenching the diffusion along [001],[81,82] that is, across the compact rows), the subtle balance of which can determine the suitable pairing geometry for the N–H dissociation to take place. In addition, STM images at 100 K (see the inset in Figure 1 d) show a molecular shape and contrast (the high density of states on the now clearly visible four peripheral phenyl rings) compatible with a reduction of the dihedral angle between the porphyrin macrocycle and the *meso*-phenyl rings compared with that at RT. A smaller dihedral angle means a shorter distance between the silver surface and the *trans*-TPP$(NH_2)_2$ amino groups. As the indirect excitation process responsible for the N–H bond breaking is distance-dependent,[48,83] temperature-induced changes in the adsorbate–substrate distance can affect the efficiency of the photoreaction.

Conclusion

We report on the formation of a new long-range ordered and mainly defect-free SCOF obtained photochemically from *trans*-TPP$(NH_2)_2$.

The STM images, C K-edge NEXAFS spectra, and thermal stability prove that the rectangular SCOF structure is not metastable and is not due to an intramolecular reaction, which in principle could lead to a different supramolecular organization of the starting monomers. In addition, comparison with DFT simulations and XPS N 1s spectra suggest that the protocol used leads to the formation of N=N bonds between porphyrin units, likely through the dissociation of N–H bonds mediated by the metallic substrate. This in turn is shown to play a key role in coupling the monomers by low-coverage/variable-temperature experiments, where the reaction is particularly efficient.

Taking in consideration the mild reaction conditions that have been used, we have obtained evidence that, in this system, light is able to induce reactions that would not occur thermally, and, most importantly, we have shown that light can be used as a further parameter to control the growth of low-density structures. In particular, with a low-to-high density approach the probability of defects formation is reduced because the starting conditions do not sterically prevent the conformational adaptation of the molecules. In contrast, the significant conformational reorganization of a densely packed structure required by a high-to-low density approach promotes frequent improper alignments of the molecular building blocks in the resulting covalent structure, as it is commonly observed in the thermally activated reactions, or it can even hamper the reaction, as observed in this work.

The use of radical photodissociation for the covalent stabilization of the supramolecular structure therefore requires that the initial superstructure does not prevent the conformational changes necessary to lead to the formation of the adduct. A low-to-high surface density approach and the use of small leaving groups promote the efficient stabilization of the SCOF. In addition, temperature control is important both to tune the rate and the spatial anisotropy of molecular diffusion and the molecular conformation in order to meet the reaction steric and photoexcitation requirements.

Experimental Section

Scanning tunneling microscopy (STM) imaging

All the experiments were performed in ultrahigh-vacuum conditions at a base pressure of 2×10^{-10} mbar with an Omicron Scanning Tunneling Microscope (VT-STM). The STM measurements were carried out at room temperature (RT, ≈298 K) and near the liquid nitrogen (LN) temperature (≈100 K) in constant-current mode by using an electrochemically etched Pt–Ir tip. All STM images were acquired at RT except for those otherwise specified. The sample bias voltage (V_{bias}) is indicated for all STM images and length measurements are calibrated against the Ag lattice parameter along the [001] direction, which was set equal to 4.09 Å. The error bars associated with length determinations represent one standard deviation, as determined from repeated measurements. The STM data were processed with the WSxM software.[84] Moderate filtering was applied for noise reduction.

Sample preparation

The Ag(110) crystal was cleaned by repeated cycles of 1 keV Ar^+ sputtering and annealing at 820 K until a clean surface with sufficiently large terraces was confirmed by STM imaging. *trans*-TPP$(NH_2)_2$ molecules were deposited from a PBN crucible held at ≈550 K with an estimated flux of ≈0.02 ML min^{-1} (1.47×10^{10} cm^{-2} s^{-1}). The molecular source was outgassed until the pressure did not increase during the sublimation. One ML is defined as a fully covering single molecular layer of *trans*-TPP$(NH_2)_2$ arranged in the $(5\pm2, \mp2\ 3)$ superstructure. The continuous-wave laser source at 405 nm (Roithner Laser Technik, GmbH; model X40LM-10, Vienna, Austria) provided a surface power density of 75 mW cm^{-2} and the beam impinged on the sample with an angle of 70° with respect to the surface normal.

X-ray photoelectron spectroscopy (XPS)

XPS measurements were performed at the ALOISA beamline[85] at the ELETTRA synchrotron radiation facility (Trieste, Italy), using linearly polarized radiation. The spectra were obtained in normal emission geometry with photon energy of 520 eV and overall XPS resolution of ~0.3 eV, by using grazing incident radiation and a home-built hemispherical electron analyzer equipped with a multichannel plate (MCP) detector.

Near-edge X-ray absorption fine structure (NEXAFS)

NEXAFS spectra were measured at the ALOISA beam-line in partial electron yield with a channeltron and a negatively biased (−230 V) grid in front of it to reject low-energy secondary electrons. The orientation of the surface with respect to the linearly polarized photon beam was changed by rotating the surface around the beam axis at a constant grazing incidence angle of ~6°.[86] The polarization is defined by the orientation of the scattering plane with respect to either the electric or the magnetic field. Transverse electric (TE) polarization corresponds to s-polarization, whereas transverse magnetic (TM) closely corresponds to p-polarization (apart

from the grazing angle). The spectra have been energy-calibrated a posteriori by the characteristic absorption signal of the carbon K-edge in the I_0 signal (drain current on the last mirror).

Density functional (DF) calculations

Density functional calculations were performed within the plane-wave pseudopotential formalism using the Quantum ESPRESSO code.[87] The PBE[88] approximation to the exchange-correlation functional was adopted, while van der Waals interactions were taken into account by means of the DFT-D2 semi-empirical correction scheme.[89,90] Ultrasoft pseudopotentials[91,92] from the QE database were employed, and the cut-offs on plane waves were set to 25 Ry and 250 Ry on the wave function and the charge density, respectively. Geometries were optimized until energy and forces converged within 1E–4 Ry and 1E–5 Ry/a_0, respectively. Reported results refer to an unsupported model of the molecular overlayer: a single layer of TPP molecules not supported by the metal surface placed in a proper cell having the periodicity of the real system. As there is no conducting substrate in our model, STM images cannot be simulated by the conventional Tersoff–Hamann[93] approach. Rather, in the same spirit of the aforementioned approach, we define the STM current at the position r simply as the integrated local density of states (ILDOS) at that point. Here, local density of states (LDOS) are integrated from the Fermi level E_f to the bias energy ($E_f + eV_b$):

$$I(\mathbf{r},eV_b) = \mathrm{ILDOS}(\mathbf{r},E_f : E_f + eV_b) = \sum_{E_f<E_i<E_f+eV_b}^{n} \varphi_i(r)^2 \qquad (1)$$

where V_b is the applied bias voltage, and the Fermi level is defined as the center of the HOMO–LUMO gap. Within this approach, the numerical value of the current does not have physical meaning, and isocurrent profiles can be qualitatively compared to STM images. To better match the appearance of the porphyrin core, the integration integral of ILDOS was extended up to +1.5 eV (−1.5 eV) to simulate STM images acquired at $V_b = 1$ V ($V_b = -1$ V). This choice doesn't affect the features related to the link between monomers, as orbitals localized in that space region are close to the Fermi level. Besides, this roughly takes into account the broadening of molecular states due to the interaction with the surface.

Acknowledgements

P. Villoresi is gratefully acknowledged for providing the laser source. This work has been partially funded by MIUR (PRIN 2010/11, Project No. 2010BNZ3F2: "DESCARTES") and by the University of Padova (Progetto Strategico STPD08RCX5 "HELIOS" and Progetti di Ricerca di Ateneo, CPDA118475/11). The authors acknowledge Cecilia Crestale for the cover illustration.

Keywords: covalent organic frameworks · on-surface synthesis · porphyrins · scanning tunneling microscopy (STM) · surface photochemistry · surface polymerization

[1] S.-Y. Ding, W. Wang, *Chem. Soc. Rev.* **2013**, *42*, 548 – 568.
[2] J. Sakamoto, J. van Heijst, O. Lukin, D. Schlüter, *Angew. Chem.* **2009**, *121*, 1048 – 1089; *Angew. Chem. Int. Ed.* **2009**, *48*, 1030 – 1069.
[3] D. Bonifazi, S. Mohnani, A. Llanes-Pallas, *Chem. Eur. J.* **2009**, *15*, 7004 – 7025.
[4] L. Zang, Y. Che, J. Moore, *Acc. Chem. Res.* **2008**, *41*, 1596 – 1608.
[5] D. Heim, D. Ecija, K. Seufert, W. Auwärter, C. Aurisicchio, C. Fabbro, D. Bonifazi, J. V. Barth, *J. Am. Chem. Soc.* **2010**, *132*, 6783 – 6790.
[6] Y. Yang, C. Wang, *Chem. Soc. Rev.* **2009**, *38*, 2576 – 2589.
[7] T. Kudernac, S. Lei, J. W. Elemans, S. De Feyter, *Chem. Soc. Rev.* **2009**, *38*, 402 – 421.
[8] M. Di Marino, F. Sedona, M. Sambi, T. Carofiglio, E. Lubian, M. Casarin, E. Tondello, *Langmuir* **2010**, *26*, 2466 – 2472.
[9] F. Sedona, M. Di Marino, A. Basagni, L. Colazzo, M. Sambi, *J. Phys. Chem. C* **2014**, *118*, 1587 – 1593.
[10] A. Dmitriev, H. Spillmann, N. Lin, J. V. Barth, K. Kern, *Angew. Chem.* **2003**, *115*, 2774 – 2777; *Angew. Chem. Int. Ed.* **2003**, *42*, 2670 – 2673.
[11] A. Langner, S. L. Tait, N. Lin, C. Rajadurai, M. Ruben, K. Kern, *Proc. Natl. Acad. Sci. USA* **2007**, *104*, 17927 – 17930.
[12] S. Stepanow, N. Lin, J. V. Barth, K. Kern, *J. Phys. Chem. B* **2006**, *110*, 23472 – 23477.
[13] R. Otero, M. Schöck, L. M. Molina, E. Laegsgaard, I. Stensgaard, B. Hammer, F. Besenbacher, *Angew. Chem.* **2005**, *117*, 2310 – 2315; *Angew. Chem. Int. Ed.* **2005**, *44*, 2270 – 2275.
[14] J. Theobald, N. S. Oxtoby, M. Phillips, N. R. Champness, P. H. Beton, *Nature* **2003**, *424*, 1029 – 1031.
[15] M. Stöhr, M. Wahl, C. H. Galka, T. Riehm, T. a. Jung, L. H. Gade, *Angew. Chem.* **2005**, *117*, 7560 – 7564; *Angew. Chem. Int. Ed.* **2005**, *44*, 7394 – 7398.
[16] A. El-Sayed, P. Borghetti, E. Goiri, C. Rogero, L. Floreano, G. Lovat, D. J. Mowbray, J. L. Cabellos, Y. Wakayama, A. Rubio, *ACS Nano* **2013**, *7*, 6914 – 6920.
[17] D. G. de Oteyza, J. M. García-Lastra, M. Corso, B. P. Doyle, L. Floreano, A. Morgante, Y. Wakayama, A. Rubio, J. E. Ortega, *Adv. Funct. Mater.* **2009**, *19*, 3567 – 3573.
[18] K. W. Hipps, L. Scudiero, D. E. Barlow, M. P. Cooke, *J. Am. Chem. Soc.* **2002**, *124*, 2126 – 2127.
[19] S. Furukawa, K. Tahara, F. C. De Schryver, M. Van der Auweraer, Y. Tobe, S. De Feyter, *Angew. Chem.* **2007**, *119*, 2889 – 2892; *Angew. Chem. Int. Ed.* **2007**, *46*, 2831 – 2834.
[20] F. Tao, S. L. Bernasek, *J. Am. Chem. Soc.* **2005**, *127*, 12750 – 12751.
[21] J. Méndez, M. F. López, J. Martín-Gago, *Chem. Soc. Rev.* **2011**, *40*, 4578 – 4590.
[22] G. Franc, A. Gourdon, *Phys. Chem. Chem. Phys.* **2011**, *13*, 14283 – 14292.
[23] F. Sedona, M. Di Marino, M. Sambi, T. Carofiglio, E. Lubian, M. Casarin, E. Tondello, *ACS Nano* **2010**, *4*, 5147 – 5154.
[24] M. Treier, N. V. Richardson, R. Fasel, *J. Am. Chem. Soc.* **2008**, *130*, 14054 – 14055.
[25] S. Weigelt, C. Busse, C. Bombis, M. M. Knudsen, K. V. Gothelf, T. Strunskus, C. Wöll, M. Dahlbom, B. Hammer, E. Laegsgaard, *Angew. Chem.* **2007**, *119*, 9387 – 9390; *Angew. Chem. Int. Ed.* **2007**, *46*, 9227 – 9230.
[26] C. H. Schmitz, J. Ikonomov, M. Sokolowski, *J. Phys. Chem. C* **2009**, *113*, 11984 – 11987.
[27] A. C. Marele, R. Mas-Ballesté, L. Terracciano, J. Rodríguez-Fernández, I. Berlanga, S. S. Alexandre, R. Otero, J. M. Gallego, F. Zamora, J. M. Gómez-Rodríguez, *Chem. Commun.* **2012**, *48*, 6779 – 6781.
[28] J. Lipton-Duffin, O. Ivasenko, D. F. Perepichka, F. Rosei, *Small* **2009**, *5*, 592 – 597.
[29] M. Bieri, S. Blankenburg, M. Kivala, C. Pignedoli, P. Ruffieux, K. Müllen, R. Fasel, *Chem. Commun.* **2011**, *47*, 10239 – 10241.
[30] L. Lafferentz, V. Eberhardt, C. Dri, C. Africh, G. Comelli, F. Esch, S. Hecht, L. Grill, *Nat. Chem.* **2012**, *4*, 215 – 220.
[31] J. Cai, P. Ruffieux, R. Jaafar, M. Bieri, T. Braun, S. Blankenburg, M. Muoth, A. P. Seitsonen, M. Saleh, X. Feng, *Nature* **2010**, *466*, 470 – 473.
[32] M. Kittelmann, P. Rahe, M. Nimmrich, C. M. Hauke, A. Gourdon, A. Kühnle, *ACS Nano* **2011**, *5*, 8420 – 8425.
[33] J. Colson, W. Dichtel, *Nat. Chem.* **2013**, *5*, 453 – 465.
[34] L. Xu, X. Zhou, Y. Yu, W. Q. Tian, J. Ma, S. Lei, *ACS Nano* **2013**, *7*, 8066 – 8073.
[35] J. F. Dienstmaier, A. M. Gigler, A. J. Goetz, P. Knochel, T. Bein, A. Lyapin, S. Reichlmaier, W. M. Heckl, M. Lackinger, *ACS Nano* **2011**, *5*, 9737 – 9745.
[36] C.-Z. Guan, D. Wang, L.-J. Wan, *Chem. Commun.* **2012**, *48*, 2943 – 2945.
[37] Y.-H. Qiao, Q.-D. Zeng, Z.-Y. Tan, S.-D. Xu, D. Wang, C. Wang, L.-J. Wan, C.-L. Bai, *J. Vac. Sci. Technol. B* **2002**, *20*, 2466.

[38] X. Zhang, S. Xu, M. Li, Y. Shen, Z. Wei, S. Wang, Q. Zeng, C. Wang, *J. Phys. Chem. C* **2012**, *116*, 8950 – 8955.
[39] A. Deshpande, C.-H. Sham, J. M. P. Alaboson, J. M. Mullin, G. C. Schatz, M. C. Hersam, *J. Am. Chem. Soc.* **2012**, *134*, 16759 – 16764.
[40] X.-L. Zhou, X.-Y. Zhu, J. M. White, *Surf. Sci. Rep.* **1991**, *13*, 73 – 220.
[41] K. Fukutani, M.-B. Song, Y. Murata, *J. Chem. Phys.* **1995**, *103*, 2221.
[42] S. K. So, R. Franchy, W. Ho, *J. Chem. Phys.* **1991**, *95*, 1385.
[43] X. L. Zhou, X. Y. Zhu, J. M. White, *Acc. Chem. Res.* **1990**, *23*, 327 – 332.
[44] X.-Y. Zhu, J. M. White, *J. Chem. Phys.* **1991**, *94*, 1555.
[45] J. L. Solomon, R. J. Madix, J. Stöhr, *Surf. Sci.* **1991**, *255*, 12 – 30.
[46] V. Poterya, L. Šištík, P. Slavíček, M. Fárník, *Phys. Chem. Chem. Phys.* **2012**, *14*, 8936 – 8944.
[47] G. King, T. Oliver, M. N. R. Ashfold, *J. Chem. Phys.* **2010**, *132*, 214307.
[48] J. Lee, S. Ryu, J. S. Ku, S. K. Kim, *J. Chem. Phys.* **2001**, *115*, 10518.
[49] J. Lee, S. Ryu, J. Chang, S. Kim, S. K. Kim, *J. Phys. Chem. B* **2005**, *109*, 14481 – 14485.
[50] J. Brede, M. Linares, S. Kuck, J. Schwöbel, A. Scarfato, S.-H. Chang, G. Hoffmann, R. Wiesendanger, R. Lensen, P. H. J. Kouwer, *Nanotechnology* **2009**, *20*, 275602.
[51] F. Buchner, I. Kellner, W. Hieringer, *Phys. Chem. Chem. Phys.* **2010**, *12*, 13082 – 13090.
[52] M. O. Sinnokrot, C. D. Sherrill, *J. Phys. Chem. A* **2006**, *110*, 10656 – 10668.
[53] E. Arunan, H. S. Gutowsky, *J. Chem. Phys.* **1993**, *98*, 4294.
[54] V. Barone, M. Casarin, D. Forrer, S. Monti, G. Prampolini, *J. Phys. Chem. C* **2011**, *115*, 18434 – 18444.
[55] G. Di Santo, S. Blankenburg, C. Castellarin-Cudia, M. Fanetti, P. Borghetti, L. Sangaletti, L. Floreano, A. Verdini, E. Magnano, F. Bondino, *Chem. Eur. J.* **2011**, *17*, 14354 – 14359.
[56] T. Yokoyama, S. Yokoyama, T. Kamikado, S. Mashiko, *J. Chem. Phys.* **2001**, *115*, 3814.
[57] F. Buchner, K.-G. Warnick, T. Wölfle, A. Görling, H.-P. Steinrück, W. Hieringer, H. Marbach, *J. Phys. Chem. C* **2009**, *113*, 16450 – 16457.
[58] G. Di Santo, C. Sfiligoj, C. Castellarin-Cudia, A. Verdini, A. Cossaro, A. Morgante, L. Floreano, A. Goldoni, *Chem. Eur. J.* **2012**, *18*, 12619 – 12623.
[59] Scalar relativistic two component zeroth-order regular approximation time-dependent-DFT (ZORA TD-DFT) calculations pertaining to H_2-TPP state that, despite the major contribution to the peak at 285.2 eV comes from C^{Ph}-based $1s\rightarrow\pi^*$ transitions, the participation of $1s\rightarrow\pi^*$ excitations involving all the macrocycle C atoms (C^{Ph} and C^{m}) is not negligible (M. V. Nardi, R. Verucchi, L. Pasquali, A. Giglia, G. Fronzoni, M. Sambi, G. Mangione, M. Casarin, submitted).
[60] Y. Lee, C. Chang, S. Yau, L. Fan, Y. Yang, L. O. Yang, K. Itaya, *J. Am. Chem. Soc.* **2009**, *131*, 6468 – 6474.
[61] M. Casarin, M. Di Marino, D. Forrer, M. Sambi, F. Sedona, E. Tondello, A. Vittadini, V. Barone, M. Pavone, *J. Phys. Chem. C* **2010**, *114*, 2144 – 2153.
[62] G. Witte, S. Lukas, P. S. Bagus, C. Wöll, *Appl. Phys. Lett.* **2005**, *87*, 263502.
[63] G. Di Santo, C. Castellarin-Cudia, M. Fanetti, B. Taleatu, P. Borghetti, L. Sangaletti, L. Floreano, E. Magnano, F. Bondino, A. Goldoni, *J. Phys. Chem. C* **2011**, *115*, 4155 – 4162.
[64] B. Dong, Y. Fang, L. Xia, H. Xu, M. Sun, *J. Raman Spectrosc.* **2011**, *42*, 1205 – 1206.
[65] Y.-F. Huang, H.-P. Zhu, G.-K. Liu, D.-Y. Wu, B. Ren, Z.-Q. Tian, *J. Am. Chem. Soc.* **2010**, *132*, 9244 – 9246.
[66] Y. Fang, Y. Li, H. Xu, M. Sun, *Langmuir* **2010**, *26*, 7737 – 7746.
[67] L.-B. Zhao, Y.-F. Huang, X.-M. Liu, J. R. Anema, D.-Y. Wu, B. Ren, Z.-Q. Tian, *Phys. Chem. Chem. Phys.* **2012**, *14*, 12919 – 12929.
[68] D. Wu, X. Liu, Y. Huang, B. Ren, X. Xu, Z. Tian, *J. Phys. Chem. C* **2009**, *113*, 18212 – 18222.
[69] M. Onoue, M. R. Han, E. Ito, M. Hara, *Surf. Sci.* **2006**, *600*, 3999 – 4003.
[70] U. Jung, S. Kuhn, U. Cornelissen, F. Tuczek, T. Strunskus, V. Zaporojtchenko, J. Kubitschke, R. Herges, O. Magnussen, *Langmuir* **2011**, *27*, 5899 – 5908.
[71] D. Brete, D. Przyrembel, C. Eickhoff, R. Carley, W. Freyer, K. Reuter, C. Gahl, M. Weinelt, *J. Phys. Condens. Matter* **2012**, *24*, 394015.
[72] G. Mercurio, E. R. McNellis, I. Martin, S. Hagen, F. Leyssner, S. Soubatch, J. Meyer, M. Wolf, P. Tegeder, F. S. Tautz, *Phys. Rev. Lett.* **2010**, *104*, 036102.
[73] D. Menzel, *Crit. Rev. Solid State Mater. Sci.* **1978**, *7*, 357 – 384.
[74] T. Nakayama, K. Inamura, Y. Inoue, S. Ikeda, K. Kishi, *Surf. Sci.* **1987**, *179*, 47 – 58.
[75] M. Piantek, J. Miguel, M. Bernien, C. Navío, A. Krüger, B. Priewisch, K. Rück-Braun, W. Kuch, *Appl. Phys. A* **2008**, *93*, 261 – 266.
[76] M. Piantek, J. Miguel, A. Krüger, C. Navío, M. Bernien, D. K. Ball, K. Hermann, W. Kuch, *J. Phys. Chem. C* **2009**, *113*, 20307 – 20315.
[77] M. Miyachi, Y. Yamamoto, Y. Yamanoi, A. Minoda, S. Oshima, Y. Kobori, H. Nishihara, *Langmuir* **2013**, *29*, 5099 – 5103.
[78] A. Mesnage, X. Lefèvre, P. Jégou, G. Deniau, S. Palacin, *Langmuir* **2012**, *28*, 11767 – 11778.
[79] J. W. Gadzuk, *J. Chem. Phys.* **2012**, *137*, 091703.
[80] S. R. Hatch, X.-Y. Zhu, J. M. White, A. Campion, *J. Chem. Phys.* **1990**, *92*, 2681.
[81] F. Montalenti, R. Ferrando, *Phys. Rev. B* **1999**, *59*, 5881 – 5891.
[82] U. T. Ndongmouo, F. Hontinfinde, *Surf. Sci.* **2004**, *571*, 89 – 101.
[83] M. Comstock, N. Levy, A. Kirakosian, J. Cho, F. Lauterwasser, J. Harvey, D. Strubbe, J. Fréchet, D. Trauner, S. Louie, *Phys. Rev. Lett.* **2007**, *99*, 038301.
[84] I. Horcas, R. Fernández, J. M. Gómez-Rodríguez, J. Colchero, J. Gómez-Herrero, A. M. Baro, *Rev. Sci. Instrum.* **2007**, *78*, 013705.
[85] L. Floreano, G. Naletto, D. Cvetko, R. Gotter, M. Malvezzi, L. Marassi, A. Morgante, A. Santaniello, A. Verdini, F. Tommasini, *Rev. Sci. Instrum.* **1999**, *70*, 3855.
[86] L. Floreano, A. Cossaro, R. Gotter, A. Verdini, G. Bavdek, F. Evangelista, A. Ruocco, A. Morgante, D. Cvetko, *J. Phys. Chem. C* **2008**, *112*, 10794 – 10802.
[87] P. Giannozzi, S. Baroni, N. Bonini, M. Calandra, R. Car, C. Cavazzoni, D. Ceresoli, G. L. Chiarotti, M. Cococcioni, I. Dabo, *J. Phys. Condens. Matter* **2009**, *21*, 395502.
[88] J. P. Perdew, K. Burke, M. Ernzerhof, *Phys. Rev. Lett.* **1996**, *77*, 3865 – 3868.
[89] S. Grimme, *J. Comput. Chem.* **2006**, *27*, 1787 – 1799.
[90] V. Barone, M. Casarin, D. Forrer, M. Pavone, M. Sambi, A. Vittadini, *J. Comput. Chem.* **2009**, *30*, 934 – 939.
[91] A. Rappe, K. Rabe, E. Kaxiras, J. Joannopoulos, *Phys. Rev. B* **1990**, *41*, 1227 – 1230.
[92] D. Vanderbilt, *Phys. Rev. B* **1990**, *41*, 7892 – 7895.
[93] J. Tersoff, D. R. Hamann, *Phys. Rev. Lett.* **1983**, *50*, 1998 – 2001.

Received: April 23, 2014
Published online on September 8, 2014